Winter 2018

A SIMPLIFIED STRUCTURAL ANALYSIS METHOD FOR A 20-FOOT CARGO SHIPPING CONTAINER

Dzijeme Ntumi
University of New Hampshire, Durham

A SIMPLIFIED STRUCTURAL ANALYSIS METHOD FOR A 20-FOOT CARGO SHIPPING CONTAINER

BY

Dzijeme A. G. Ntumi

BS, UNIVERSITY OF NEW HAMPSHIRE, 2017

THESIS

Submitted to the University of New Hampshire in Partial Fulfillment of the Requirements for the Degree of

Master of Science in Civil and Environmental Engineering

December, 2018

This thesis/dissertation has been examined and approved in partial fulfillment of the requirements for the degree of

Masters of Science in Civil and Environmental Engineering by:

Dr. Robert Henry, Associate Professor in Civil and Environmental Engineering

Dr. Erin Santini Bell, Associate Professor in Civil and Environmental Engineering

Dr. Ricardo Medina, Associate Professor in Civil and Environmental Engineering

On December 4th, 2018

Original approval signatures are on file with the University of New Hampshire Graduate School.

TABLE OF CONTENTS

LIST OF FIGURES

ABSTRACT
A SIMPLIFIED STRUCTURAL ANALYSIS METHOD FOR A 20-FOOT CARGO SHIPPING CONTAINER

by

Dzijeme A. G. Ntumi

University of New Hampshire, December, 2018

Cargo containers are utilized around the globe as structural components in the design of buildings. Kevin Giriuanas [1] wrote a thesis on the finite element analysis of a 20-foot cargo shipping container, which was comprised of mostly shell elements. This thesis aims to develop a simplified beam model which compares well with the displacement and stresses of a finite element shell model of a 20-foot cargo shipping container. The simplified beam model is comprised of columns with rectangular cross sections and four panels developed using the modified box frame model presented in a thesis by Deborah L. Calvin [2]. The displacements determined by the simplified beam model are with 10% difference of the displacements determined by the finite element shell models of the cargo container structural system. The stresses determined by the simplified beam model are within 15% of the finite element shell models.

Dedication

This thesis is dedicated to Solace and Etoenyo Ntumi. Two wonderful parents who nurtured and supported me through my education. I couldn't have asked for better parents.

I love you both,

Dzijeme Afua Gbo Ntumi

Acknowledgements

Dr. Robert Henry

Thank you for helping me on my journey and being very supportive throughout my education years here at UNH. I couldn't have done this without you.

Dr. Ricardo Medina:

Thank you for your words of wisdom and constant reassurance during my journey in graduate school.

Dr. Erin Bell:

Thank you for always being there to bounce ideas off of and answer questions pertaining to my thesis.

Shokoufeh Zargar:

Thank you for your constant encouragement and help learning AbaqusCAE.

Duncan McGeehan:

Thank you for helping me learn AbaqusCAE and helping me understand the results of my modeling.

Kathryn Kaspar:

Thank you for the motivation you provided day in and day out.

Chapter 1

Introduction

1.1 Background

Cargo containers have become an intriguing component of the United States tiny home construction process in the last five or so years. Shows such as *Tiny Homes*, and *Containables* [3] have made their way onto television channels such as, the DIY channel and the Home Improvement Channel. These shows demonstrate the wide range of uses and capabilities of using cargo containers to construct homes and buildings. However, the United States is just now stepping into the realm of building in which many parts of the world have already ventured. Some examples are, the QUO Container Center in Buenos Aires, Boxpark Shoreditch in London, and 27 Boxes in South Africa.

Figure 1 QUO Container Center in Buenos Aires, Argentina

Cargo containers are an interesting source of structural building component because they can be considered a sustainable material. Cargo containers are built using steel or aluminum. However, they are comprised mostly of steel, a material which is widely used in structures around the world. As the social environment in the United States and the world move to useing more sustainable resources, existing steel cargo containers could help decrease pollution due to the reduction in steel fabrication, as well as make use of containers that are sitting in "graveyards". Another advantage to building with the containers is that they can serve as building blocks, i.e. like Legos, which can reduce construction time. Cargo containers are available in an array of sizes in the United States. These container grave yards tend to be at a port of entry or nearby.

One significant question that arises when one is considering using cargo containers as structural elements in buildings is:

- What is the structural behavior of a cargo container under a variety of loads?

The primary goal of this thesis is to:

- Develop a computer model that can reasonably predict the structural behavior of an ISO cargo shipping containers. An ISO container is a cargo shipping container that meets the design standards of the International Organization for Standardization (ISO).

It is crucial to understand the structural capacity and behavior of ISO cargo containers when they are used as a structural building component. The containers are built to safely

hold a large load of goods, the payload capacity, that are transported overseas. They are designed to be stacked as high as nine containers.

The structural investigation of the cargo container will attempt to answer the following questions:

- How does the container behave under different applied loads?
- What structural components in the containers control how the loads applied to the containers are supported?
- What is the critical load path to transfer the load from the top of the container to its support points?

These questions must be answered in order to fully use the cargo shipping container as a structural building component.

1.2 Potential Value of New Model

The primary beneficiary of the information developed in this thesis is the research community that is interested in exploring new structural components for building and innovative use of materials as structural building elements. Another is civil engineering and construction professions in the United States.

While there is some research being conducted by companies that manufacture cargo shipping container, obtaining this information has proven to be difficult. Even securing the dimensions and material properties of the structural members used in the construction of an ISO cargo shipping container has proven hard to obtain. Manufacturers appear to be hesitant to share their information because they have to remain a competition in the cargo container manufacturing industry, stated by Kevin Banes a public affairs coordinator at ACM USA [4]. This thesis will provide some fundamental knowledge of the behavior of the structural components of a typical cargo container. The information generated will be available to the structural engineering community. Thus enabling them to further explore the uses of cargo containers and expand how one might incorporate ISO cargo containers into a variety of structural systems.

There are several different aspects of value added for the civil engineering profession. The analysis approach that will be detailed in this thesis will provide engineers with an efficient method to analyze cargo shipping container structural components and its assembly. There are many used ISO cargo shipping containers resting in "graveyards" around the United States. Using these containers for the construction of new structures could bring a new meaning to reuse, reduce, and recycle. The reuse of the cargo containers would be an essential approach in areas where steel, masonry, or timber as a building material are limited. Engineers could use the containers as building blocks reducing the need for the use of virgin building materials. The understanding of the

structural capability of ISO cargo shipping containers could significantly help sustainable building practices in the United States.

1.3 Goals

The goal of this thesis is to develop a simplified beam analytical model of a typical cargo container. The model will consist of a simplified beam model for the corner post and a simple beam/truss system for the corrugated walls. This model would provide information on the structural behavior of a cargo container and would enable one to use ISO cargo shipping containers as the primary structural building component.

Chapter 2

Literature Review

2.1 Overview

This chapter reviews the available background information for this thesis. The chapter will go over the early history of the cargo shipping container. It will present relevant previous research associated with the analytical methods used in the thesis.

2.2 History of Cargo Shipping Container

The modern cargo shipping container, Figure 2, was first developed and patented by Malcolm Mc Lean in 1956. Mc Lean owned the largest trucking fleet in the southern part of the United States. He began his operation in 1934 with the purchase of his first truck [5]. The inspiration for the creation of the cargo shipping container came after twenty years of watch inefficient loading and unloading of the trucks in his fleet. He noted that the irregular sized wooden crates in which goods were shipped were a major factor in the inefficiency. [6] In addition to the creation of the cargo shipping container McLean designed and renovated cargo ships so that they could stack the containers below and above the deck. [5]His newly created business was given the name of Sea-Land with its first ship named the Ideal X.

Figure 2 Cargo Shipping Container (20ft)

Soon after the deployment of the Ideal X other companies began using this approach to ship goods. Within two years Matson Navigation Company deployed its own cargo container ship, the Hawaiian Merchant [6]. This competition led to an efficiency optimization in the cargo container shipping industry. There was a need to create a set of standards that could aid in transferring shipping containers between ships, trains, cranes and trucks. By 1961 the International Organization for Standardization [7] set standards for the cargo containers.

2.3 Information Search

The background information used in this thesis comes from three primary sources; the Tilton Trailer Company [8], the 2013 version of the ISO codes [9], a thesis written by Kevin Andre Giriunas [1], and a thesis written by Deborah L. Calvin [2]. Tilton Trailer is a company in Tilton, New Hampshire that modifies cargo containers to be used as field offices on construction sites. Tilton Trailer works with twenty-foot and forty-foot long cargo shipping containers. They provided a piece of the exterior wall of a typical cargo shipping container that was used to create test specimens to determine some material properties of the metal used for the cargo shipping container corrugated walls.

The ISO (International Organization for Standardization) standard has sections for the design of cargo shipping container [9]. The standards referenced were ISO 1496, ISO 668, ISO 6346. The ISO standards for cargo shipping containers are used by many companies in the United States for designing and building their cargo shipping containers. The ISO standard for cargo shipping containers was last updated in 2016. The idea of this thesis is to structurally evaluate used cargo shipping containers as a building component. Therefore, the 2013 version of the ISO standards will be utilized because the ISO cargo shipping containers that would be used as a structural component today were likely built prior to 2016. There wasn't a significant change in the 2016 ISO standards when compared to the 2013 standards.

2.4 Previous Research

In 2012 Kevin Andre Giriunas, a graduate at Ohio State University completed a thesis called "Evaluation, Modeling, and Analysis of Shipping Container Building Structures" [1]. The main objective of the thesis was to develop structural guidelines for ISO designed containers that would be used in non-shipping applications. Giriunas performed a finite element analysis (FEA) of a twenty-foot cargo shipping container, shown in Figure 3. It included some interesting foundation designs. Giriunas' thesis allows for a comparison of analytical methods in both theses. It also provides a computation verification data for analysis portion of this thesis. Giriunas talked to many professionals who were able to provide him with dimensions and suggestions for the 20-foot container analysis. He made several conclusions based upon his research. The following four conclusions directly relate to the research being conducted in this thesis:

1. The twenty-foot cargo shipping container tested reached or exceeded the maximum loads set by ISO standards for all the loading scenarios
2. The roof of the cargo shipping container did not offer any significant structural contribution to the building system.
3. The direction of the lateral load determined which side components of the cargo shipping container contributed most to the lateral resistance system.
4. When subject to gravity loads on the corner fittings, the ranking of the structural components from strongest resisting to weakest are:
    a. End walls

b. Side walls

c. The roof had no structural resistance

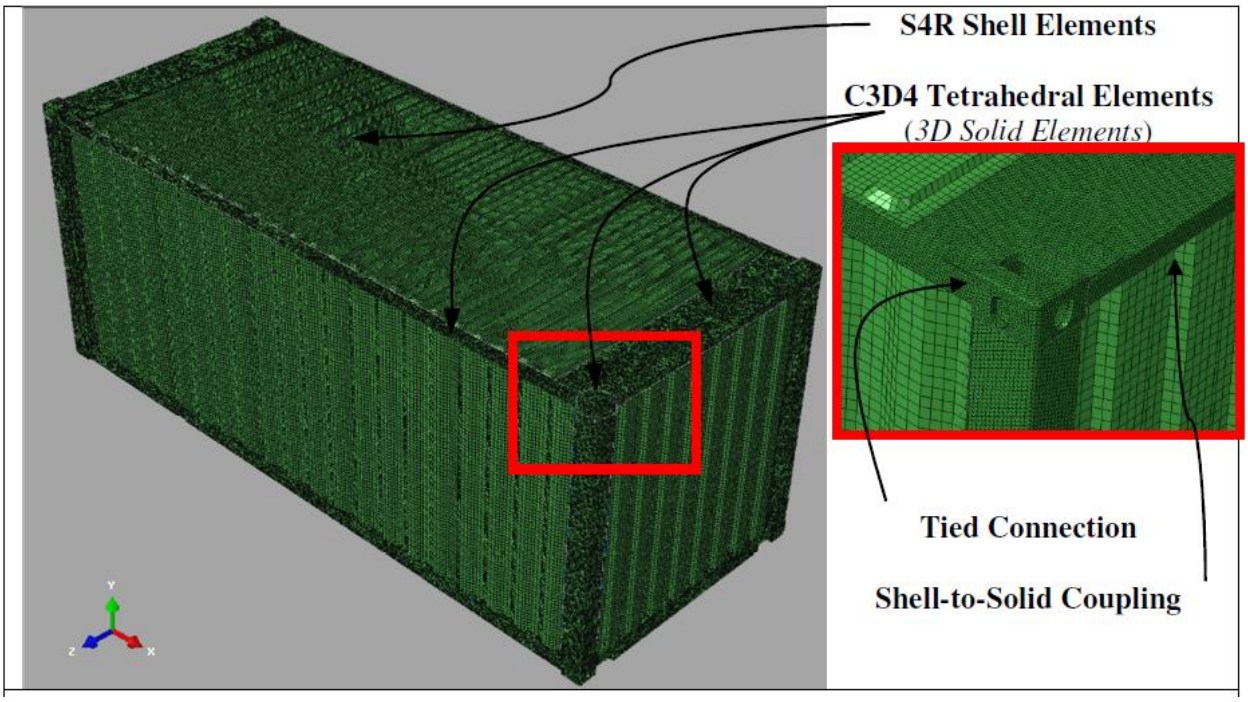

Figure 3 Model 4 & 5 (Giriunas)

Giriunas utilized many different types of elements in the finite element analysis of the twenty-foot cargo shipping container. The main one being the element S4R shell element as detailed by AbacusCAE. The same elements will be used to model the corrugated siding of a twenty-foot cargo shipping container in this thesis. Chapter 4 will detail specifics such as shape function and degrees of freedom of an S4R shell element.

Deborah Calvin completed a thesis in 1986 titled "A Simplified Box Frame Model For Structural Cladding" [2]. In the thesis Calvin explores the structural capabilities of precast concrete cladding. The purpose of the thesis was two-fold. The first was to create a

computer model that would simulate a conventional flat plane stress concrete cladding panel using truss and beam elements. The second was to see if the cladding could be used as a structural component in a building system. Calvin determined she could use a box frame analysis along with a numerical scale to reasonably, within 10%, determine the structural behavior of the concrete cladding. A numerical scale is a number multiplied to each quantitative result to produce a new quantitative result. This idea of simplified analysis will be utilized within this thesis to develop part of a combined simplified beam model.

The box frame model consists of four boxes connected with pin connections, shown in Figure 4. Each box consists of two horizontal members (#1) and two vertical members (#2) rigidly connected at the corners. In total the entire box frame model consists of sixteen beam elements, eight horizontal (#1) and eight vertical (#2), that simulate the structural behavior of the cladding panel. In order to reasonably simulate the behavior of the concrete cladding, Calvin developed several equations that sized the horizontal and vertical members. The sizing is based on the properties and geometry of the cladding panel. Each horizontal member has the same dimensions and the same is true for all of the vertical members. The length of each horizontal member corresponds to half the length of the concrete cladding, while the length of each vertical member corresponds to half the height of the concrete cladding. Figure 4 details the model and equations Calvin used. A1 corresponds to cross sectional area of the horizontal member and A2 corresponds to the cross sectional area of the vertical member.

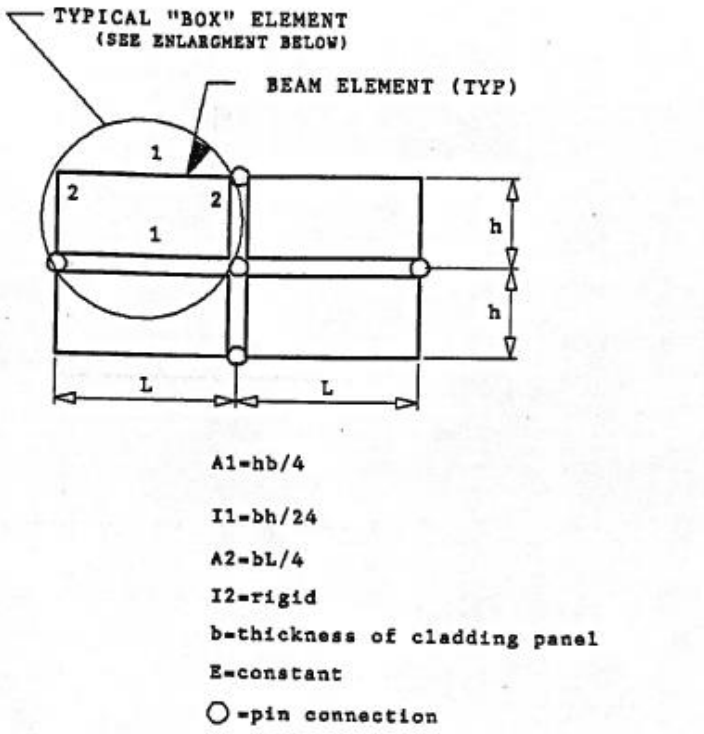

FIGURE 2.2.1

Figure 4 Box Frame Model Calvin 1986

Chapter 3

Coupon Testing

3.1 Introduction

The purpose of Chapter 3 is to detail the methods used to determine the material properties associated with the corrugated metal siding used in later chapters of the thesis. The material properties will be used in the computer models of a typical forty-foot cargo container. The test was completed in order to make sure that the material properties are known for the siding, since cargo container manufacturers were not willing to provide the information. In order to perform the tests, it was necessary to obtain a piece of corrugated metal siding from a used ISO cargo shipping container. A piece of corrugated steel siding from a cargo container was obtained from Tilton Trailer Company in Tilton, New Hampshire.

In this case the material properties of interest are the material type, 0.2% offset yield stress, ultimate yield strength, modulus of elasticity, and percent elongation. To get the material properties a coupon test was performed. A coupon is a precisely sized specimen of the material that is used in a uniaxial tension test to obtain material properties. This test is to determine what type of steel material the corrugated siding is composed of. The test will verify the material based on the value of the modulus of elasticity as well as the stress strain relationship it produces. Below is a reference of what a typical steel stress strain curve looks like.

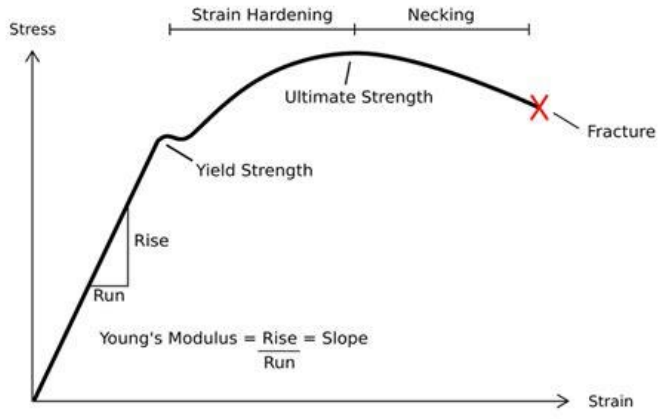

Figure 5 Typical Steel Stress Strain curve (Google)

3.2 Material Preparation

In the United States there are many standards that have been established in relation to how each material should be tested [10]. Using the standards one can compare the results of laboratory tests completed in one lab to that of tests completed in another lab. The set of standards that were used for this material testing program are the American Society for Testing and Materials Standards (ASTM) [10]. Before the test method was selected, clear goals for the test needed to be determined. The objective of this test was to determine the material type, 0.2% offset yield stress, ultimate yield strength, modulus of elasticity, and percent elongation. These results were picked because they specifically correlate to how the material behaves in a uniaxial tension test. This is needed in order to understand what to expect the cargo shipping container to behave like under loading. The standard that details the exact methods to be used to determine the parameters is the ASTM E8/E8M-16a "Standard Test Methods for Tension Testing of Metallic Materials" [11].

According to ASTM E8/E8M-16a, the corrugated steel plate needed to be cut into several small sections that would be used for the laboratory test. The original piece of material was approximately 762 mm X 762 mm (2.5 ft X 2.5 ft). Twelve specimens of steel were obtained from the original piece, all measuring 8 inches in length. Figure 6 is an image of the original piece of corrugates siding obtained from the Tilton Trailer Company. It was determined that the proper specimen type would be a Sheet-Type specimen [11]. A sheet type specimen requires a sample of certain dimensions and the thickness of the material. By following the ASTM E8 standard, Figure 7, each specimen was cut to the specified dimensions show in Figure 8.

Figure 6 Original Piece of Steel Siding 2.5' X 2.5'

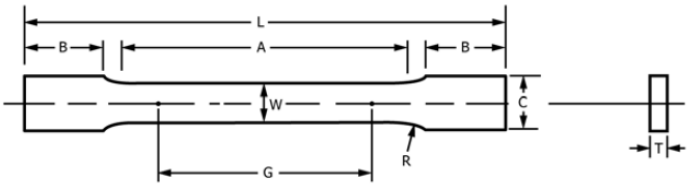

	Dimensions		
	Standard Specimens		Subsize Specimen
	Plate-Type, 40 mm [1.500 in.] Wide	Sheet-Type, 12.5 mm [0.500 in.] Wide	6 mm [0.250 in.] Wide
	mm [in.]	mm [in.]	mm [in.]
G—Gauge length (Note 1 and Note 2)	200.0 ± 0.2 [8.00 ± 0.01]	50.0 ± 0.1 [2.000 ± 0.005]	25.0 ± 0.1 [1.000 ± 0.003]
W—Width (Note 3 and Note 4)	40.0 ± 2.0 [1.500 ± 0.125, -0.250]	12.5 ± 0.2 [0.500 ± 0.010]	6.0 ± 0.1 [0.250 ± 0.005]
T—Thickness (Note 5)		thickness of material	
R—Radius of fillet, min (Note 6)	25 [1]	12.5 [0.500]	6 [0.250]
L—Overall length, min (Note 2, Note 7, and Note 8)	450 [18]	200 [8]	100 [4]
A—Length of reduced parallel section, min	225 [9]	57 [2.25]	32 [1.25]
B—Length of grip section, min (Note 9)	75 [3]	50 [2]	30 [1.25]
C—Width of grip section, approximate (Note 4 and Note 9)	50 [2]	20 [0.750]	10 [0.375]

Figure 7 ASTM E8/E8M-16a Coupon Standard Used

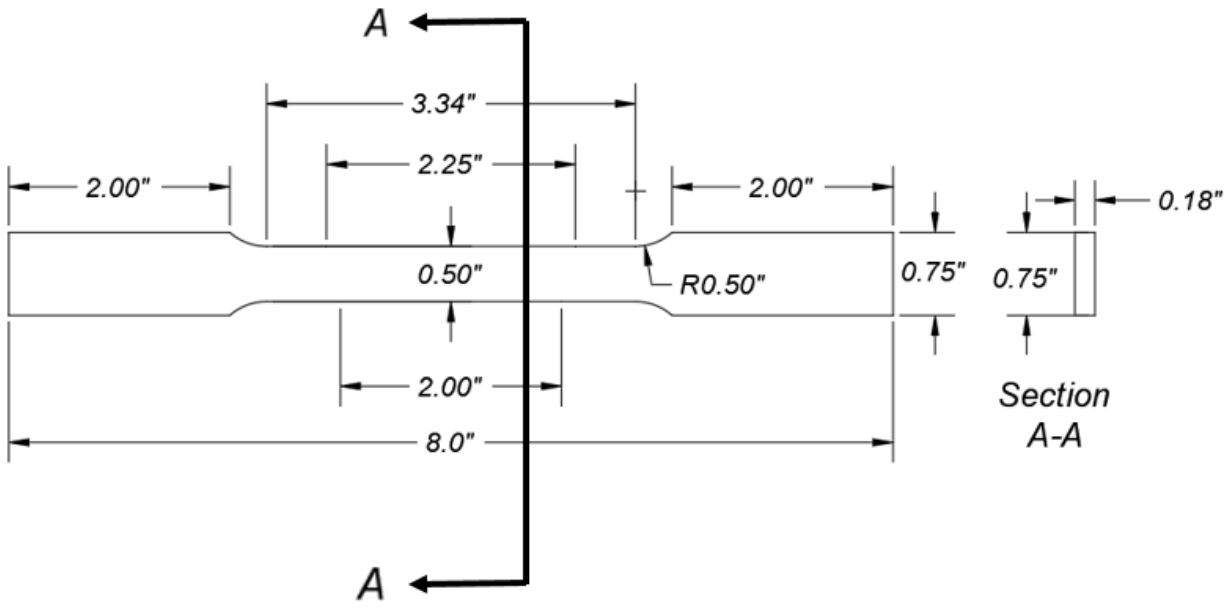

Figure 8 Drawing of Coupon Specimen

Using the dimensions shown in Figure 9 the specimens were cut and prepared for testing. Note that specimen twelve is not shown in Figure 9. This is because the picture was taken as specimen twelve was being tested.

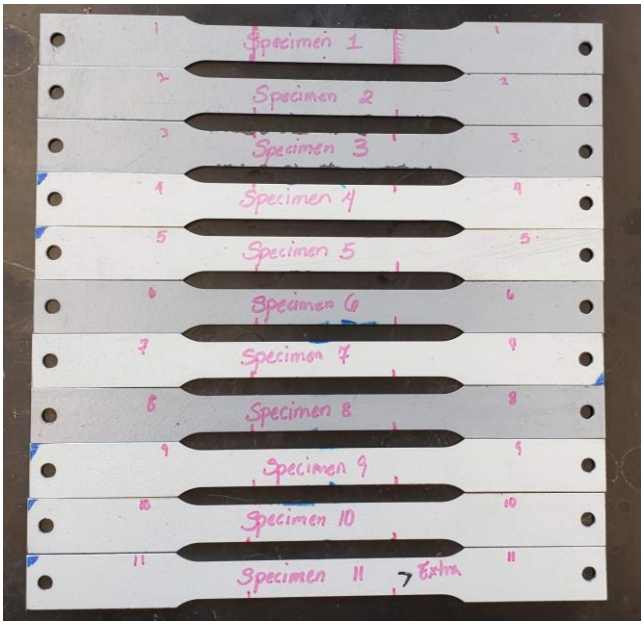

Figure 9 Coupon Specimens

3.3 Test Procedure

1. Label and gather measurements for each specimen.
    - Length (L)
    - Gauge Length (G)
    - Width (W)
    - Thickness (T)
    - Width of Grip Section (C)
    - Length of Grip Section (B)

2. Calculate the cross sectional area of each specimen

a. Take each measurement three times and use the average as the value for the specific measurement to insure accuracy

Coupon Data												
Specimen Number	L	B	W	C	T	G	G	Rate	Elongation Distance	Time of Test	Rounded Time	Time
Units	in	in	in	in	in	in	mm	mm/sec	mm	sec	sec	min
1	8	2.00	0.498	0.750	0.058	2	50.8	0.0508	15	295.3	300	5.0
2	8	2.00	0.499	0.749	0.058	2	50.8	0.0508	25	492.1	500	8.3
3	8	2.00	0.500	0.749	0.059	2	50.8	0.0508	25	492.1	500	8.3
4	8	2.00	0.500	0.749	0.058	2	50.8	0.0508	25	492.1	500	8.3
5	8	2.01	0.510	0.748	0.058	2	50.8	0.0508	25	492.1	500	8.3
6	8	2.01	0.499	0.749	0.058	2	50.8	0.0508	25	492.1	500	8.3
7	8	2.00	0.499	0.750	0.058	2	50.8	0.0508	25	492.1	500	8.3
8	8	2.00	0.500	0.749	0.058	2	50.8	0.0508	25	492.1	500	8.3
9	8	2.00	0.500	0.749	0.058	2	50.8	0.0508	25	492.1	500	8.3
Average	8	2.00	0.501	0.749	0.058	2.0	50.8	0.0508	24	470.3	478	8.0

3. Specify the duration of the test (time span) and elongation distance.
4. Specify loading rate based upon the experience of a professional or professor or specific data known about material. The loading rate was 0.0508 mm/s based upon the gauge length and the experience of Dr. Todd Gross, Professor of Mechanical Engineering at the University of New Hampshire
    a. The loading rate is a function of the gauge length over one thousandths of a second.
5. Place the specimen in the bottom grips of the Instron Model 1350, making sure to align the specimen all the way to the back side of the grip and close the grips.
6. Attach the extensometer to the specimen with a resolution of +/- 5mm
7. Attach the top grips to the specimen making sure to align the specimen all the way to the back side of the grip and close the grips.

8. Zero out the load indicator and the extensometer on the Instron Model 1350
9. Check to make sure values entered into computer match the ones calculated for time span, elongation, and loading rate.
10. Run the test for the total time span specified earlier.
11. Store Data
12. Repeat for all specimens

Specimen twelve was the first specimen tested and it was used to calibrate the Intron Model 1350 machine. Specimen eleven was tested next and the data from both specimens was post processed. The post processed data produced stress-strain data that had a linear range that resembled a heart monitor graph. This can be seen in (). From this it it was obvious that the specimen was slipping back and forth within the grips thus not providing usable data. Based upon this information it was decided that the paint on the coupons would need to be removed in order to enable the grips to properly set. Not wanting to add residual stresses to the specimens by sanding them with a high pressure sander the paint was removed with a chemical solvent. The remaining 10 specimens were placed in a paint remover for an hour and then the surfaces were cleaned.

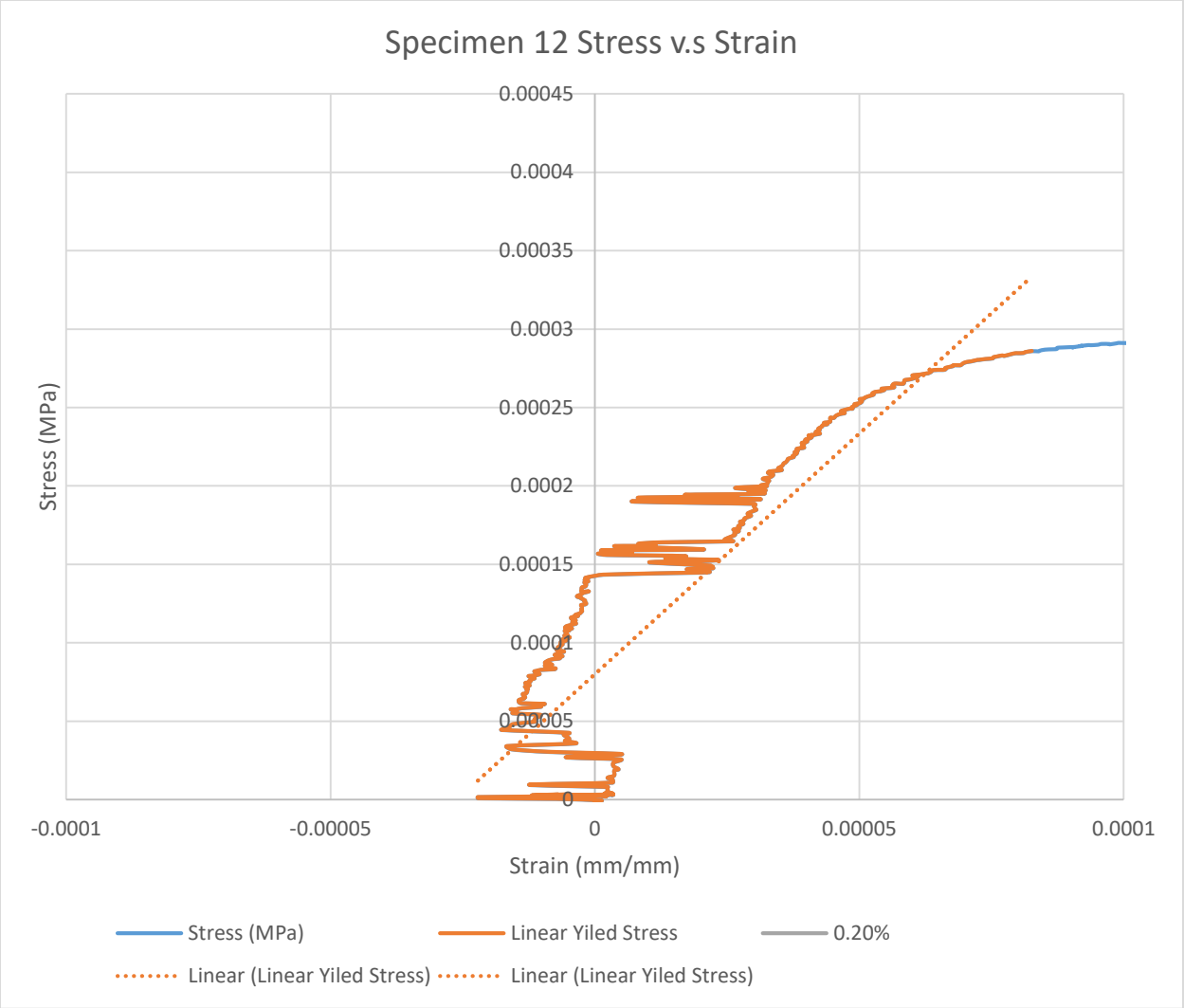

Graph 1 Specimen 12 of Coupon Testing Linear Range

3.3 Results and Conclusion

Once the laboratory testing of the specimens was completed, the data for each specimen was gathered and post processed. During post processing, certain specimens were eliminated based upon errors that occurred during the test. Two major errors that occurred during testing were not properly attaching the extensometer to the specimen and entering the wrong duration value for the test into the computer. The data for five

specimens was used to complete the calculations necessary to identify the desired material properties of the corrugated steel siding.

The data from each specimen was used to create a stress-strain diagram, Graph 2. From the graph a 0.2% offset of the data was determined. The methods used to determine the 0.2% offset are detailed in Appendix B. Then using points on the graphs as well as the cross sectional information for each specimen, the material properties were determined. The Modulus of Elasticity (E) is the slope of the linear portion of the stress-strain curve. In order to find the Modulus of Elasticity, the LINEST function in Excel was utilized on the set of data exhibited in linear format. The LINEST function calculates the statistics of a line which includes the slope of a first order equation. The slope corresponds to the linear portion of the stress strain data which provides the Modulus of Elasticity. The 0.2% offset yield strength was obtained by finding the stress at the point where the offset line crossed the graph of the original data, as shown in Graph 2. Below are the equations used to calculate the ultimate strength and % elongation.

Graph 2 Specimen 6-2 Stress Strain Curve

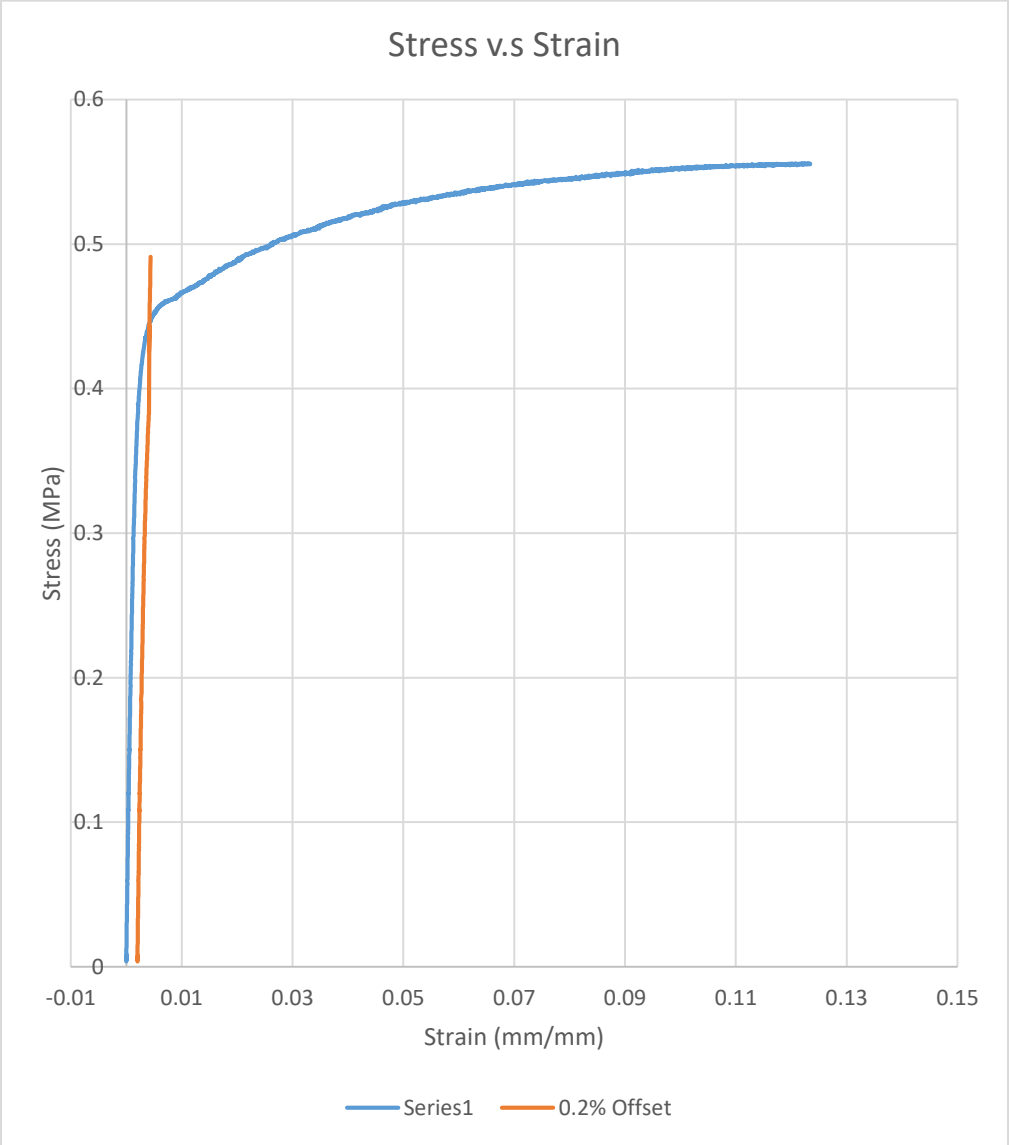

$$Ultimate\ Stength = Maximum\ Stress * 0.145037738 * 1000 = ksi \quad EQ\ 1\ [3.3\text{-}1]$$

$$\%\ Elongation = \frac{Change\ in\ Length}{Extensometer\ Gauge\ Length} \quad EQ\ 2\ [3.3\text{-}2]$$

Once all of the data was post processed, it was reviewed to identify other issues. It can be seen that specimen 2-2 and 4-2 have Modulus' of Elasticities that are much higher than

the rest of the specimens. The ultimate strength of the specimens are within 1.6% difference of each other. It is not clear why specimens sp2-2 and sp4-2 have Modulus' of Elasticities that are much higher than the rest. There are many possible reasons. Based upon the data presented specimens sp6-2, sp7-2, and sp9-2 were used to determine the Modulus of Elasticity, 200GPa, that was used for the computer modeling. This choice was made because those numbers were very close and the data from specimens sp2-2 and sp4-2 provided modulus values that were not realistic for common steel. The information gathered from the testing and the information drawn from the Engineers handbook [12] were used to make the conclusion that the steel in the corrugated siding is G10350 Cold Drawn Steel with a Yield strength of 67 ksi and ultimate strength of 80 ksi.

Table 1 Results of Coupon Testing

Results								
Specimen	Modulus of Elasticity		Ultimate Strength	Ultimate Strength	Yield Stress	Yield Stress	Elongation	% Elongation
	GPa	ksi	ksi	Gpa	ksi	Gpa	in	%
sp2-2	556.61	80,729.44	79.69	549.43	71.76	494.77	0.55	2.16
sp4-2	472.22	68,489.85	79.92	551.02	65.18	449.39	0.55	2.15
sp6-2	204.52	29,662.93	80.82	557.24	64.38	443.88	0.56	2.19
sp7-2	184.36	26,739.79	79.98	551.42	70.16	483.76	0.55	2.16
sp9-2	209.33	30,360.26	79.61	548.91	63.22	435.89	0.55	2.15
Average	199.40	28,920.99	80.00	551.61	66.94	461.54	0.55	2.16

Chapter 4

Mathematical Modeling of Cargo Container Structural Components

4.1 Overview

This chapter reviews the means and methods used to create the mathematical models of typical structural components of a twenty-foot ISO cargo shipping container. A mathematical model is a set of equations that represent the structural behavior of a physical building system. The computer program used to create and analyze the mathematical models was AbaqusCAE (2017). Parameters such as material properties, mesh generation, model assumptions, comparisons, and boundary conditions will be discussed for each structural component modeled. The mathematical models developed and discussed in this chapter will be comprised of typical shell elements. The results from these models will be compared to the simplified mathematical models based upon the simplified rectangular beam and modified box frame model approach presented in Chapter 5.

Each structural component of a typical cargo container will be modeled using shell elements as part of a finite element analysis (FEA). Shell elements are typically used to model thin walled structures in a finite element analysis. The shell elements used in the models are quadrilateral elements. This is an isoparametric quadrilateral element that consists of four corner nodes with two displacement degrees of freedom at each node (u & v). This type of element is called a S4R element in AbaqusCAE. S4R is described as "A

4-noded doubly curved thin or thick shell, reduced integration, hourglass control, finite membrane strains." In this case all of the models are classified as thick shell elements because the height to length ratios are greater than 0.1 and less than 0.6. The degrees of freedoms in the element are characterized by two types of displacement fields. The first is u(x,y) which describes the displacement in the x direction. The second is v(x,y) which describes the displacement in the y direction. Figure 10 shows the element schematic as define by AbaqusCAE. Equations [4.1-1] through [4.1-4] are the shape functions for the S4R element. Figure 11 shows the auxiliary coordinate system used so that the quadrilateral element can be considered non-rectangular. The system is called $\zeta\eta$ and its defines the "natural" coordinate system of the element.

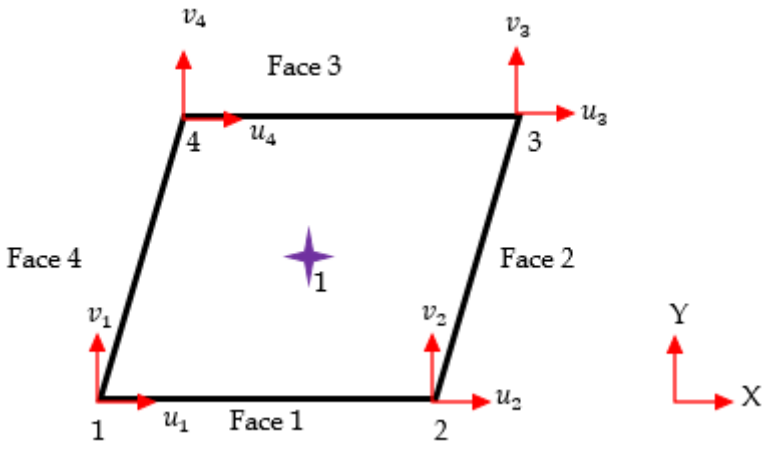

Figure 10 (4-Noded) Reduced Integration Element in Local x-y plane

$$N_1(x,y) = \frac{1}{4}(1-x)(1-y) \qquad EQ\ 3\ [4.1\text{-}1]$$

$$N_2(x,y) = \frac{1}{4}(1+x)(1-y) \qquad EQ\ 4\ [4.1\text{-}2]$$

$$N_3(x,y) = \frac{1}{4}(1+x)(1+y) \qquad EQ\ 5\ [4.1\text{-}3]$$

$$N_4(x,y) = \frac{1}{4}(1-x)(1+y) \qquad EQ\ 6\ [4.1\text{-}4]$$

$u(x)$ ➔ displacement field in the x-direction

$v(x)$ ➔ displacement field in the y-direction

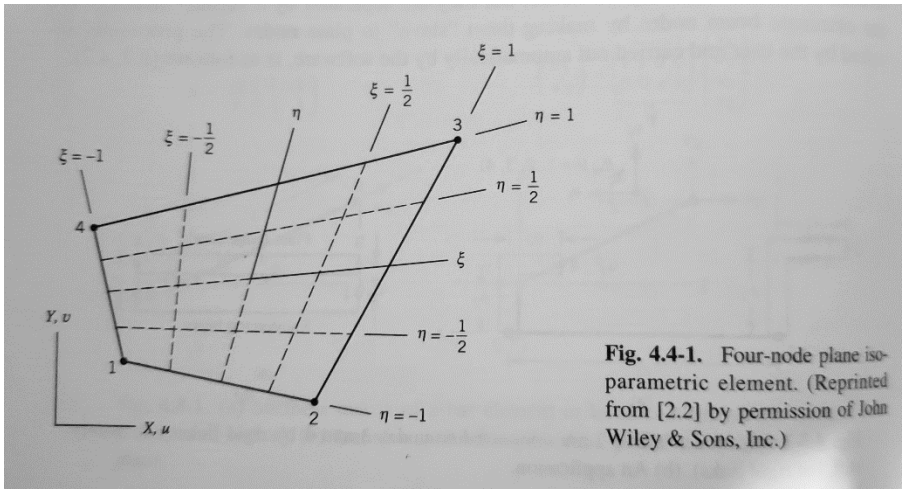

Fig. 4.4-1. Four-node plane isoparametric element. (Reprinted from [2.2] by permission of John Wiley & Sons, Inc.)

Figure 11 Auxiliary Coordinate System

$$\xi = x, \eta = y$$

The corner post was subject to a sensitivity analysis. A sensitivity analysis checks solution convergence of the model question to see how the mesh quality influences the calculation results. All of the other models utilized reasonable aspect ratios. An aspect ratio is the ratio between the longest edge of the element to the shortest edge of the element. In many geometric cases as the aspect ratio increases beyond 2:1 the inaccuracy of the solution also increases. The goal of utilizing appropriate aspect ratios in element meshing of the geometry is to decrease the inaccuracy of the solution. Not every element mesh will meet

this requirement. As a rule, this thesis used the aspect ratios that were not be higher than 2.5. This is based upon the findings by Daryl L Logan, in which he finds that with aspect ratios less than 3.6, the error in the solution accuracy is less than 12% [13].

4.2 Structural Components

4.2.1 Corner Post

The cross section of the corner post is shown Figure 12. The dimensions shown in **Error! Reference source not found.** represent the center line dimensions for the cross section. AbaqusCAE adds one half of the thickness to these dimensions to calculate the cross-sectional properties (i.e. area, moment of inertia, etc.) All of the dimensions shown in **Error! Reference source not found.** are in units of millimeters. The wall thickness of each p art of the cross section is 3.77 mm [14]. The longitudinal (z-axis) length of the corner post corresponds to the height of the cargo shipping container of 2440 mm (8 ft).

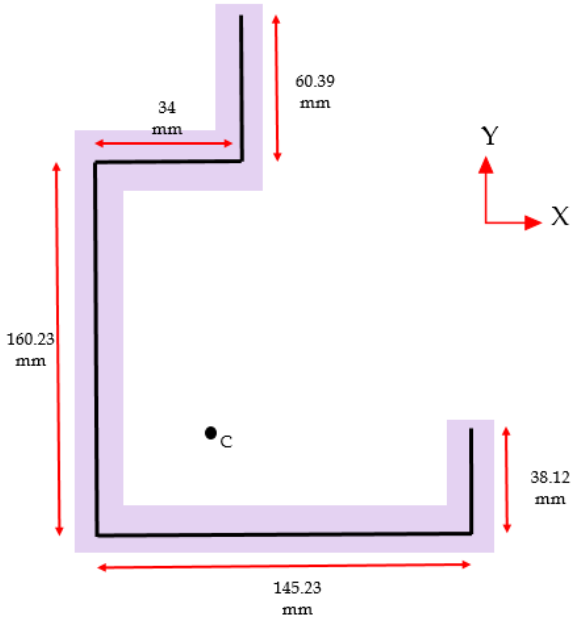

Figure 12 Corner Post Cross Section

From the material coupon testing presented in Chapter 3 all of the structural components of the container were assumed to be composed of cold drawn steel. With a Modulus of Elasticity of 200 GPa (200,000 N/mm^2) approximately 29,000 ksi and a Modulus of Rigidity of 75,000 N/mm^2 (approximately 10,900 ksi). The geometric properties of the corner post cross section are listed below. Ix and Iy stand for the moment of inertias about the x-axis and y-axis respectively, whilst c is the centroid of the cross section. The centroid can be seen in Figure 12.

- Ix = 8,408,010 mm^4 (20.2 in^4)
- Iy = 3,514,895 mm^4 (8.45 in^4)
- C = (42.73, 69.66, 0.0) mm (x,y,z)

Once the geometric properties are assigned to the structural member, a FEA mesh is generated by AbaqusCAE to fit the geometry of the member. The mesh was composed of 10,736 isoparametric quadrilateral shell elements. All the elements within the mesh had an aspect ratio of 1.13 or less, well within the limit of 2.5. The mathematical model was analyzed for a uniaxial an arbitrary vertical load of 10 kN placed at the centroid of the cross section. Loading a structural member at its centroid prevents out of plane bending. It also gives a more reasonable representation of the maximum displacement and stress the member will experience To make this possible within AbaqusCAE a reference point was positioned at the centroid of the cross section at the top of the member. The top edges of the cross section were kinetically coupled to the reference point. The kinetic couple restrains the corner post geometry to move and behave exactly as the point at which it is coupled to. The uniaxial load was applied at the reference point as shown in Figure 13.

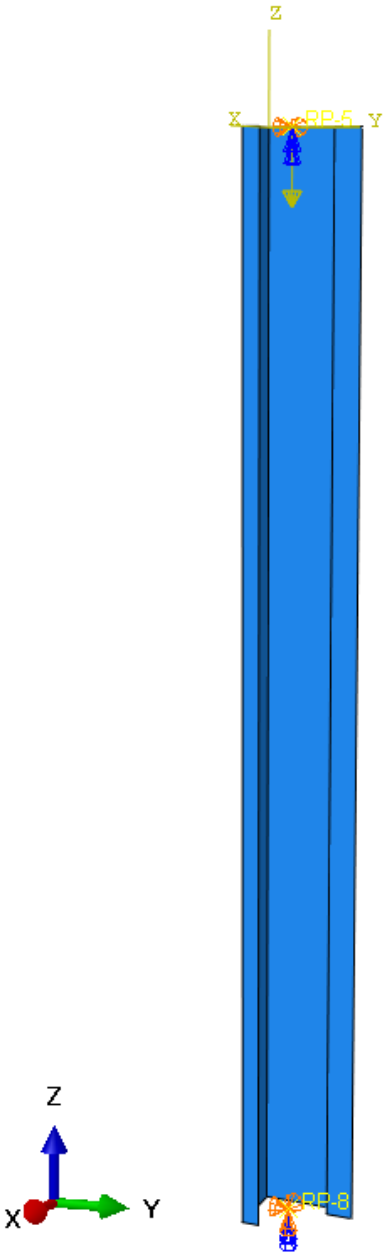

Figure 13 Corner Post With Boundary Conditions and Loading

The boundary conditions were placed at the centroids corresponding to the top and bottom cross sections of the member. The top cross section of the member, where the load was applied, had a vertical roller support that only allowed movement in the direction parallel to the load. Another reference point was set at the centroid of the cross section at the bottom of the member. The edges of the bottom cross section were kinetically coupled to the reference point. A pin support, which restrains the transverse movement, was placed at the bottom of the corner post model. The model was analyzed under a linear elastic condition and the displacement and stresses were obtained.

Figure 14 shows the axial displacement and stress of the member due to a vertical load of 10kN. The top edge of the image corresponds to the top of the member, where the load is applied (vertical roller support point), while the bottom edge corresponds to the bottom (or pinned support point) of the member. Figure 14 shows that most of the member experiences the same stress, except for the points at which the supports and uniaxial load are located. There are localized stress contours at the location of the supports and applied load. This phenomenon is known as Saint Venant's effect and is discussed later at the end of the chapter.

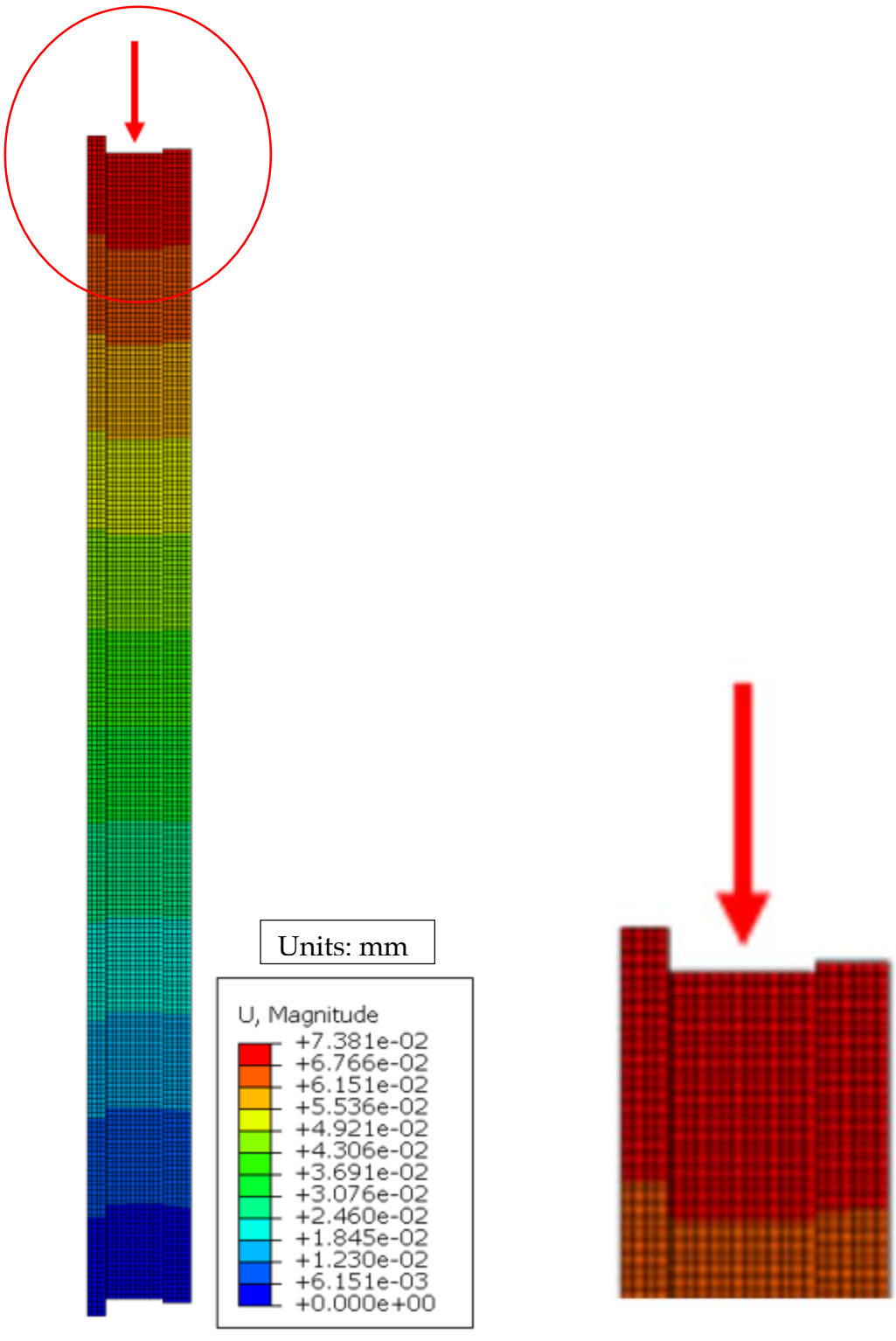

Figure 14 Displacement Contours of Corner Post

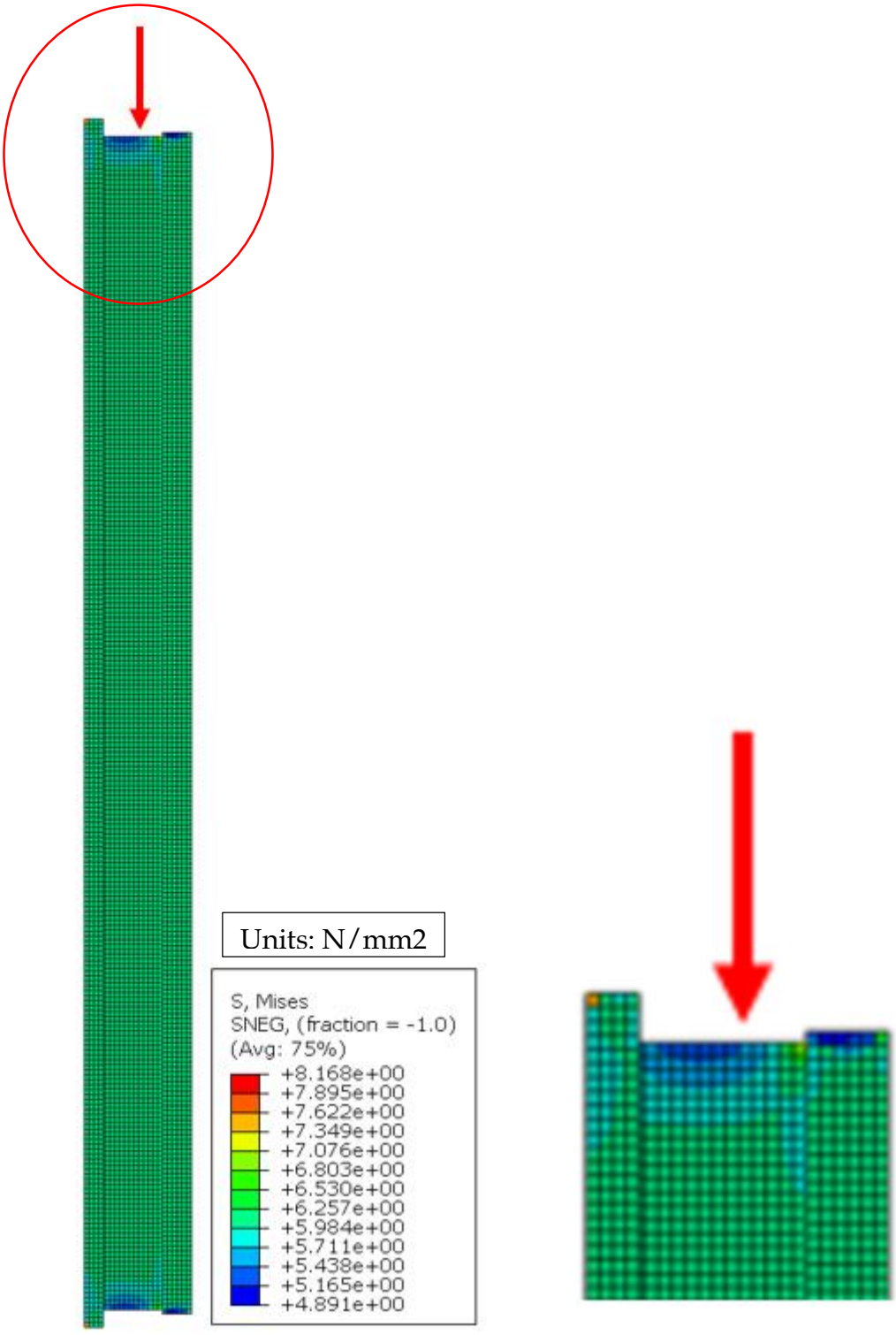

Figure 15 Stress Distribution of Corner Post

The mesh size for the model shown in Figure 14 and Figure 15 is very fine, with an aspect ratio of 1:1.03. This fine mesh is not necessarily useful in terms of data collection and showing the behavior of this mathematical structural system. Therefore, a sensitivity check of the mesh was conducted in order to better understand the fineness of mesh that would be necessary to obtain good results while maintaining a reasonable aspect ratio fineness. Table 2 shows the global mesh size of the mathematical model compared to the results that were obtained. The maximum deflection and average Von Mises stress were compared to hand calculations, shown on page 40, of the predicted stress and displacement.

Table 2 Sensitivity Check on Corner Post Model

Corner Post						
Global Mesh Size	Worst Aspect Ratio	Maximum Deflection	% Difference from Hand Calcs	Von Mises	% Difference from Hand Calcs	Maximum Stress (In-Plane Principal)
unitless	unitless	mm	unitless	N/mm2	unitless	N/mm2
10	1.13	0.07381	0.11%	6.53	8%	0.6334
20	1.18	0.07382	0.09%	6.291	4%	0.7678
30	1.27	0.07382	0.09%	6.093	1%	0.4005
40	1.32	0.07382	0.09%	6.052	0%	0.4439
50	1.46	0.07383	0.08%	6.103	1%	0.3151
60	1.75	0.07384	0.07%	6.095	1%	0.3149
70	2.05	0.07385	0.05%	6.072	0%	0.4427
80	2.31	0.07384	0.07%	6.067	0%	0.4447
90	2.66	0.07384	0.07%	6.07	0%	0.4392
100	2.99	0.07386	0.04%	6.064	0%	0.4151
110	3.26	0.07384	0.07%	6.063	0%	0.3435
120	3.59	0.07384	0.07%	6.089	1%	0.3285
130	3.78	0.07384	0.07%	6.093	1%	0.3198

140	4.22	0.07384	0.07%	6.071	0%	0.2928
150	4.49	0.07383	0.08%	6.075	0%	0.3054
160	4.78	0.07384	0.07%	6.073	0%	0.2627
170	5.13	0.07383	0.08%	6.08	0%	0.2955
180	5.13	0.07383	0.08%	6.08	0%	0.2955
190	5.52	0.07384	0.07%	6.097	1%	0.2373
200	5.98	0.07383	0.08%	6.103	1%	0.2795

The predicted stress and displacement were calculated from simple beam equations. Simple beam equations were utilized because symmetry about the cross section geometry does not affect the outcome. Geometric properties such as cross section area and member length are the factors that affect calculations the most. Equation [4.2.1-1] is the axial stress calculation and equation [4.2.1-2] is the maximum deflection calculation for the member at the top end where the vertical roller support is located.

$$\sigma = \frac{P}{A} = \frac{10{,}000N}{1{,}651.1\ mm^2} = 6.06\ \frac{N}{mm^2} \qquad \textit{EQ 7 [4.2.1-1]}$$

$$\Delta_{max} = \frac{PL}{AE} = \frac{(10{,}000N * 2440mm)}{(1{,}651.1mm^2 * 200{,}000\frac{N}{mm^2})} = 0.07389\ mm \qquad \textit{EQ 8 [4.2.1-2]}$$

Graph 2 shows a clear view of the global mesh size versus the percent difference in stress compared to the hand calculations. As can be seen in Graph 2, for global mesh sizes smaller than 25 there is a significant increase in percent difference. This is due to the size of the element within the mesh. Fine meshes allow the mathematical model to take into account significantly small amounts of out of plane movement. This increases the stress

values possible in the model. Whereas the beam equation for stress does not take into account the out of plane movement of the member. Note that for global mesh sizes greater than 25 the percent difference in stress is below 1%. It is sufficient to say that for global mesh sizes between 25 and 205 the results for the Von Mises stress will be within reason for the corner post model.

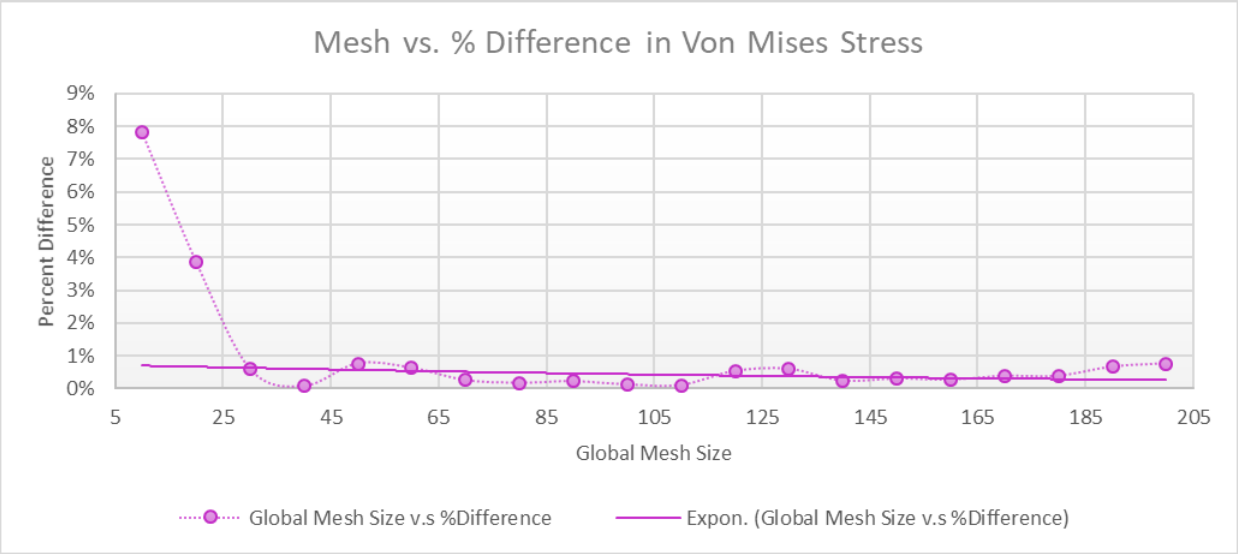

Graph 3 Mesh vs. Error in Von Mises Stress

Graph 3 shows the global mesh size versus the percent difference in the longitudinal displacement determined from the model compared to the hand calculation. The maximum difference between the computer model results and the hand calculations is 0.11% for a global mesh size of 5. The longitudinal displacement determined by the computer model is much less sensitive to the global mesh size than the Von Mises stresses calculated.

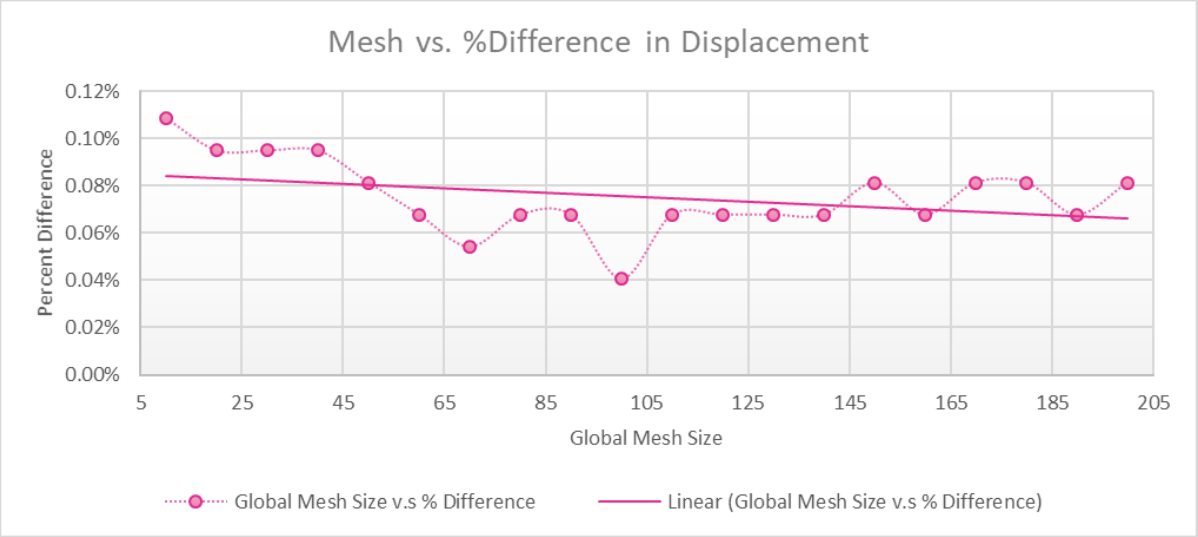

Graph 4 Mesh vs. Error in Displacement

Based on the results shown in Table 2 the optimal global mesh size for the corner post model is 30. This yields about 0.09% error between the hand calculations and the computer model results output.

4.2.1 Corrugated Walls

Figure 16 shows a portion of the cross section of the corrugated walls. The dimensions of the corrugated siding are along the center line of the cross section. AbaqusCAE takes into account the wall thickness as part of the analysis The side wall spans a total length of 6066 mm (19.90 ft.) while the end wall spans 2377 mm (7.80 ft.). The thickness of the corrugated wall is 1.47mm. The height of the walls corresponds to the height of the cargo shipping container of 2440 mm (8 ft.).

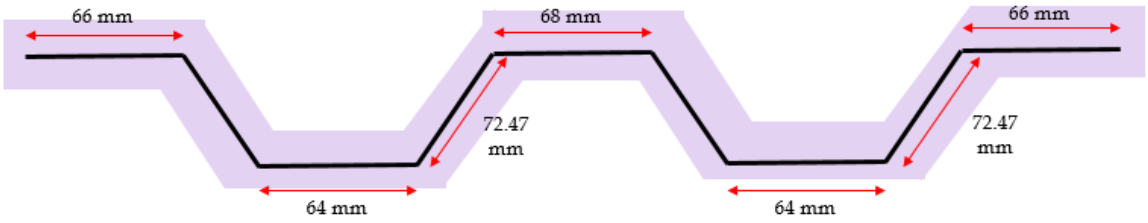

Figure 16 Corrugate Wall Centerline Cross Section

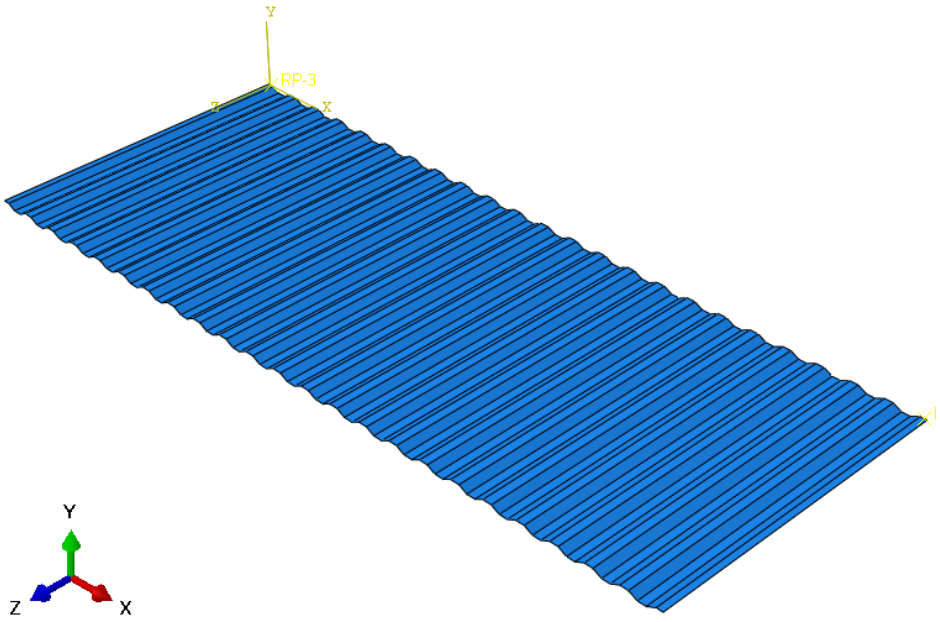

Figure 17 Side Wall 3D View

The mesh utilized created 39,650 isoparametric quadrilateral shell elements for the sidewall and 5,994 isoparametric quadrilateral shell elements for the end wall. All the elements within the sidewall mesh had an aspect ratio 1.18 or less. The elements within the end wall mesh had an aspect ratio of 1.23 or less. Both models are well within the

maximum aspect ratio of 2.5. The mathematical models were analyzed under an arbitrary shell edge load of 0.6803 N/mm, this number is based on a 1 N/mm^2 load over the wall cross sectional area. This load was divided by the wall thickness of 1.47mm to get a distributed edge load of 0.6803 N/mm.

The boundary conditions at both ends were set for the member, this can be seen in Figure 18. The sidings were analyzed as simply supported members. Therefore, reference points were assigned to the two bottom corners of the models. For each model the bottom edge of the first and last panel of corrugation were kinematically coupled to their respective reference points. One reference point (point A) was set with a pin support which restrains the transverse movement in all direct6ions. The other reference point (point B) was set with a roller support that only allowed movement in the x-direction. The computer model was completely restrained in the out of plane direction so that the member could not bend out of plane. A static analysis was performed on the model and the displacement and stresses were obtained.

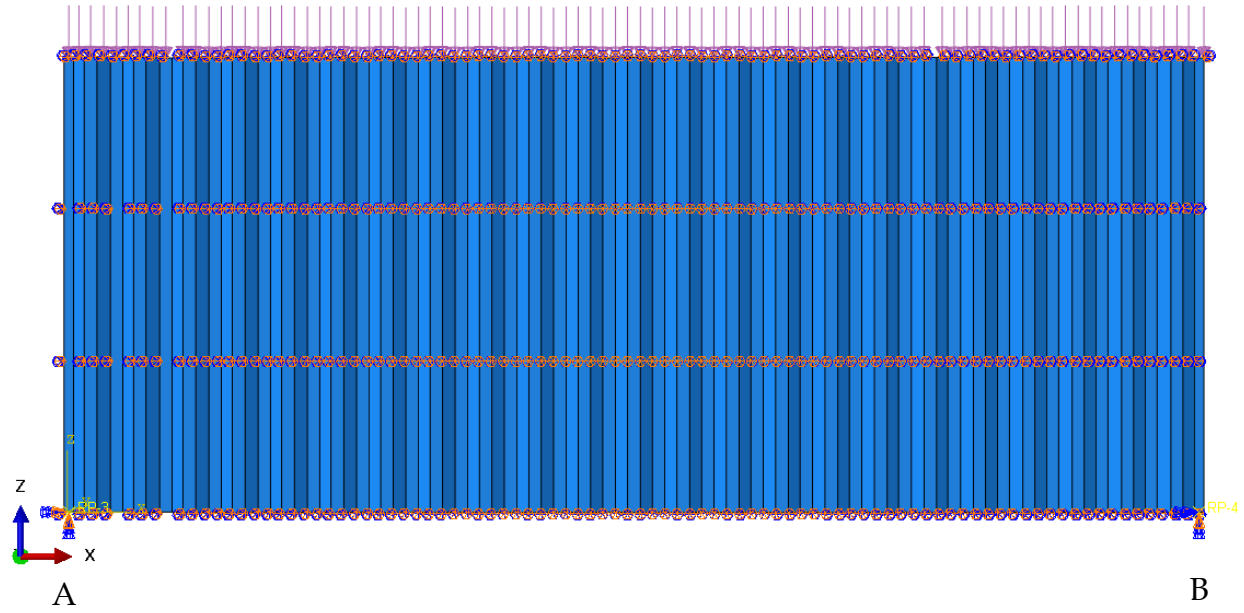

Figure 18 Boundary Conditions and Loading for Sidewall

Figure 19 shows the displacement response of the sidewall model to the shell edge load along the top edge of the siding. The top edge of the image corresponds to the top of the member, where the load is applied, while the bottom edge corresponds to the bottom of the sidewall model, where the supports are located. Figure 19 shows that the maximum displacement is located in the middle (longitudinally) of the corrugated siding. This make sense for a structural component that is simply supported. Figure 21 shows that most of the member experiences the same stress, except for the points at which the supports and vertical load are located. There are localized stress contours at the location of the supports due to Saint Venant's principle.

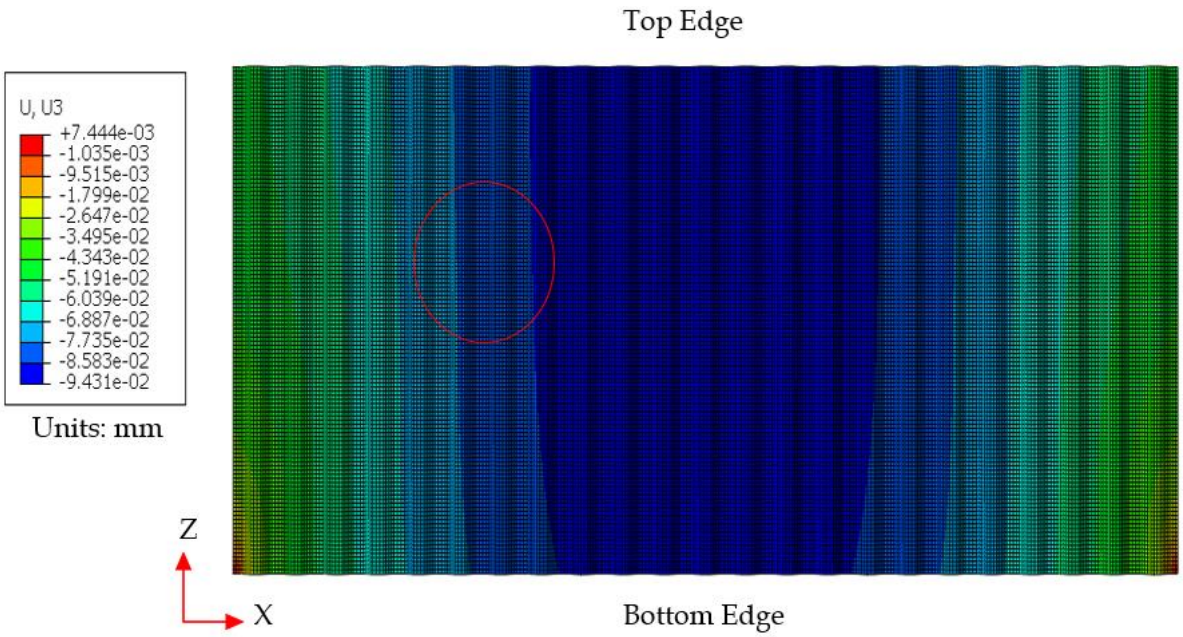

Figure 19 Side Wall Displacement

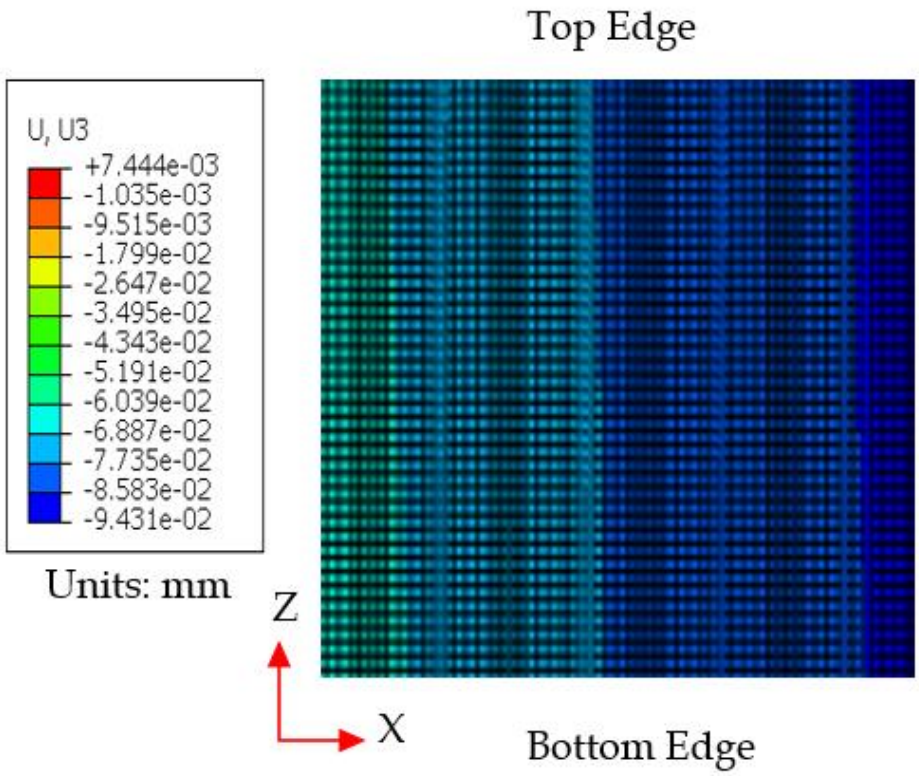

Figure 20 Close Up of Wall Displacement

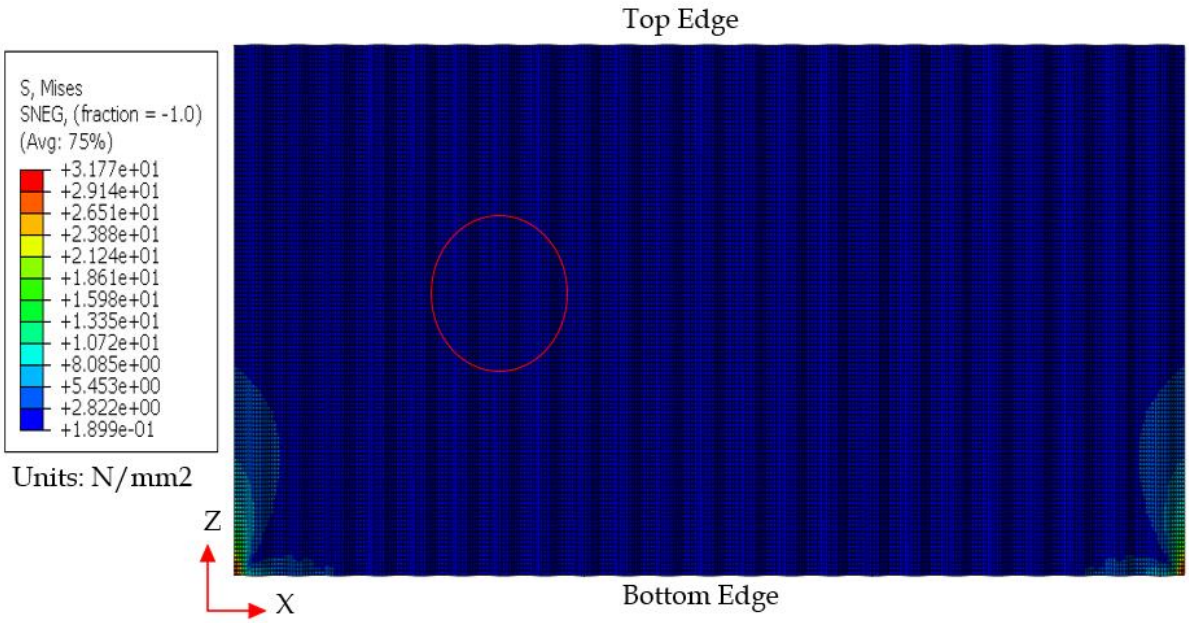

Figure 21 Side Wall Stress Distribution

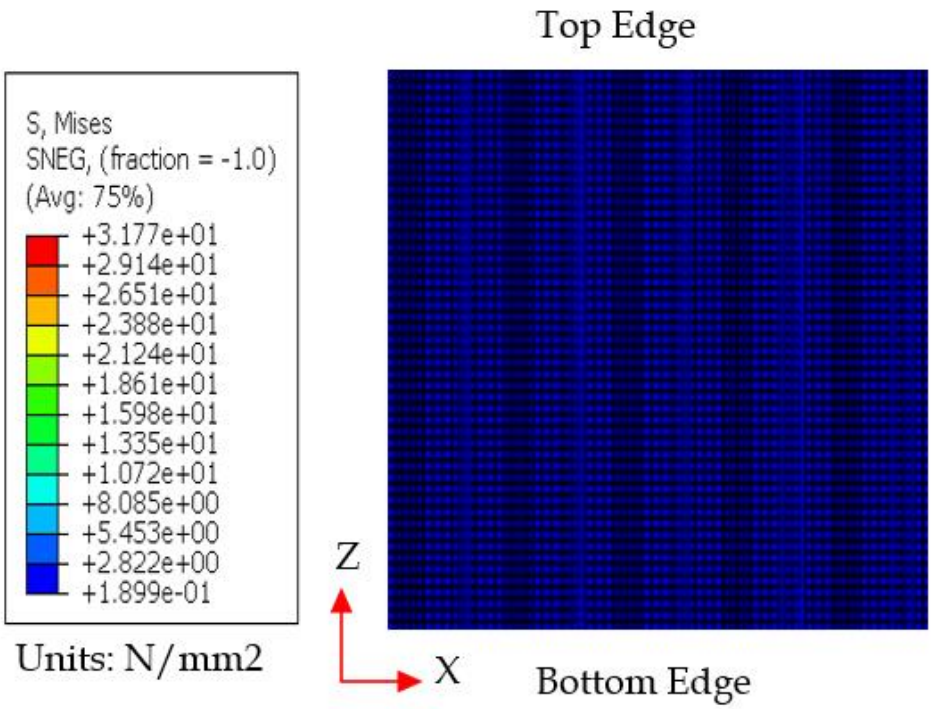

Figure 22 Close Up of Stress Distribution

4.3 Localized Stress Contours

Figure 21 depicts the Von Mises stress distribution within the models. As previously noted each numerical model shows localized high regions of stress near the supports. This is due to stress singularities that occur in the mesh. A stress singularity is a point in a mesh that the stress does not converge, with finer and finer meshes the stress at those points increase infinitely, theoretically. The singularities occur at areas that correspond to point loads and boundary restraints. St. Venant's principle states that the effect of local disturbances to a uniform stress fields remain local [15]. Therefore, these localized stresses can be ignored when the stress at these points are not of interest.

The displacement and stress results developed using finite element models of the corner post and corrugates walls will be used in Chapter 6 to compare to results obtained by the simplified models developed in Chapter 5.

Chapter 5

Simplified Mathematical Model of Cargo Structural Components

5.1 Overview

This chapter reviews the methods used to develop simplified mathematical models of the twenty-foot cargo shipping container structural components discussed in Chapter 4. The purpose of the simplified models is to reduce the complexity associated with modeling the cargo shipping container using shell finite elements. The simplified model needs to have behavior similar to the higher order shell elements FEA mathematical. AbaqusCAE 2017 was used to analyze the simplified models discussed in this chapter. The material properties, model assumptions and boundary conditions for each model are similar to the assumptions used with the FEA shell models analyzed in Chapter 4. The difference between the mathematical models in this chapter and those of Chapter 4 are the element types and mesh generations used.

Each structural component of the cargo shipping container will be modeled using beam elements for the structural analysis. The types of beam elements used in this chapter are called B31 elements in AbaqusCAE. B31 elements are one dimensional beam elements, also known as simple beams. Beam element B31 uses a linear interpolation and has a shear factor of 0.44 in AbaqusCAE. A shear factor is the distant a point of interest can move due to shear divided by the perpendicular distance of the point from an invariant line. A one dimensional beam element can resist in-plane bending, axial force, and

transverse shear force [16]. AbaqusCAE utilizes the Timoshenko beam theory which accounts for shear deformation and rotational bending effects. When the length to depth ratio of a beam is significantly large (L/D > 6) the Timoshenko beam behaves like a typical Euler- Bernoulli beam. The smallest length to depth ratio of one of the horizontal members of the modified box frame model is 9. Therefore, all the modeled beams will behave as Euler-Bernoulli beam elements. A simple beam element has six degrees of freedom identified as u(x), v(x), and θ(x). The displacement field u(x) describes the displacement in the longitudinal x direction. The displacement field v(x) describes the transverse displacement in relation to the longitudinal axis of the beam. The rotational field θ(x) describes the rotational displacement in relation to the longitudinal axis of the beam. Figure 23 shows the element nodal schematic whilst equations [5.1-1] through [5.1-9] show the shape functions.

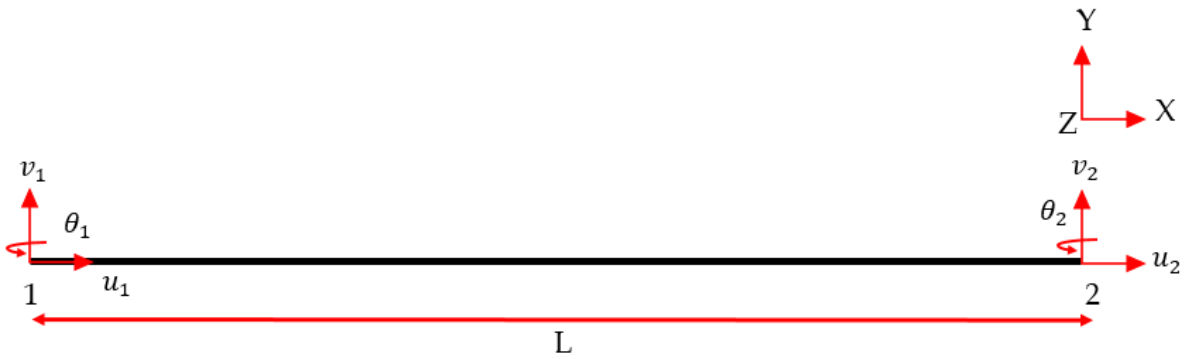

Figure 23 (2-Noded) Simple Beam Element

$$N_1(x) = \left(1 - \frac{x}{L}\right) \qquad EQ\ 9\ [5.1\text{-}1]$$

$$N_2(x) = \frac{x}{L} \qquad \textit{EQ 10 [5.1-2]}$$

$$N_3(x) = \left(1 - \frac{3x^2}{L^2} + \frac{2x^3}{L^3}\right) \quad \textit{EQ 11 [5.1-3]}$$

$$N_4(x) = L\left(x - \frac{2x^2}{L} + \frac{x^3}{L^2}\right) \quad \textit{EQ 12 [5.1-4]}$$

$$N_5(x) = \left(\frac{3x^2}{L^2} + \frac{2x^3}{L^3}\right) \qquad \textit{EQ 13 [5.1-5]}$$

$$N_6(x) = \left(\frac{-x^2}{L} + \frac{x^3}{L^2}\right) \quad \textit{EQ 14 [5.1-6]}$$

$$u(x) = N_1(x)u_1 + N_2(x)u_2 \qquad \textit{EQ 15 [5.1-7]}$$

$$v(x) = N_3(x)v_1 + N_4(x)\theta_2 + N_5(x)v_1 + N_6(x)\theta_2 \quad \textit{EQ 16 [5.1-8]}$$

$$\theta(x) = \frac{dv(x)}{dx} \qquad \textit{EQ 17 [5.1-9]}$$

5.2 Modeling The Structural Components Of The Cargo Container

5.2.1 Corner Post

A simplified beam approach for the corner post is necessary because a generalized prismatic beam member does not output stresses in AbaqusCAE 2017, it only outputs displacement. A comparison of stress and displacement is needed to verify the compatibility of the simplified models to the FEA shell models, therefore a simplified method for the corner post was developed. The method used for the simplified beam approach stems from the fact that the cross sectional area of the post directly affects the stresses and displacements an element will experience. Structural elements bend and move according to whether the load was implemented along the strong or weak axis. It was important to keep the ratio of the moment of inertias about the strong and weak axes for the simplified beam the same as for the beam model with FEA shell elements. A method was developed to convert the corner post cross section into a solid rectangular beam cross section so that both mathematical models (FEA shell and simplified rectangular beam) have the same ratio of inertias and similar cross-sectional areas. AbaqusCAE allows inputs of the cross-sectional dimensions so that the program can solve for stresses within the beam. AbaqusCAE has another type of part called the generalized beam. The generalized beam in the program does not allow input of the cross-sectional dimensions so stresses cannot be calculated using that type of part structure.

To start the method, the moment of inertias about the cross section axes for the corner post were obtained. A rectangular section is utilized because it allows different moment of inertias about the x and y axes, which allows the implementation of the moment of inertia ratio. A beam with the same moment of inertias (I_x & I_y) about the cross sectional axes was calculated. This can be completed using equations [5.2-1] through [5.2.1-6]. The base (b) and height (h) dimensions of the cross section were reduced by a percentage until the cross section area was similar to that of the original corner post. The cross section of the simplified rectangular beam model is shown in Figure 24. The length of the model corresponds to the height of the cargo shipping container of 2440mm (8 ft.). Appendix B shows the calculations for determining the cross sectional properties of the rectangular section.

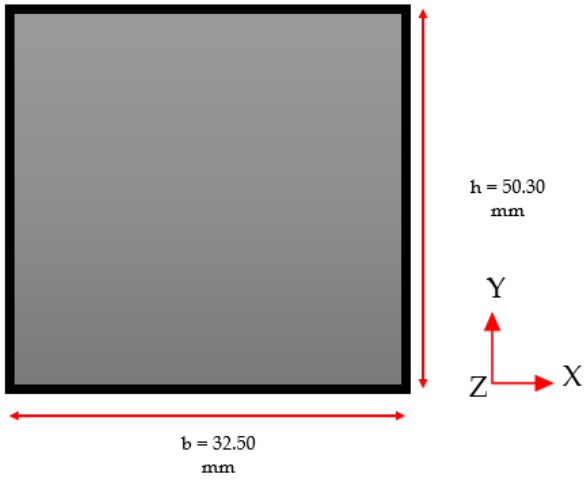

Figure 24 Cross Section of Simplified Corner Post

$$A_x = b * h \qquad \textit{EQ 18 [5.2-1]}$$

$$I_x = \frac{1}{12} bh^3 \qquad \textit{EQ 19 [5.2.1-2]}$$

$$I_y = \frac{1}{12} hb^3 \qquad \textit{EQ 20 [5.2.1-3]}$$

$$Given\ I_x\ ,I_y\ ,and\ A_x$$

$$h = \frac{I_y * 12}{b^3} \qquad \textit{EQ 21 [5.2.1-4]}$$

$$I_x = \frac{1}{12} * b * \left[\frac{I_y * 12}{b^3}\right]^3 \qquad EQ\ 22\ [5.2.1\text{-}5]$$

$$b = \sqrt[8]{\frac{144 * {I_y}^3}{I_x}} \qquad EQ\ 23\ [5.2.1\text{-}6]$$

The rectangular beam model was subjected to a uniaxial vertical load of 10 kN applied at the centroid of the cross section at the top of the member. The top of the member, where the load is applied, has a roller support that only allows movement in the longitudinal direction. A pin support which restrains the transverse movements was placed at the bottom of the rectangular beam model. The end support conditions are shown in Figure 25. A 3D analysis was performed. Stress and displacement results were calculated by AbaqusCAE and compared to the FEA shell model of the corner post that was discussed in Chapter 4. The results of the analyses and comparisons will be presented in Chapter 6.

Figure 25 Rectangular Beam Loading and Boundary Conditions

Table 3 Corner Post Simplification Results

Corner Post Simplification			
	Units	Original Corner Post	Simplified rectangular Beam
A	mm2	1651	1,636
Ix	mm4	8,408,010	344,781
Iy	mm4	3,514,895	144,133
b	mm	72.3	32.5
h	mm	111.8	50.3

5.2.2 Corrugated Siding of Cargo Container

In 1986 Deborah created a simplified box frame method to represent the behavior of concrete cladding related structural system [2]. Her simplified model was able to predict the structural behavior within 10% of the FEA model. Her thesis determined the sizes of the box frame members by using an area based method. Calvin related the surface area of the concrete cladding to the cross sectional areas of the horizontal and vertical frame members.

This method did not work for developing a model of the corrugated siding of the cargo shipping container. The approach Calvin used produced a model that was not as stiff as the FEA shell model of the corrugated siding. This could be due to the fact that the geometry of siding of the cargo shipping container is three dimensional while the concrete cladding is planar. Therefore, a different method for developing the cross sectional properties of the beam members in the box frame would be needed. The following describe the method that was developed.

The method used to develop the box frame model for the corrugated siding differs from the method used by Calvin to model flat concrete panels. The method used in this thesis is named the modified box frame model (MBFM). The modified box frame model consists of four boxes tied together, each box consists of two horizontal beam members and two vertical beam members that are rigidly connected to each other. Figure 26 shows the

assembly of one box in the MBFM. Both horizontal members have the same cross sectional properties and both vertical members have the same cross sectional properties. The MBFM uses a volumetric approach as the basis for developing the model of the corrugated sidings. Volume is directly proportional to stiffness, equations [5.2.2-1] through [5.2.2-3] shows how the volume was used to relate to the stiffness of the model. If the MBFM could predict the same displacements as the FEA shell model of the corrugated siding, then the stiffness of the modified box frame model would be equivalent to the FEA model for the siding.

$$k = \frac{F}{\delta} \qquad EQ\ 24\ [5.2.2\text{-}1]$$

$$F = ma = Volume * Density * Acceleration = \forall * \rho * a \qquad EQ\ 25\ [5.2.2\text{-}2]$$

$$k = \frac{\forall \rho a}{\delta} \qquad EQ\ 26\ [5.2.2\text{-}3]$$

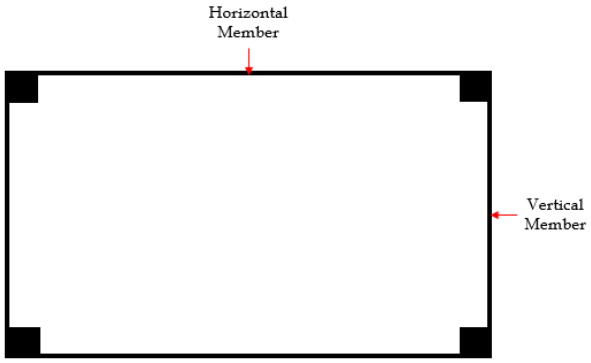

Figure 26 Members Used In Modified Box Frame Model

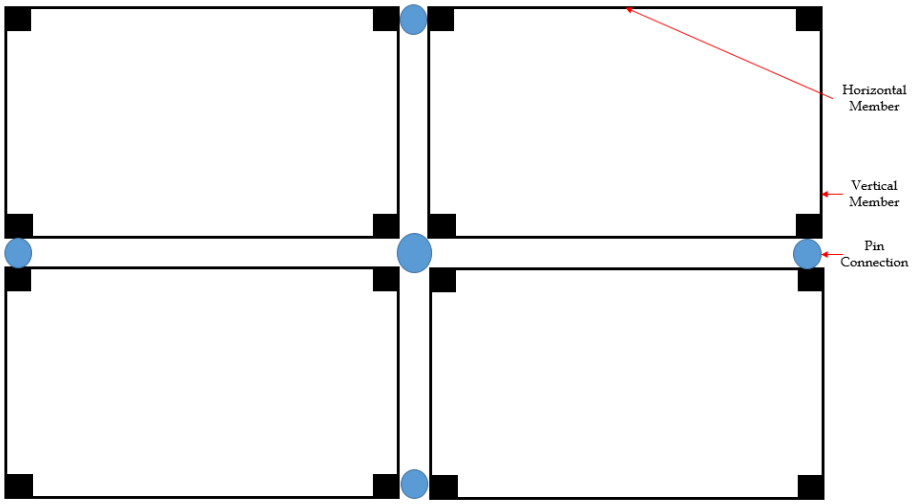

Figure 27 Calvin 1986 Box Frame Model

Each box in the modified box frame method theoretically holds a fourth of the volume of the entire siding. The cross sectional properties of the members within each box were calculated using 25%of the total volume of the siding. The length of the horizontal members is equal to half the total length of the siding and the length of the vertical members is equal to half the height of the siding. A square cross section means that only one dimension (b) of the cross section needs to be calculated, adding to the simplicity. Assuming a square cross section for both the vertical and horizontal beam elements, the base dimension of the cross sectional area can be found by dividing one fourth of the total volume by the length of the presumed member then multiplying it by a cross section modification factor (n).

The cross section modification factor (n) was derived from the relationship of the volume of a corrugated siding with respect to the volume of the sidewall of a twenty-foot cargo

shipping container. Iterative models were run in order to develop the cross section modification factor (n) that would be needed in each beam element to retain the same stiffness as the FEA shell model. The cross section modification factor (n) is equal to the square of the ratio of volumes (Vf) divided by the member sizing factor (Si). Where the member sizing factor (Si) correlates to the numerical scale used in the cross section sizing of the MBFM to account for the necessary member stiffness that relates to the stiffness shown by the FEA shell model of the corrugated side wall. For the corrugated side wall it was found that the member sizing factor is 3.1. This was obtained by running numerous models to check for the overall stiffness in relation to the stiffness of the corrugated siding of the side wall. Equations [5.2.2-4] through [5.2.2 − 9] show what was described above. Hand calculations for MBFM's corresponding to the sidewall and end wall corrugation can be found in Appendix B.

$$b = \sqrt{\frac{0.25 * V_s}{L_{Member}}} * n \qquad EQ\ 27\ [5.2.2\text{-}4]$$

$$for\ V_s \neq V_i$$

$$n = \frac{{V_f}^2}{S_i} \qquad EQ\ 28\ [5.2.2\text{-}5]$$

$$V_f = \frac{V_i}{V_s} \qquad EQ\ 29\ [5.2.2 - 6]$$

$$for\ V_s = V_i$$

$$n = 3.1 \qquad EQ\ 30\ [5.2.2\text{-}7]$$

$$for\ Volume\ Opening$$

$$for\ V_o \leq 0.25 V_i \rightarrow n = V_f * S_i \qquad EQ\ 31\ [5.2.2 - 8]$$

$$for\ V_0 \leq 0.25V_i \rightarrow V_f = \frac{V_s}{V_i} \qquad EQ\ 32\ [5.2.2-9]$$

$S_i = Member\ sizing\ factor$= 3.1

$V_s = Volume\ of\ corrugated\ siding$

$V_o = Volume\ of\ opening$ in corrugated siding

$b = Thickness\ of\ cross\ sectional\ area$

$n = Cross\ section\ modification\ factor$

$L_{member} = Length\ of\ respective\ member$

$V_i = Volume\ of\ 20ft\ container\ sidewall$ = 23,143,076 mm^3

$V_f = Volume\ \ factor\ of\ siding\ to\ 20ft\ container\ sidewall$

Figure 28 shows a schematic of the connections of the modified box frame model. The blue circles correspond to circumferential ties in AbaqusCAE 2017. The ties connect the two members of interest so that they move in unison. The tie constraint allows two different surfaces to move together translationally and rotationally. A tie also allows equal movement in the active degrees of freedom. Each box corresponds to a box in the modified box frame system which consists of four boxes. Each small rectangle denotes the ninety-degree rigid connection. The variables L and H refer to the length and heights, respectively, of the corrugated siding being modeled.

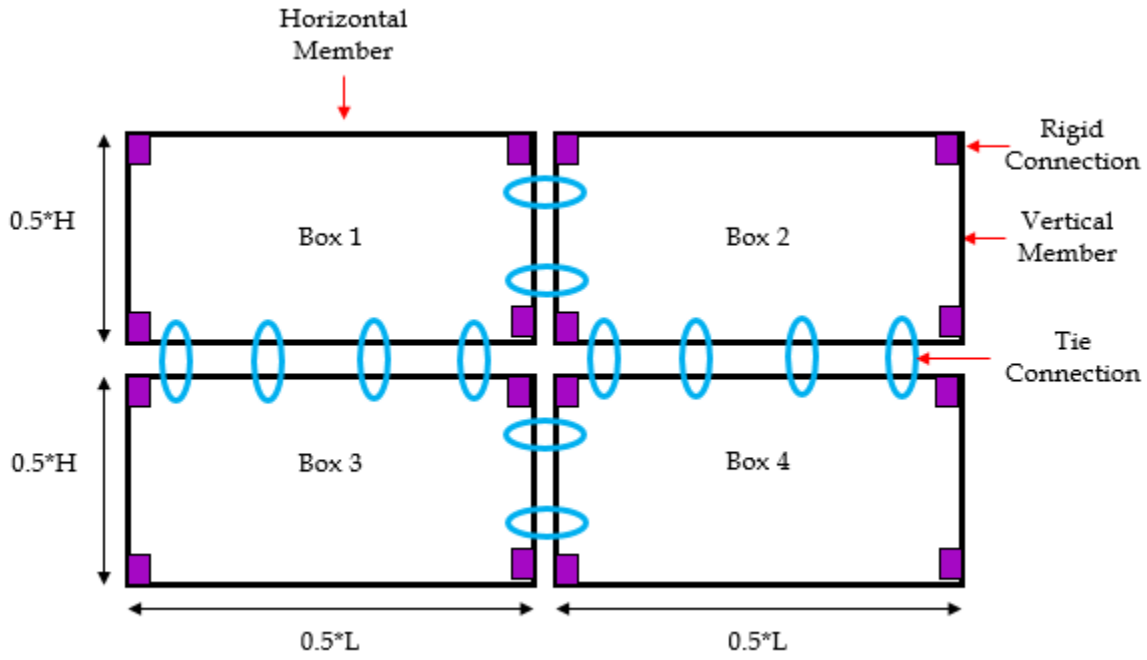

Figure 28 Schematic of the Modified Box Frame Model

Figure 31 shows a schematic of the vertical loading scenario necessary for the box frame to displace like that of the corrugated siding. When an edge load is applied to the top of the corrugated siding the loading disperses through the whole siding. The modified box frame model behaves like a beam/truss system. When the load is applied to only the top of the modified box frame model, the top two beams displace and the load travels to the vertical beams and down to the supports. This means there is little to no interaction of the middle section of the modified box frame model. It is important to distribute the load in a manner that mimics the load path the corrugated siding experiences. The vertical loading scenario used is based upon the tributary areas associate with the horizontal

members in the modified box frame. Figure 29 shows the tributary areas corresponding to the beams in the MBFM for a vertically applied load. The variable, w, in Figure 31 utilizes that represents the uniformly distributed edge load applied to the top of the corrugated siding. Each new uniform load corresponds to the percent of the entire tributary area distributed to that specific area. Figure 30 and Figure 32 show the tributary widths and loading scenario corresponding to a lateral load applied, to the modified box frame model. The lateral loading applies the same principles as the vertical loading does in terms of application to the modified box frame model.

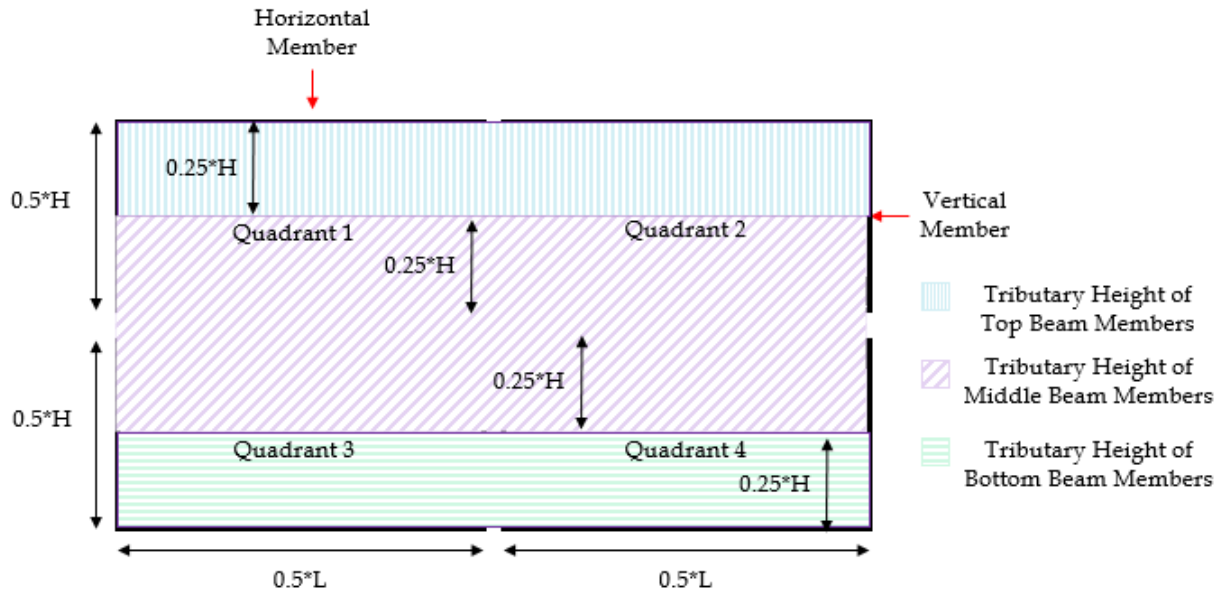

Figure 29 Tributary Height Distribution for MBFM

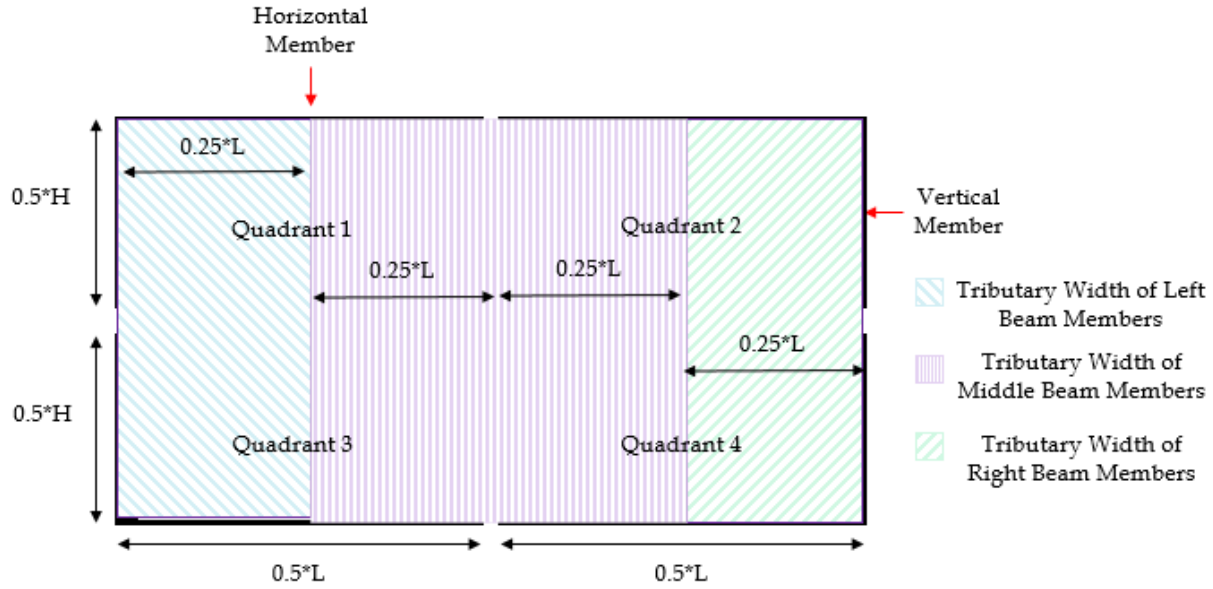

Figure 30 Tributary Width Distribution for MBFM

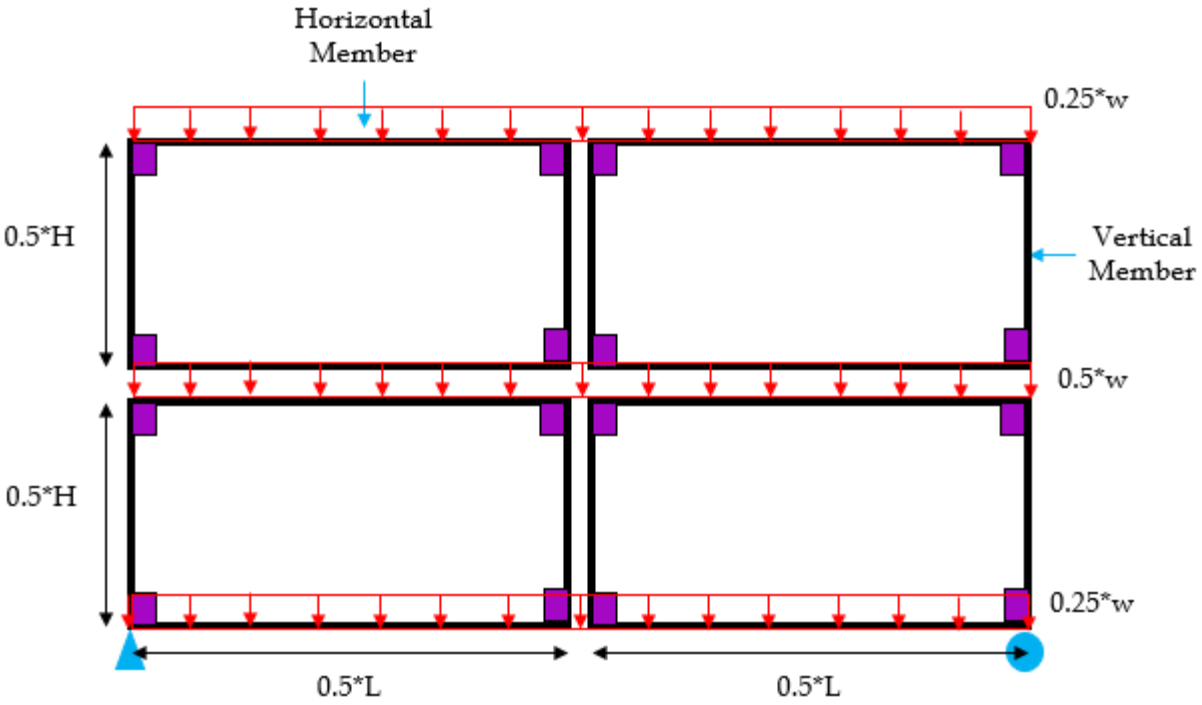

Figure 31 Modified Box Frame Vertical Loading

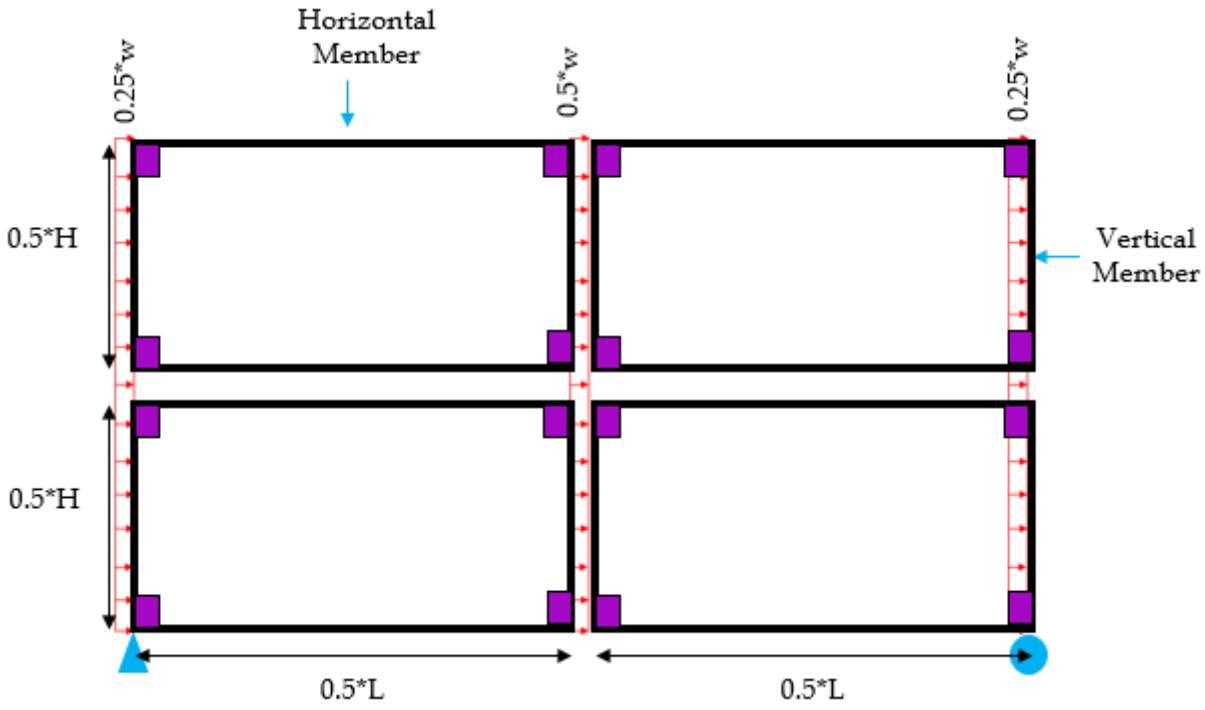

Figure 32 Modified Box Frame Lateral Loading

Findings for the structural behavior of the modified box frame model subject to lateral loading compared to the FEA shell model in Chapter 6. After analyzing different modified box frame models the maximum displacement of the modified box frame method under a vertical load is within 10% difference to the maximum displacement of the FEA models of the corrugated sidings.

The stress results are a bit different. There are two different types of stress data relationships to consider. The first is the relationships of the Von Mises stress distributions for both models. The Von Mises stress distributions represents the critical values of energy stored in a ductile isotropic material. This means that he Von Mises distribution correlates to the yielding and plasticization of the system. In terms of the Von

Mises relationship it was found that the modified box frame model has the relationship specified in equations 5.3-4 and 5.3-5 to the corrugated siding.

The second type of stress relationship is the principal stress. The principal stress distribution corresponds to the stress in relation to the nature of the applied loading in each model. The in-plane principal stress of the modified box frame model has almost a one to one relationship with in plane principal stress of the FEA shell model of the corrugated siding.

$$\sigma_{VC} = \left(0.5 - \left[1 - \frac{V_f}{S_i}\right]\right) * \sigma_{VMB} \qquad \textit{EQ 33 [5.3-4]}$$

$$\Delta_C = \Delta_{MB} \qquad \textit{EQ 34 [5.3-5]}$$

$$\sigma_{PC} = \sigma_{PMB} \qquad \textit{EQ 35 [5.3-6]}$$

$S_i = Member\ sizing\ factor$
$\sigma_{VC} = Von\ Mises\ stress\ of\ corrugated\ siding$
$\Delta_C = Maximum\ deflection\ of\ corrugated\ siding$
$\sigma_{VMB} = Von\ Mises\ stress\ of\ modified\ box\ frame$
$\Delta_{MB} = Maximum\ deflection\ of\ modified\ box\ frame$
$\sigma_{PC} = In\ plane\ principal\ stress\ of\ corrugated\ siding$
$\sigma_{PMB} = In\ plane\ pricipal\ stress\ of\ modified\ box\ frame$
$V_f = Volume\ \ factor\ of\ siding\ to\ 20ft\ container\ sidewall$

In Chapter 6 the results of comparing the modified box frame model and the FEA shell model of the corrugate siding will be discussed.

Chapter 6

Result Comparison of Mathematical Models

6.1 Overview

This chapter compares the results of the FEA shell mathematical models discussed in Chapter 4 and the simplified siding model discussed in Chapter 5. This chapter will examine the accuracy with which the simplified mathematical models predict the stress and displacement in relation to the original mathematical models. The simplified models utilized beam elements whilst the FEA shell models utilized FEA shell elements. The simplified models require a cross section input that allows AbaqusCAE to calculate stresses along the beam. The loading schemes for these models are described in Chapters 4 and 5.

To compare the different types of models, percent difference equations [6.1-1] through [6.1-3] will be utilized. Equation [6.1-1] describes the percent difference the simplified rectangular beam has in relation to the FEA shell model of the corner post. Equation [6.1-2] will be used when comparing the two models. Equation [6.1-2] describes the percent difference the modified box frame method has in relation to the FEA shell model of the corrugated sidings. Equation [6.1-2] will be used when comparing the two models. Equation [6.1-3] describes the percent difference of the assembled siding of the cargo container using the simplified beam method in relation to the assembled siding of the

cargo container using the FEA shell models. Equation [6.1-3] will be used to compare the different models

$$\%Diff = \frac{FEA\ Shell\ Model - Rectangular\ Beam\ Model}{FEA\ Shell\ Model} \quad EQ\ 36\ [6.1\text{-}1]$$

$$\%Diff = \frac{FEA\ Shell\ Model - Modified\ Box\ Frame\ Model}{FEA\ Shell\ Model} \quad EQ\ 37\ [6.1\text{-}2]$$

$$\%Diff = \frac{FEA\ Shell\ Model - Simplified\ Beam\ Model}{FEA\ Shell\ Model} \quad EQ\ 38\ [6.1\text{-}3]$$

There are three different types of stress relationships that AbaqusCAE will calculate, Tresca stresses, Principal stresses, and Von Mises stresses. Tresca stress distributions represent the critical value of maximum shear stress in an isotropic material [17]. This stress distribution stems from the assumption that yielding starts when the maximum shear stress in the material equals the maximum shear stress at yielding in a simple tension test. Principal stress shows the maximum amount of normal stress a material can have at a certain point.

The Von Mises principal was initially proposed by Maksymilian Hurber in 1904 and developed further by Richard Von Mises in 1913 [18]. Von Mises stresses represent the critical values of distortional energy stored in an isotropic material [17]. The stress distribution stems from the assumption that yielding starts when the maximum distortion/strain energy in the material equals the maximum distortion/ strain energy at

yielding in a simple tension test, such as a coupon test [17]. Steel shows plastic deformation and yielding before failure as shown in Figure 5 in Chapter 3.

Von Mises stress accounts for six stress components in a 3D stress states. This includes stress parallel to loading, stress perpendicular to loading, and shear stress. Von Mises stress can be looked at as a measurement to determine whether a structure has started to yield at any point [17]. One of the assumptions in the mathematical models of the structural container components is linear elastic behavior. "Von Mises stress is commonly used to present results because the structural safety for many engineering materials show elasto-plastic properties (for example, steel or aluminum alloy) can be evaluated using Von Mises stress." [19]. Therefore, Von Mises stresses distribution will be used to compare the results of the mathematical models.

6.2 Vertical Load Comparison

6.2.1 Corner Post

Table 5 shows the comparison of two mathematical models and hand calculations. As can be seen in Table 5 the mathematical model of the corner post has a 0% percent error in displacement and stress distribution when compared to hand calculations. In terms of the simplified beam model the percent error in relation to hand calculations and the corner post model is about 1%. With this error lower than 5% it is safe to say the simplified beam model which

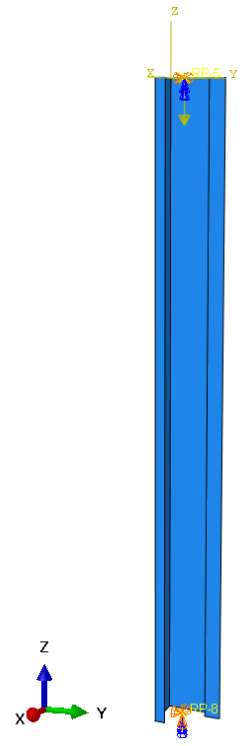

Figure 33 Corner Post With Boundary Conditions and Loading

represents the corner post as a rectangular cross section predicts the behavior of the corner post accurately.

Table 4 Corner Post Simplification

Corner Post Simplification			
Item	Units	Calculated Dimensions	Reduction Factor
			0.55
b	mm	72	33
h	mm	112	50
Area	mm^2	8,077	1,636

Table 5 Comparison of Corner Post Models

Comparison Table of Corner Post Simplification (Axial Compression Load of 10kN)										
Model	Area	Over all Stress	Description	Overall Displacement	Description	Stiffness	Predicted Displacement	%Difference in Displacement	Predicted Stress	%Difference in Stress
	mm^2	N/mm^2		mm		N/mm	mm		N/mm^2	
Beam Element	1635.6	6.113	Same Throughout Element	0.0746	Changes throughout element	134,048.26	0.0739	0.96%	6.06	0.9%
Corner Post (Shell Element)	1651.1	6.060	Based on Stress Graph	0.0738	Changes throughout element	135,462.81	0.0739	0.09%	6.06	0.1%

The corner post section of the cargo shipping container acts like an eight-foot long column braced every 32 inches within the assembly. Using the material properties calculated in Chapter 3, a nominal compressive strength can be calculated using the AISC 14th Edition Steel Manual. Noting that simplified beam model produces a viable behavior for the corner post, its cross section will be used to compute the compressive strength. Chapter E of the AISC 14th Edition Manual denotes the checks needed to calculate the compressive strength of a member. Due to its symmetry the simplified beam does not consist of any slender elements, section E3 of the steel manual governs. The rectangular beam will be checked for the limit state of flexural bucking. The material properties are assumed to be

equal to those found in Chapter 3 through the coupon tests. The yield strength and ultimate strength of the member will be assumed to be 67 ksi and 80 ksi respectively. The nominal compressive strength for the corner post is found to be 126.2 kips. Appendix B shows the calculation for the compressive strength of the corner post.

6.2.2 Corrugated Walls

The results from the modified box frame models detailed in Chapter 5 were compared to the results from the FEA shell models detailed in Chapters 4. It is important to compare similar areas of interest when looking at the similarities and differences between the modified box frame models and the FEA Shell. Table 6 compares stresses and displacements at different areas of interest for the side wall in both models. The legend details what each abbreviation stands for in the table. Stress 90% means that 90% of the model is showing stresses at the specified value whilst the other 10% is showing stresses at a different specified value.

Table 6 Vertical Load Comparison Table

Corrugated Walls Subject to Compression Distributed Load of 0.6803 N/mm							
Model	**Stress 90%**	**Stress 10%**	**Max Stress**	**Max Disp.**	**Stress At Bottom Middle**	**Displacement at 1/4 H Distance**	**Displacement At Bottom Middle**
Units	**N/mm2**	**N/mm2**	**N/mm2**	**mm**	**N/mm2**	**mm**	**mm**
CSWS	0.1899	2.8220	31.1770	0.1095	0.1899	0.0913	0.1095
BFSS	0.3642	1.0930	1.0930	0.1130	0.3642	0.0464	0.1113
% Difference	91.79	61.27	96.49	**3.20**	91.79	49.22	**1.64**
CEWS	0.0163	1.0010	11.8300	0.0242	0.0163	0.0222	0.0242
BFES	0.0552	0.0002	0.6606	0.0247	0.5505	0.0165	0.0247
% Difference	239.27	99.98	94.42	**2.27**	3283.53	25.75	**2.27**

Legend:

- CSWS: FEA shell model of corrugated side wall that is simply supported.
- BFSS: Box frame side wall that is simply supported.
- CEWS: FEA shell model of corrugated end wall that is simply supported.
- BFES: Box frame end wall that is simply supported.

Table 6 shows that the maximum displacements in the modified box frame models are within a 5% difference range of those produced by the FEA shell models. However, the stresses at the areas of interest are completely different when comparing the modified box frame models to the FEA shell models. Both types of models produce similar outputs in terms of displacement, therefore there must be a relationship between the two models in terms of stress calculations. This relationship is shown by equations [5.3-4] and [5.3-6] in Chapter 5.

Figure 34 shows the displacement contours of the FEA shell model of the corrugated side wall. The bottom left hand side of the model has a pinned support whist the bottom right hand side has a roller support. The model is restrained from out of plane movement. As can be seen in the displacement contours, the load is applied to the siding and the FEA shells compress and expand continually in the x direction. Figure 35 shows the displacement due to the distributed vertical load, it also shows that the maximum displacement occurs in the middle of the FEA shell model. Figure 36 shows the displacement contours for the modified box frame model. The maximum displacement in the modified box frame model is within a 2% difference of the FEA shell model of the corrugated siding. Figure 34 through Figure 36 show the results for the models of the side wall of the cargo shipping container. Images corresponding to the end wall of the cargo shipping container can be found in Appendix A. Note that the displacements are shown in units of millimeters.

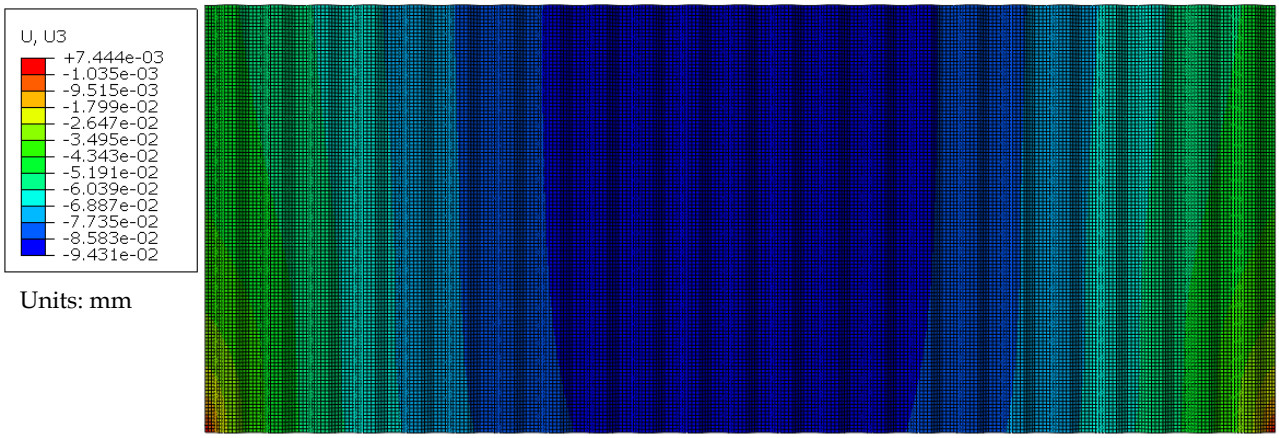

Figure 34 In-Plane Displacement of FEA Shell Model of Corrugated Side Wall Subject to Vertical Loading

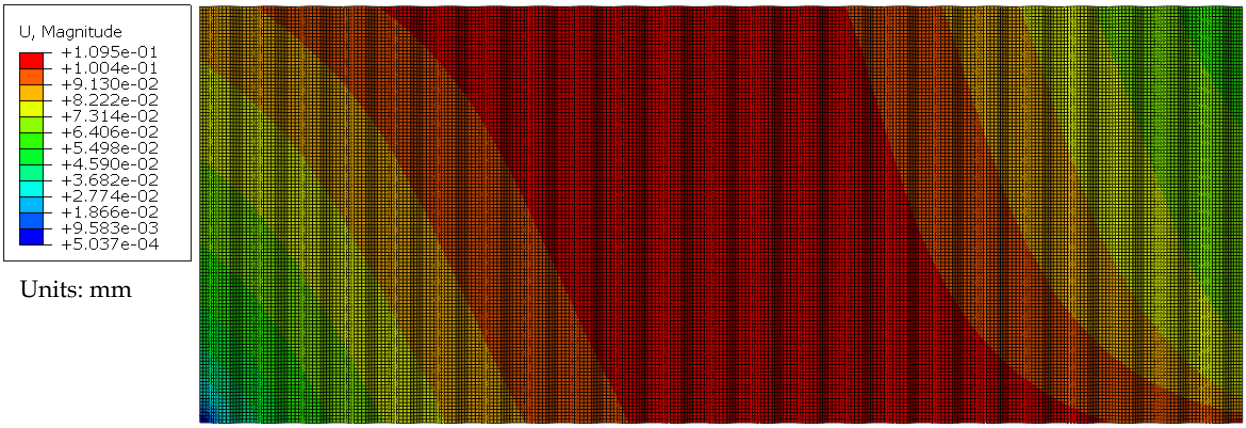

Figure 35 Displacement of FEA Shell Model of Corrugated Side Wall Subject to Vertical Loading

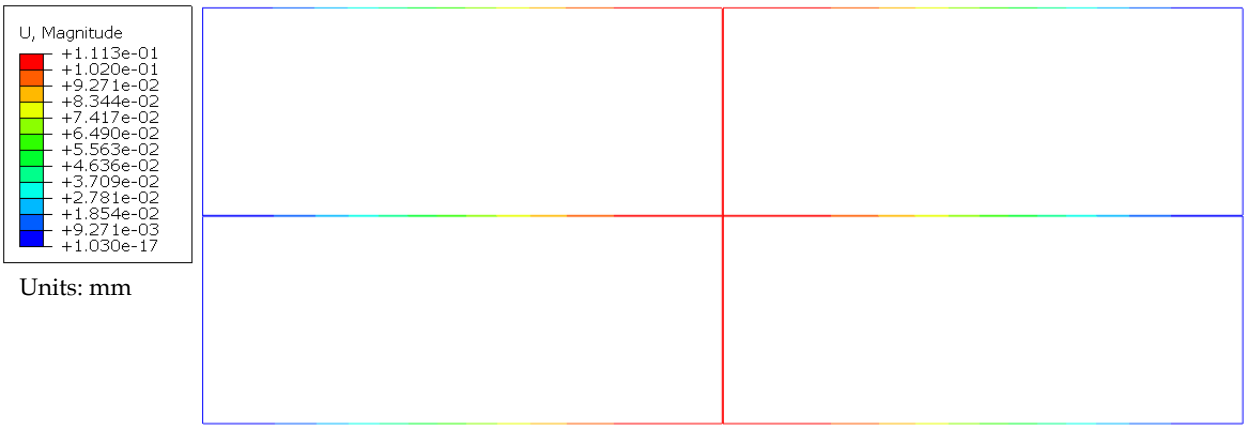

Figure 36 Displacement of Modified Box Frame Side Wall Model Subject to Vertical Loading

The stress distributions for the side wall, modified box frame model and the FEA shell model, are shown in Figure 37 and Figure 38. Respectively it can be seen in Figure 37 that most of the corrugated siding experiences the same stress, while the bottom corners near the supports experience stress concentrations. Table 7 shows the results of the stress distributions with equation [5.3-4] applied.

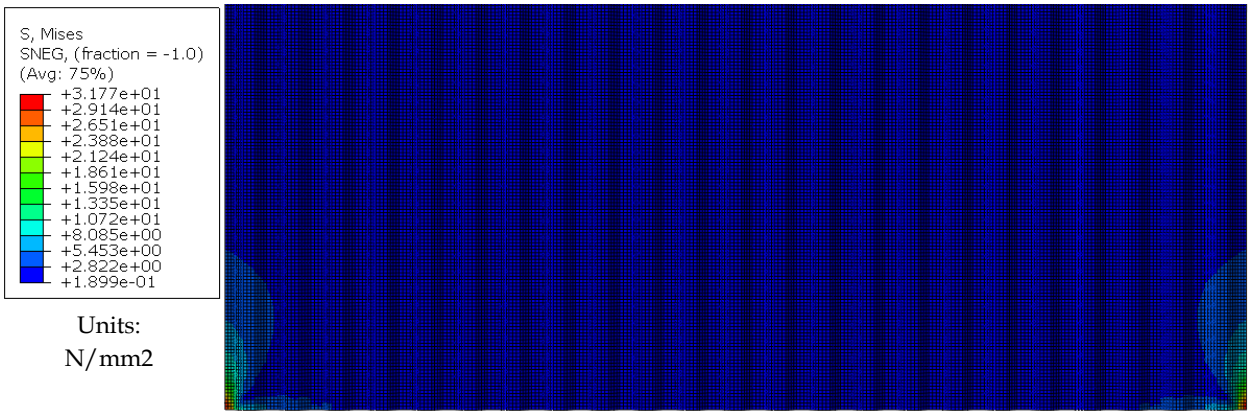

Figure 37 Von Mises Stress Distribution Corrugated Side Wall

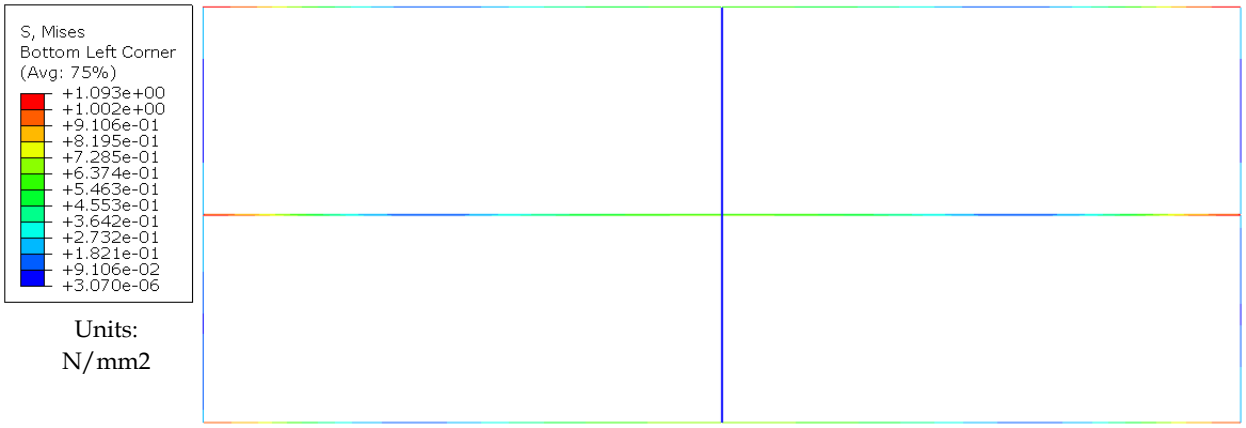

Figure 38 Von Mises Stress Distribution Box Frame Sidewall

Table 7 Vertical load Comparison utilizing Equation [5.3-5]

Compression Comparison of Methods Corrugated Walls								
Model	**Stress 90%**	**Displacement At Bottom Middle**	**Modification Factor for Stress**	**Factored Sress**	**%Difference Stress**	**Modification Factor for Displacement**	**Factored Displacement**	**%Difference Dsiplacement**
Units	**N/mm2**	**mm**	**N/A**	**N/mm2**	**N/A**	**N/A**	**mm**	**N/A**
CSWS	0.1899	0.1095	1.0000	0.1899	0%	1.000	0.110	0%
BFSS	0.3642	0.1113	0.5000	0.1821	4%	1.000	0.111	2%
CEWS	0.0163	0.0242	1.0000	0.0163	0%	1.000	0.024	0%
BFES	0.0552	0.0247	0.3100	0.0171	5%	1.000	0.025	2%

Legend:

- CSWS: FEA shell model of corrugated side wall that is simply supported.
- BFSS: Box frame side wall that is simply supported.
- CEWS: FEA shell model of corrugated end wall that is simply supported.
- BFES: Box frame end wall that is simply supported.

Figure 39 and Figure 40 show the principal stresses for the sidewall in the FEA shell model and modified box frame model. The area of interest for comparison is marked by a red circle. It can be seen from Figure 39 to Figure 40 that the relationship is about one to one for 80% of the FEA shell model of the cargo container side wall. The FEA shell model shows a principal stress of 0.4209 N/mm² while the modified box frame model shows a principal stress of 0.4531 N/mm². This gives a percent difference of 7.7% between the modified box frame model and the FEA shell model.

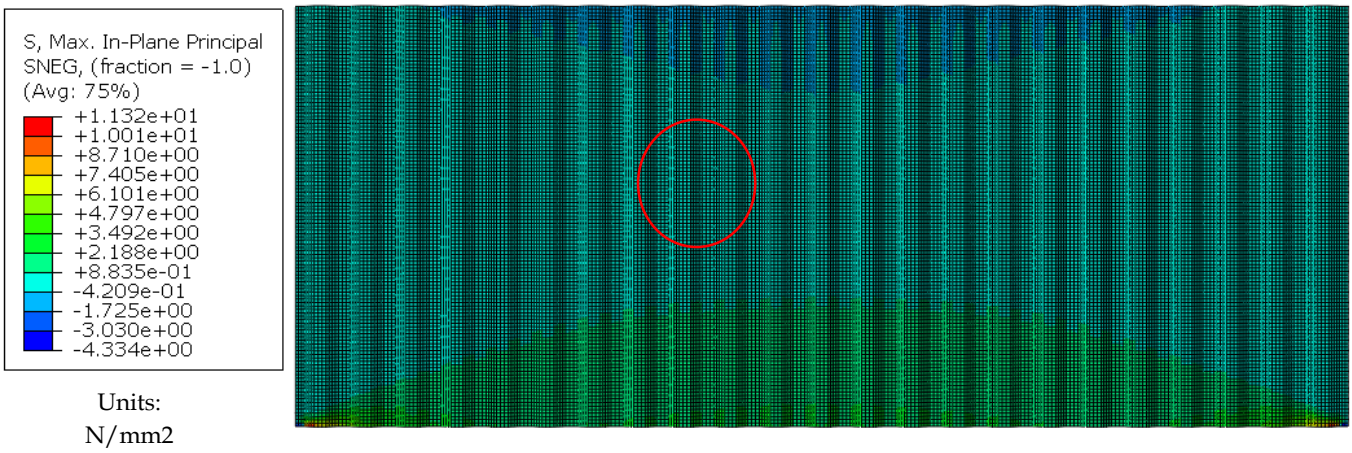

Figure 39 Principal Stress of Corrugated Siding

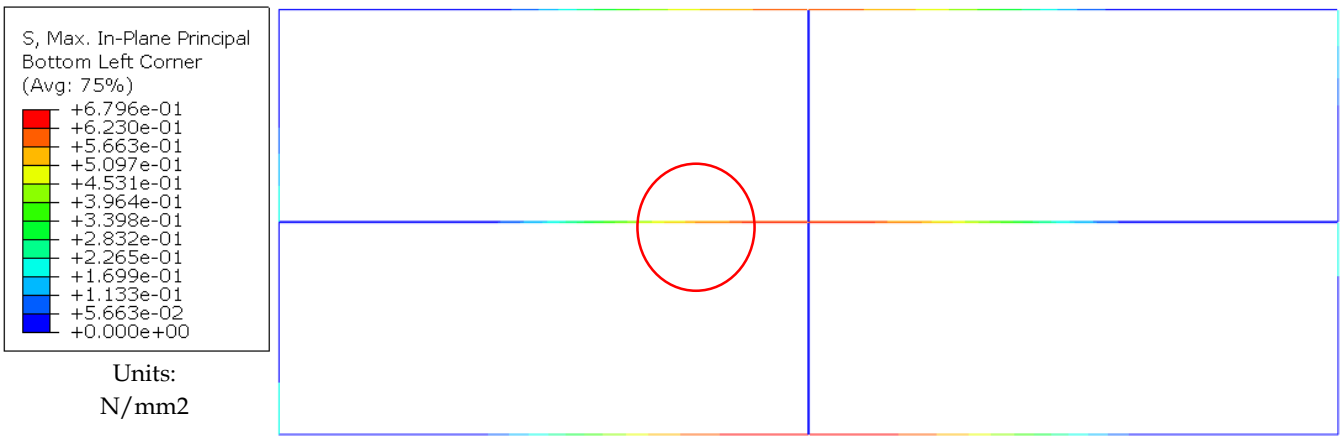

Figure 40 Principal Stress Modified box frame model Side Wall

6.3 Lateral Load Comparison

6.3.1 Corner Post

To evaluate the lateral stability of the corner post models, the simplified rectangular beam and FEA shell, the models were subject to lateral loads. The boundary conditions of both models were changed. This was to ensure the models could satisfy equilibrium. A lateral load applies a moment therefore a fixed support must be used to resist the moment. The models were treated as cantilevered members subject to loading perpendicular to the member itself. Figure 41 through Figure 44 show the stresses and displacements for the simplified rectangular beam and the FEA shell model of the corner post alone. The simplified rectangular beam model does not predict either the stress or displacement of the corner post well. This may be due to the effects of torsion on the asymmetric corner post that is not accounted for in the simplified model.

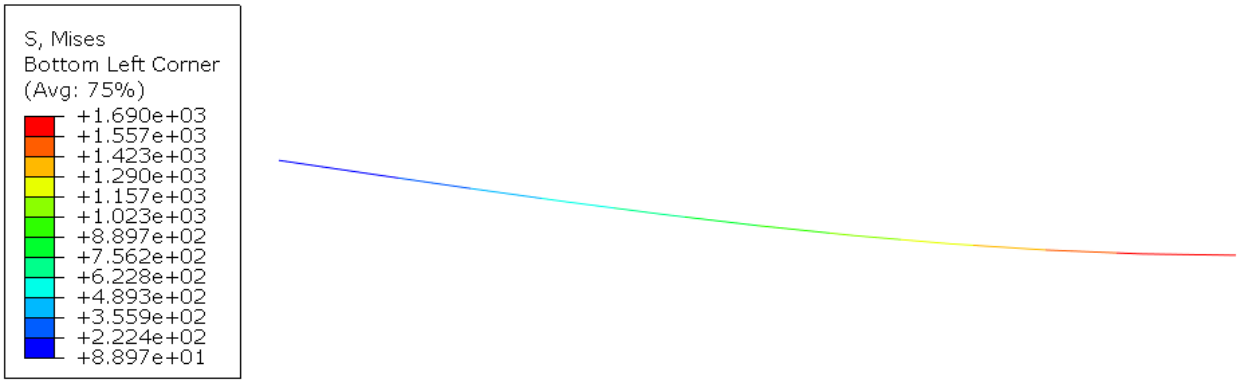

Units:
N/mm2

Figure 41 Lateral Von Mises Stress of Simplified Beam

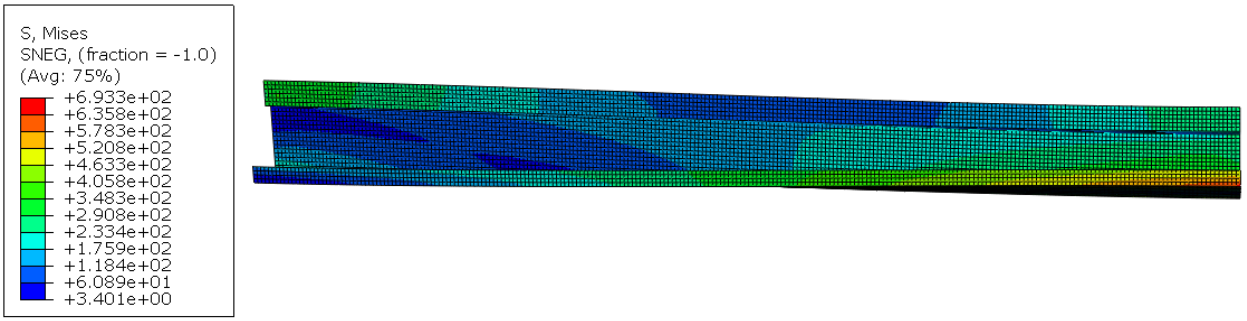

Units:
N/mm2

Figure 42 Lateral Von Mises Stress of Corner Post

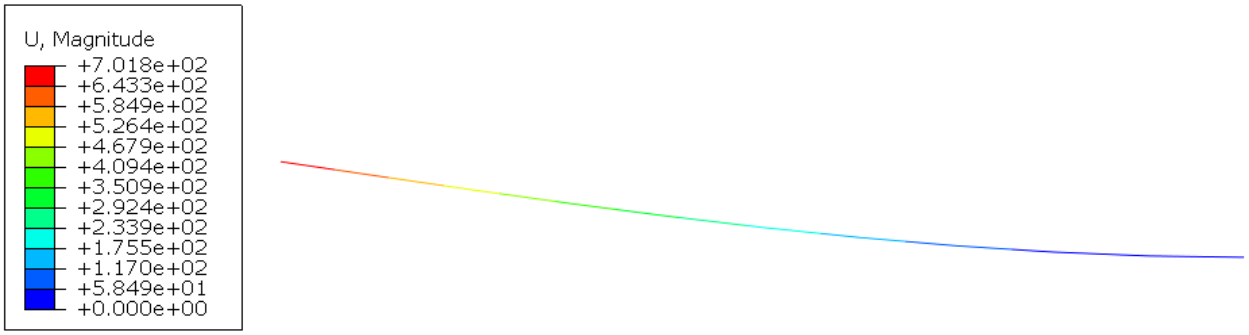

Units: mm

Figure 43 Lateral Displacement of Simplified Beam

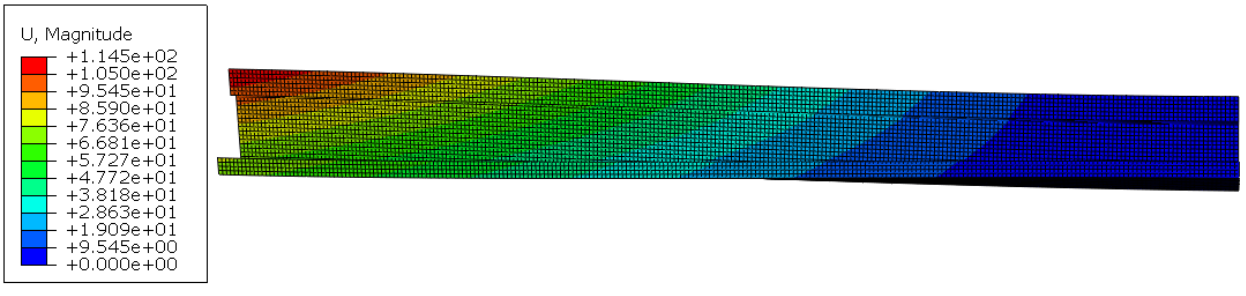

Units: mm

Figure 44 Lateral Displacement of Corner Post

6.3.2 Corrugated Walls

Figure 45 shows the loading schematic for the modified box frame model subjected to a lateral loading. Figure 46 shows the corresponding FEA shell model subjected to the same lateral load. The simulations follow the same assumptions for the models when subject to a vertical load.

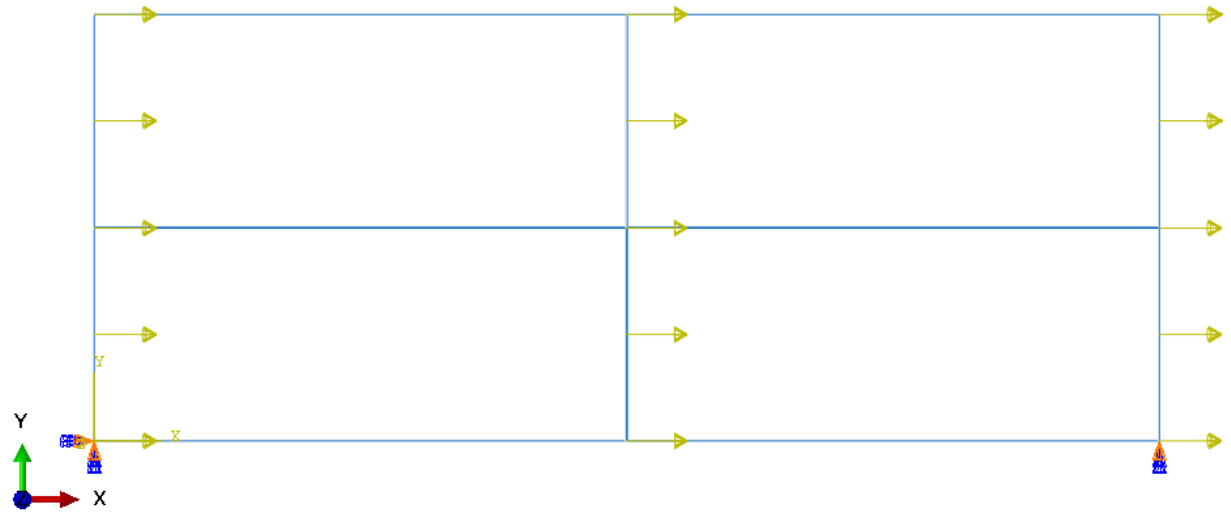

Figure 45 Lateral Loading Box Frame Sidewall

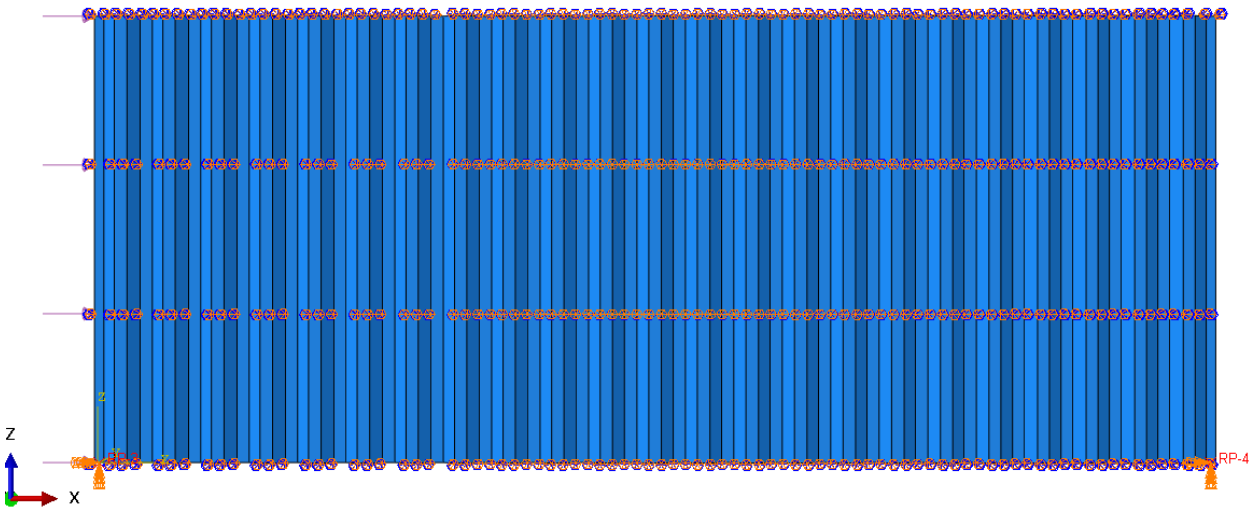

Figure 46 Lateral Loading Corrugated Sidewall

Table 8 compares different areas of interest for the side wall in both models. The legend details what each abbreviation stands for in the table. Table 8 shows that the modified box frame model does not predict the displacement or stress well. The displacement of the modified box frame model of the sidewall subject to lateral load is about half that of the FEA shell model. However, the displacement of the modified box frame model of the end wall is significantly higher than that of the corresponding FEA shell model, a figure of this can be seen in Appendix A. This shows that the modified box frame method does not work to simplify response of the corrugated walls when subject to lateral loads. Suggestions for remedying this can be found in Chapter 8.

Table 8 Container Walls Subject to Lateral Loads

Corrugated Walls Subject to Lateral Distributed Load of 0.6803 N/mm						
Model	**Stress 90%**	**Max Stress**	**Max Disp.**	**Stress At Bottom Middle**	**Displacement at Top Midpoint**	**Displacement At Middle**
CSWSL	0.002639	41.64	0.0118	0.0026	0.0605	0.0605
BFSSL	0.03355	0.40	0.0307	0.0003	0.0307	0.0179
% Difference	1171.31	99.04	**160.17**	89.26	49.26	**70.40**
CEWSL	0.003227	29.13	0.063100	0.003227	0.063100	0.054830
BFESL	0.773000	1.788000	0.134000	1.788000	0.134000	0.100500
% Difference	23854.14	93.86	**112.36**	55307.50	112.36	**83.29**

Legend:

- CSWSL: Corrugated side wall that is simply supported subject to lateral loading.
- BFSSL: Box frame side wall that is simply supported subject to lateral loading.
- CEWSL: Corrugated end wall that is simply supported subject to lateral loading.
- BFESL: Box frame end wall that is simply supported subject to lateral loading.

6.4 Opening in Corrugated Sidings

6.4.1 Model Configurations

The objective of cutting out an area of the corrugated side wall of the cargo shipping container is to evaluate the strength of the side walls with openings for doors and windows. This procedure is to analyze the ability for the modified box frame model to predict the behavior of the FEA shell corrugated walls when an opening has been made the within them. An arbitrary rectangular volume was removed from the quadrant one of the wall. Figure 53 shows a diagram of the corrugated wall of the cargo shipping container which has been divided four quadrants. The four quadrants correspond to the four boxes used in a modified box frame model. The location and size of the opening is important to the process of creating a representative modified box frame model. The location of the opening dictates which box in the modified box frame model will experience changes to the cross sectional properties of its members. Utilizing the modified box frame member sizing equations detailed in Chapter 5 the new cross section dimensions were calculated for the horizontal and vertical members of the box located in quadrant one. All of the calculations can be found in Appendix B. Table 9 through Table 11 summarize the calculations made for the volume openings in the box frame corresponding to the respective corrugated walls.

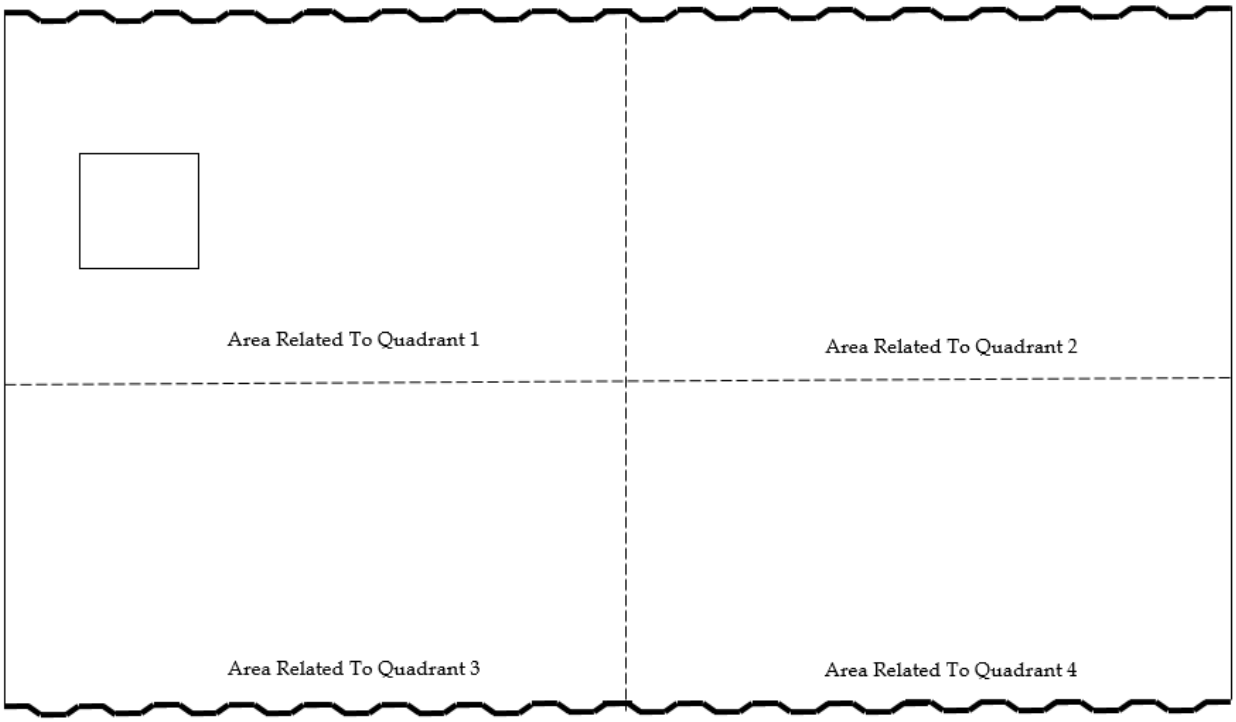

Figure 47 Quadrant Sections for Volume Opening

Table 9 Volume Opening Table

Volume Cut Out Table					
	Volume of siding with opening	**Volume of siding without opening**	**Volume of Opening**	**Surface Area of opening**	**Quadrant of Cut Out**
Units	mm3	mm3	mm3	mm2	N/A
Side Wall	22,578,462	23,143,076	564,614	384,091	1
Endwall	8,784,801	9,132,870	348,069	236,782	1

Table 10 Volume Resize of Modified box frame model for Sidewall

Box Frame Side Wall Volume Cut							
Quadrant	**Effective Volume**	**Vs**	**Vi**	**Vf**	**n**	**Horizontal Cross Section**	**Vertical Cross Section**
Units	**mm^3**	**mm3**	**mm3**	**unitless**	**unitless**	**mm**	**mm**
1	2,610,578	22,578,462	23,143,076	0.98	3.02	88.9	139.9
2	5,785,769	23,143,076	23,143,076	1	3.1	135.6	213.5
3	5,785,769	23,143,076	23,143,076	1	3.1	135.6	213.5
4	5,785,769	23,143,076	23,143,076	1	3.1	135.6	213.5

Note Calculations in Appendix B

Table 11 Volume Resize of Box Frame for End Wall

Box Frame End Wall Volume Cut							
Quadrant	**Effective Volume**	**Vs**	**Vi**	**Vf**	**n**	**Horizontal Cross Section**	**Vertical Cross Section**
Units	**mm^3**	**N/A**	**mm3**	**unitless**	**unitless**	**mm**	**mm**
1	1,935,149	8,784,801	23,143,076	2.634445	2.24	90.1	89.2
2	2,283,218	9,132,870	23,143,076	2.534042	2.07	90.4	89.5
3	2,283,218	9,132,870	23,143,076	2.534042	2.07	90.4	89.5
4	2,283,218	9,132,870	23,143,076	2.534042	2.07	90.4	89.5

Note Calculations in Appendix B

6.4.2 Vertical Load

The modified box frame model and FEA shell corrugated wall model were subject to a vertical distributed load of 0.6803N/mm. Figure 48 shows the side view of the opening in the corrugated sidewall. The overall stress of the corrugated siding was not significantly affected by the opening. However, stress concentrations can be seen at the edges of the opening, shown in Figure 49. The stress distribution shows a slight increase in stresses near the corners of the opening in comparison to the stress in other areas of the corrugated siding.

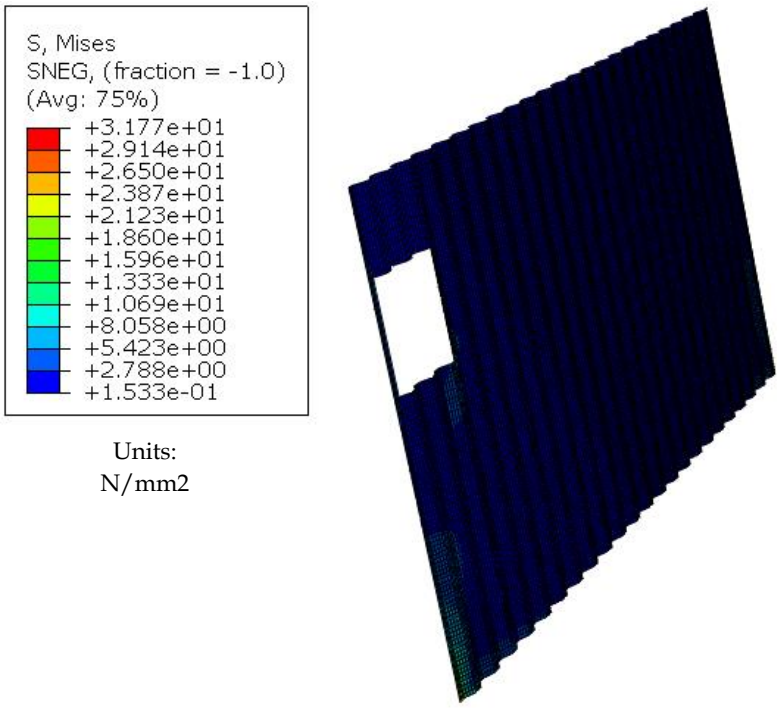

Figure 48 Sideview of Sidewall Volume Opening

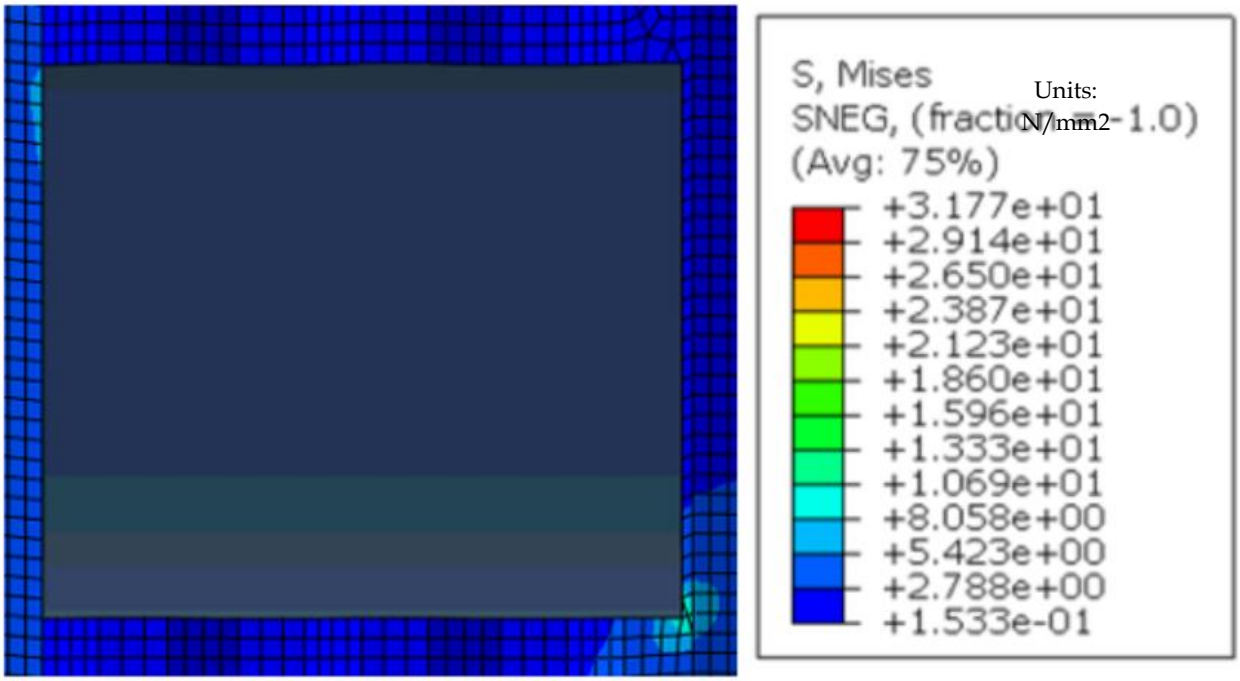

Figure 49 Zoomed in View of Stress Contours Around Sidewall Volume Opening

Figure 50 shows the displacements of the corrugated siding in the vertical direction in response to the vertical edge load applied. Figure 51 shows the vertical displacements in modified box frame model. The red circle in each the figure shows the areas of comparison. The difference in displacement prediction between the FEA shell model of the sidewall and the modified box frame model of the sidewall is 6%. Using equation from Chapter 5 Von Mises stress was calculated from the modified box frame results and compared to the FEA shell corrugated sidewall. The differences in stresses predicted by the two models is 13%. The results from the FEA shell corrugated end wall model and modified box frame model show that the predicted displacement was within 9% difference. The modified box frame method can predict the displacement response of the corrugated siding within 10% difference of the FEA shell model for the volume opening in quadrant 1.

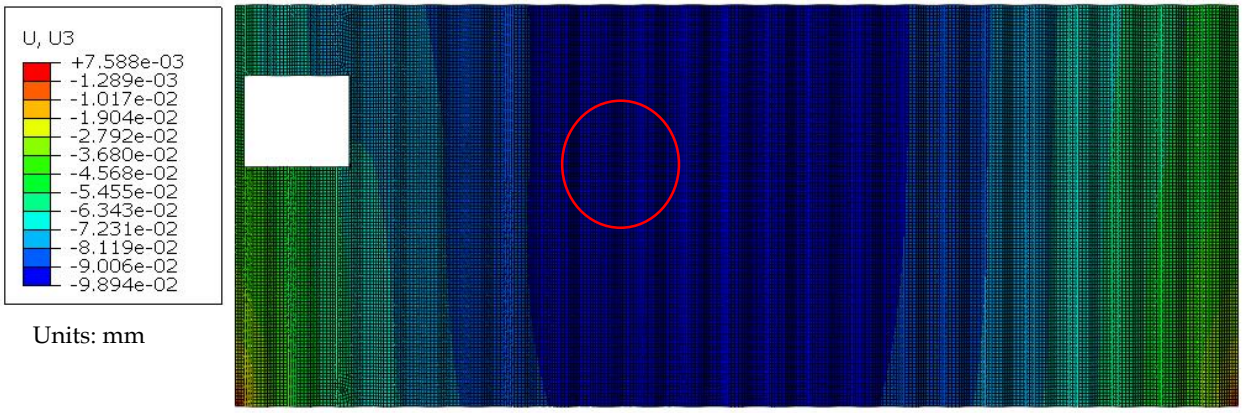

Figure 50 Displacement in Direction of Loading for Sidewall with Volume Opening

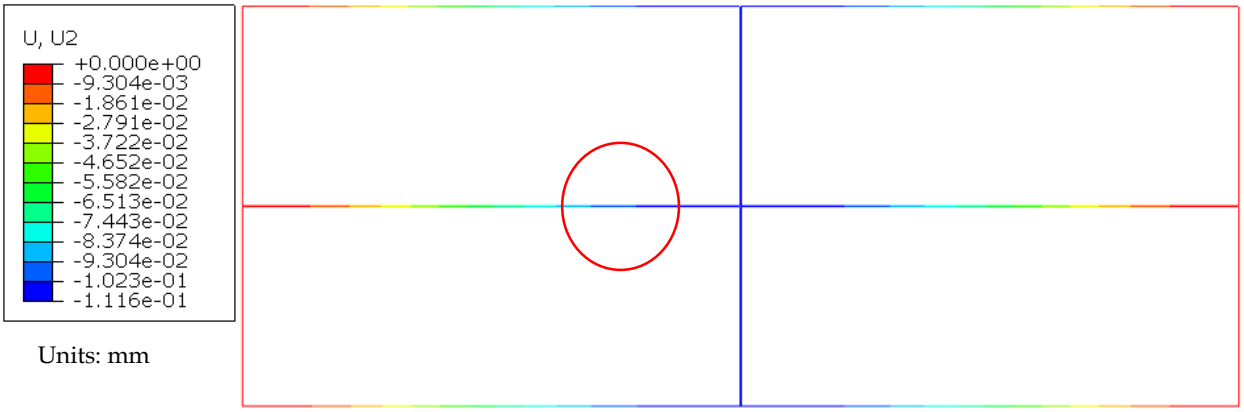

Figure 51 Displacement in Direction of Loading for Box Frame of Sidewall with Volume Opening

6.5 Assemblage of Siding and Framing

6.5.1 Vertical Load

Mathematical models of the corrugated sidings connected to framing as it would be in a cargo shipping container were created for both the side and end walls. The models were analyzed under a vertical load of 0.6803 N/mm (46.63 lb/ft) along the top beam of the model. Figure 52 shows the model of the frame and corrugated siding of the sidewall of the cargo shipping container with the applied loads and support conditions. Figure 53 shows the FEA shell model displacement response to vertical loading. A computer model was constructed using the simplified beam method, a combination of the modified box frame method and simplified beam method, for the side and end walls. Figure 54 shows the displacement of simplified beam model of the sidewall assembly subject to loading in the vertical direction.

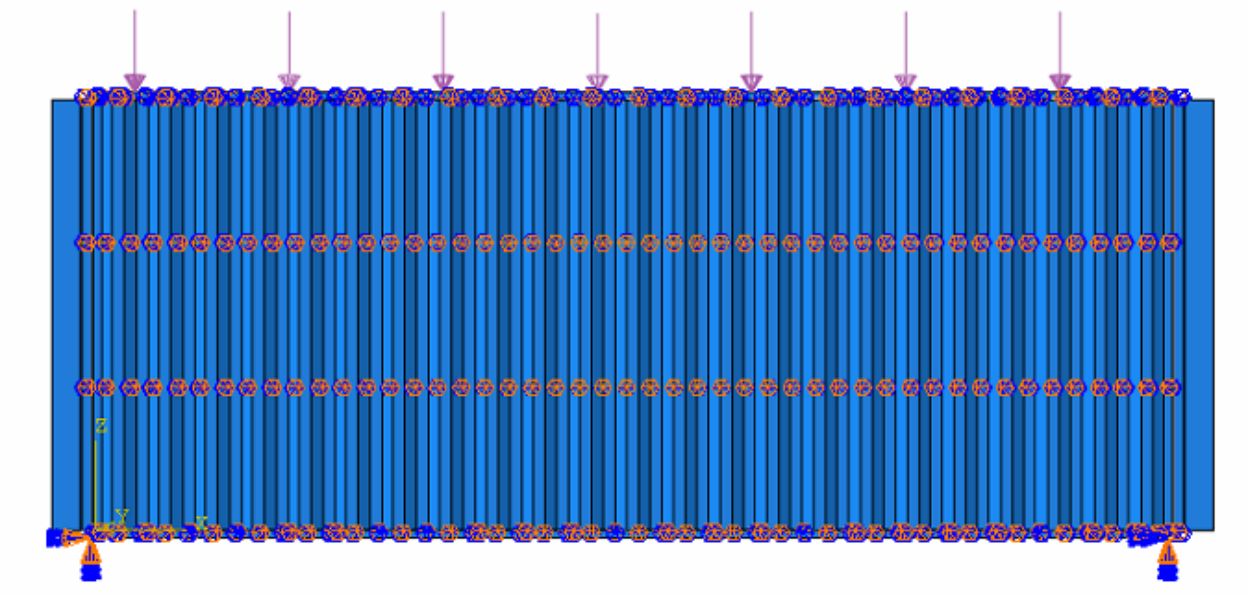

Figure 52 Assembly of FEA Shell Model of Corrugated Sidewall

Figure 53 shows the results for the assembly of the FEA shell model of the sidewall whilst Figure 54 shows the results for the assembly of the simplified model. The simplified model predicts displacement of the sidewall assemble within a 4% difference range. The red circles on each figure shows the area of comparison for the models, this area is about the same area used for comparison throughout this thesis. The difference in displacement for the assembly of the end wall in terms of the simplified model is 15%. Images for the results of the end wall models can be found in Appendix A.

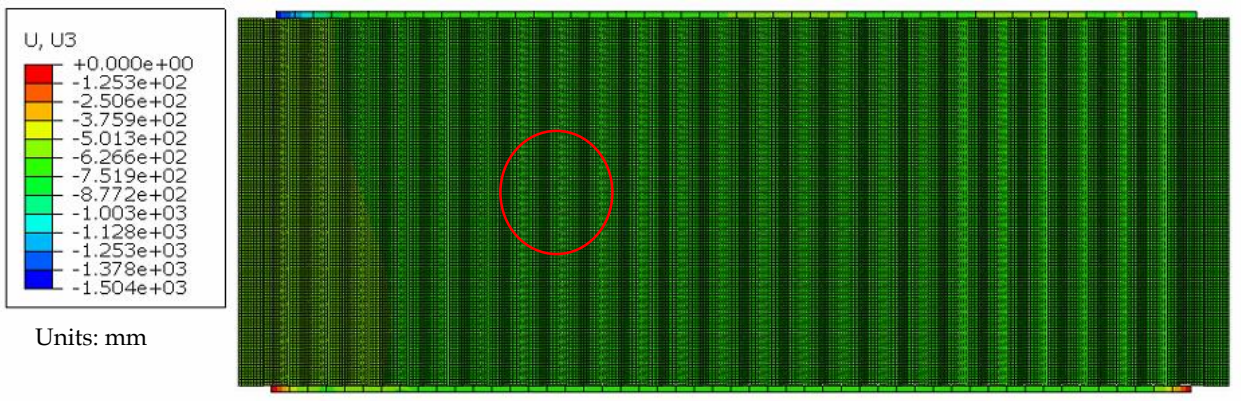

Figure 53 Sidewall Assembly Displacement Response

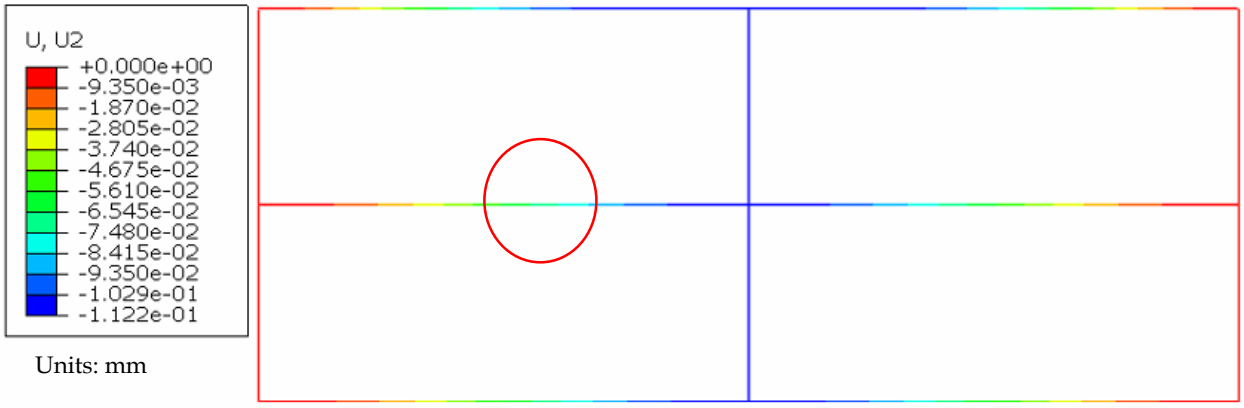

Figure 54 Sidewall Box Frame Assembly Displacement Response

6.5 Comparison of Results to Giriunas Results

Kevin Giriunas created an FEA shell model of a twenty-foot cargo shipping container for his thesis. As part of the analysis he conducted a yielding analysis in which he modeled the cargo shipping container with different structural elements eliminated. This analysis allowed him to estimate the maximum force that can be applied to a cargo shipping container at yielding. One of the models analyzed the frame of the cargo shipping container at yielding. The container was subjected to point loads at the corner fittings that connected the frame. His results noted that the maximum loading at yielding was approximately 725 kN. The cross sectional area for the corner post used in Giriunas thesis was 1479.6 square millimeters. The yield strength of the steel used in his modeling was 70 ksi (490 N/mm^2). Equation [6.5-2] was used to find the maximum displacement, 5.98mm, of the FEA shell frame model that Giriuanas created.

The steel used to model the cargo shipping container in this thesis has a yield stress of 67 ksi (461 N/mm^2). Therefore, and equivalent load to the one Giriunas used was need. Equations [6.5-1] shows the calculations for the load. Figure 55 trough Figure 56 show displacement and stress values of a simplified beam model of the cargo container frame subject to the 753,735 N vertical load at each top node. Each bottom node was restrained by pin connections. The maximum displacement of the simplified beam model was 5.625 mm. This is a 6% difference from the displacement calculated using Giriunas data.

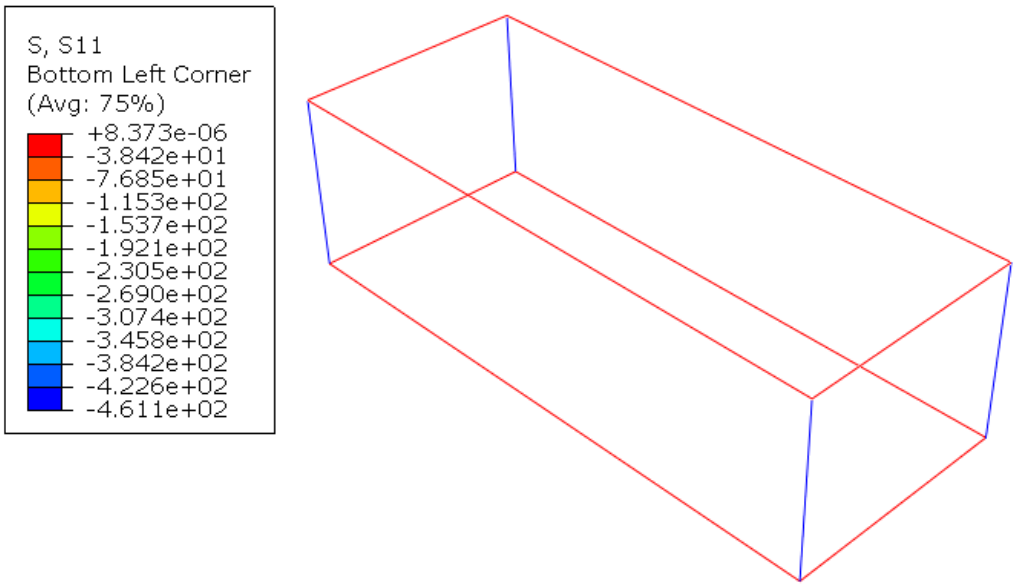

Figure 55 Stress Distribution of Simplified Beam Model of Cargo Container Framing

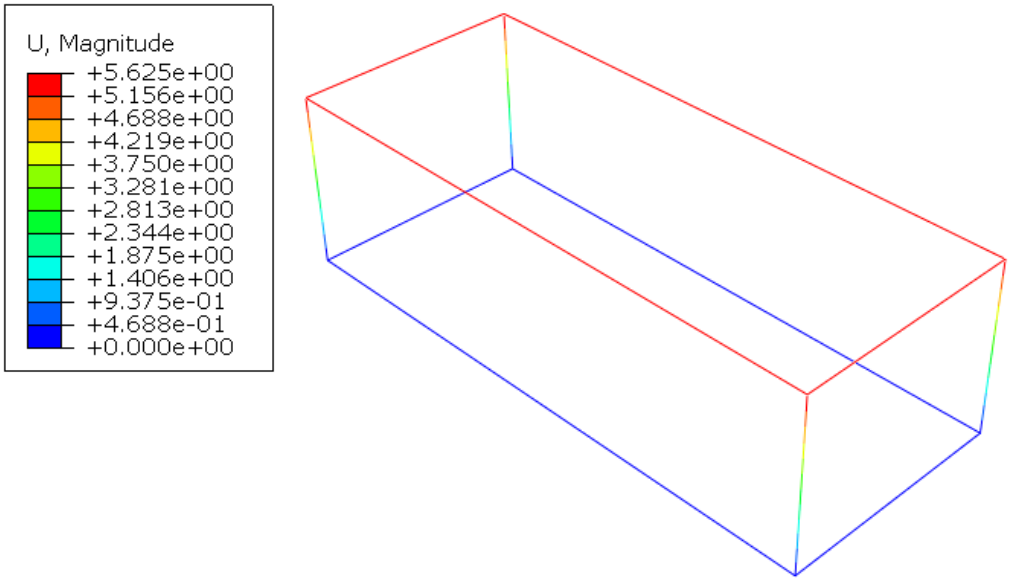

Figure 56 Displacement of Simplified Beam Model of Cargo Container Framing

$$\sigma = \frac{P}{A} \rightarrow P = \sigma * A = 461 \frac{N}{mm^2} * 1634.9 = 753{,}735\ N \qquad \textit{EQ 39 [6.5-1]}$$

$$\Delta = \frac{PL}{AE} = \frac{725{,}000N * 2440mm}{1479.6mm^2 * 200{,}000 \frac{N}{mm^2}} = 5.98mm \qquad \textit{EQ 40 [6.5-2]}$$

Chapter 7

Conclusion

7.1 Discussion

The use of FEA modeling is complex dues to the geometry and meshing of the cargo container structural components. The approach was to develop a simple model that comprised of two components. The first component being a simplified rectangular beam member, the second being a MBFM composed of beams for the corrugated sidings. This approach allows one to go from a complex FEA model to just beam elements that can be analyzed in most FEA software's. Some FEA software packages do not preform beam analysis the same way AbaqusCAE does, therefore selection of software is key to this modeling. This thesis did not include a simplification of the roof and flooring systems. During the development of the models the approach used was not able to predict the behavior of an FEA shell model subjected to lateral loads within a 15% difference. At the moment one will still have to use an FEA shell model of a cargo shipping container to model lateral loading. The FEA shell siding models of the cargo shipping container were restrained in out of plain movement. If there is a chance of out of plane movement the FEA shell model predictions in displacements and stresses would need to be verified.

7.2 Conclusions and Restrictions

This model has only been verified using a 20-foot cargo shipping container model, it has not been evaluated for other sizes. Currently there are four standard lengths of cargo containers, 10 ft, 20 ft, 30 ft, 40 ft. There are also four standard heights for the cargo shipping container height, 8ft, 8.5 ft, 9 ft, and 9.5 ft. The simplified beam method estimates the stresses and displacements for a FEA shell model of a 20ft cargo shipping container, but prediction difference for other sizes of containers has not been evaluated.

The maximum percent difference in predictions of displacements using the simplified beam method was 10%. The maximum percent difference in predictions of the stresses using the simplified beam method was 15%. Based on the results presented in Chapter 6 the simplified beam method can predict the displacement and stress of an FEA shell model within 10% and 15% respectively. A benefit to the simplified beam method is that it can be run on a variety of different software's. The model also provides stresses at key locations. This method could be used to simplify analysis for cargo shipping containers used as structural components for non-shipping applications. Load factorization using the LRFD method should allow for conservative calculations and designs for simplified rectangular beam components of the corner post.

7.3 Future Study

There is a lot that can be improved with the simplified beam method. The list below details possible future work that could simplify the method even further.

- How does the use of axial stiffeners in the direction of lateral loading effect the prediction of the simplified beam model?
- Can the method be used to simplify the roof and floor systems?
- What are the effects of out of plane bending for the corrugated siding?
    - Can effect of out of plane bending be solved using rotational stiffeners or a different method for calculating the cross sectional areas of the members
- Can this model be used in dynamic loading?
    - Can the MBFM be used for structures subjected to dynamic loading?

References

[1] K. A. Giriunas, Evaluation, Modeling, and Analysis of Shipping Container Building Structures, Ohio State Univeristy, 2012.

[2] D. L. Calvin, A Simplified Box Frame Model For Structural Cladding, Durham: University of New Hampshire, 1986.

[3] *Containables.* [Performance]. HGTV, 2018.

[4] K. Banes, Interviewee, *Cargo Container Specifications.* [Interview]. 2017.

[5] "Malcom McLean," [Online]. Available: https://www.pbs.org/wgbh/theymadeamerica/whomade/mclean_hi.html.

[6] "Shipping Container History," 2015. [Online]. Available: http://www.priceandspeed.com.au/about-us/history-shipping-containers/.

[7] I. O. f. Standardization, *Series 1 freight containers- Classification, dimensions and ratings,* International Organiztion for Standardization, 2013.

[8] *Tilton Trailer Company,* 2018.

[9] I. O. f. Standardization, *Freight containers- Coding, identification, and marking,* International Organiztion for Standardization, 1995.

[10] ASTM, *ASTM Standards,* American Association State Hiway and Transportation Officials Standard.

[11] ASTM, *Standard Test Methods for Tension Testing of Metallic Materials,* American Association State Hiway and Transportation Officials Standard, 2018.

[12] "Properties of Steel," 2006. [Online]. Available: www.engineershandbook.com/Tables/steelprop.htm.

[13] D. L. Logan, A First Course in the Finite Element Method, Wadsworth Group, 2001.

[14] "ISO 20' Shipping Container," 2017. [Online]. Available: http://www.residentialshippingcontainerprimer.com/Shipping%20Container%20Models%20and%20Drawings.

[15] A. Harish, "What Is the Meaning of the Von Mises Stress and Yield Criterion," 14 November 2018. [Online]. Available: https://www.simscale.com/blog/2017/04/von-mises-stress/.

[16] R. D. Cook, Finite Alement Modeling For Stress Analysis, John Wiley & Sons Inc., 1995.

[17] R. M. Christensen, "How Do Mises and Tresca Fit In," 2018. [Online]. Available: https://www.failurecriteria.com/misescriteriontr.html.

[18] "What is Von Mises Stress?," [Online]. Available: https://www.simscale.com/docs/content/simwiki/fea/what-is-von-mises-stress.html.

[19] P. M. Kurowski, *FEA Failure Assesment,* 2012.

[20] C. K. Inc, "Corner Castings/Corner Fittings," March 2018. [Online]. Available: http://www.chassisking.com/products/parts-and-accessories/corner-castings-corner-fittings/.

[21] "Container Design," 2018. [Online]. Available: http://www.containerhandbuch.de/chb_e/stra/index.html?/chb_e/stra/stra_03_01_00.html.

[22] "Cargo Shipping Container Parts," 2018. [Online]. Available: http://www.pacificmarine.net/marine-deck/cargo-container-parts/iso-container-corner-castings.htm.

[23] "Krisry International," 2018. [Online]. Available: https://www.krisryinc.com/products/corner-castings.

[24] A. Obianyor, "Packing and Handling Instruction for Type TC03(2989), TC04(3550), TC06(2968) & TC09(2910B) IP-2 ISO Containers," LLW Respository Ltd, 2012.

[25] "History of Containerization," 2018. [Online]. Available: http://www.worldshipping.org/about-the-industry/history-of-containerization.

[26] D. A. Andriyana, "Failure Criteria for Yielding," Sophia Antipolis, 2018.

[27] AZoM, "AISI 1035 Carbon Steel (UNS G10350)," 21 September 2012. [Online]. Available: https://www.azom.com/article.aspx?ArticleID=6540.

[28] I. O. f. Standardization, *Series 1 freight containers-Specification and testing,* International Organiztion for Standardization, 2013.

[29] AISC, Steel Construction Manual, American Institute of Steel Construction, 2011.

Appendix A

Results

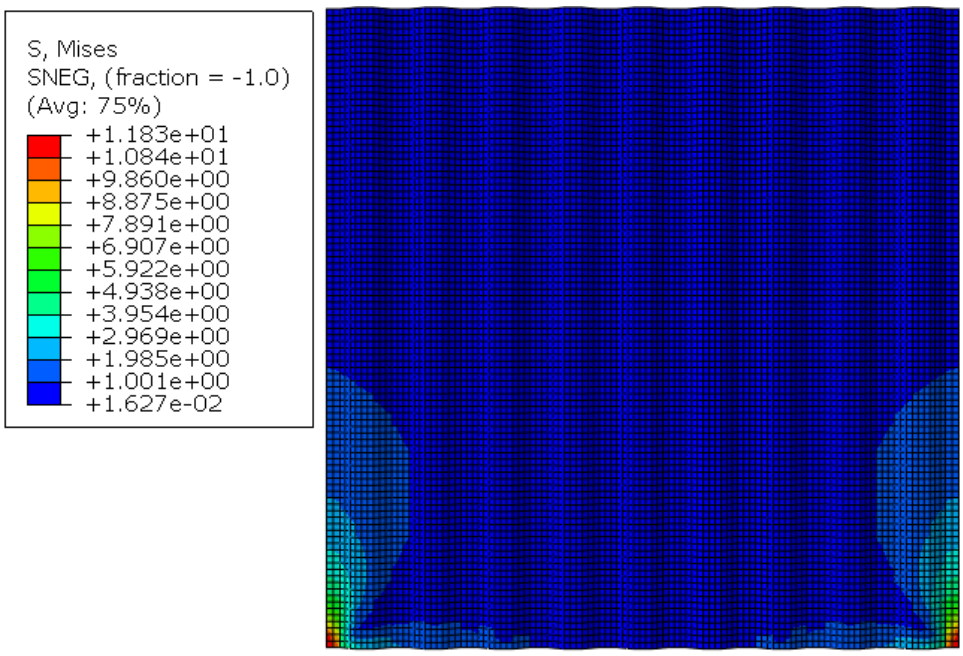

Appendix Figure 1 Stress Distribution of FEA Shell Model of End Wall Subject to Vertical Loading

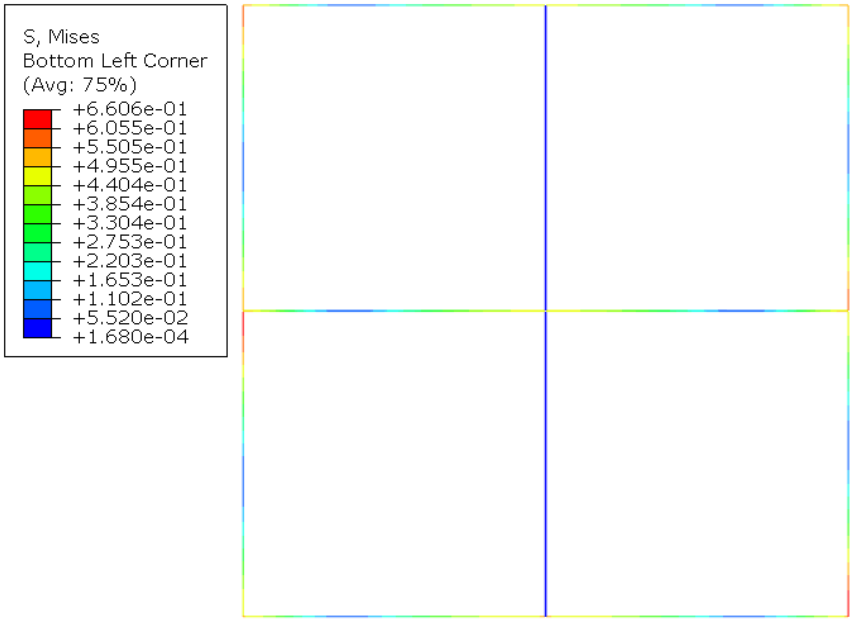

Appendix Figure 2 Stress Distribution of MBFM of End Wall Subject to Vertical Loading

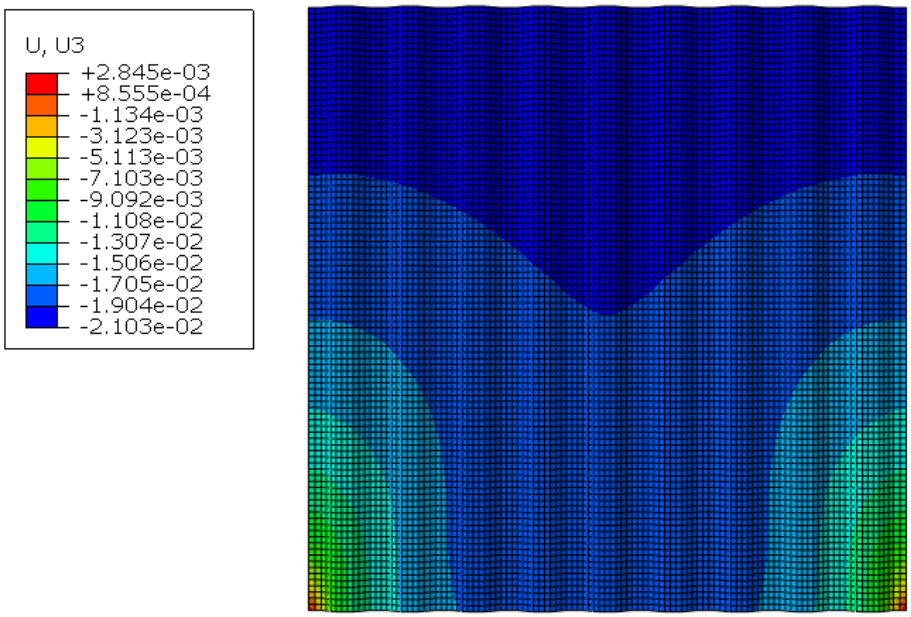

Appendix Figure 3 Displacement Distribution of FEA Shell End Wall Subject to Vertical Loading

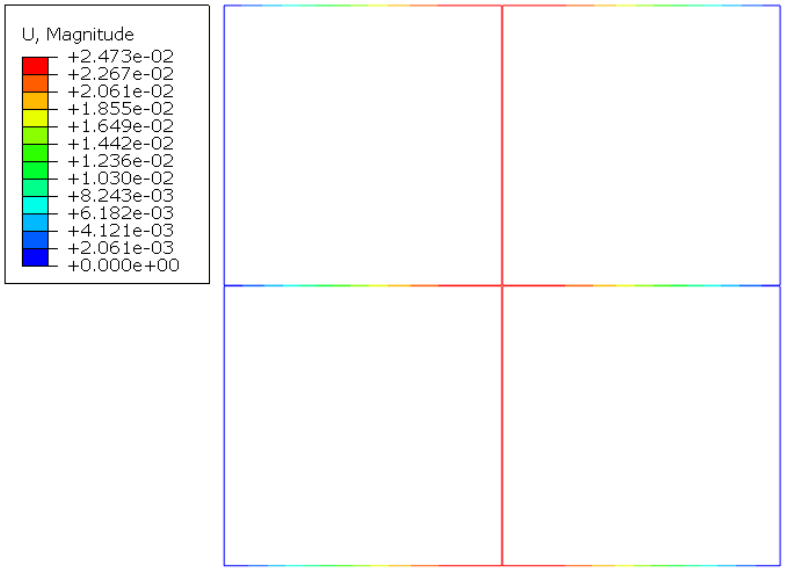

Appendix Figure 4 Displacement Distribution of MBFM of End Wall Subject to Vertical Loading

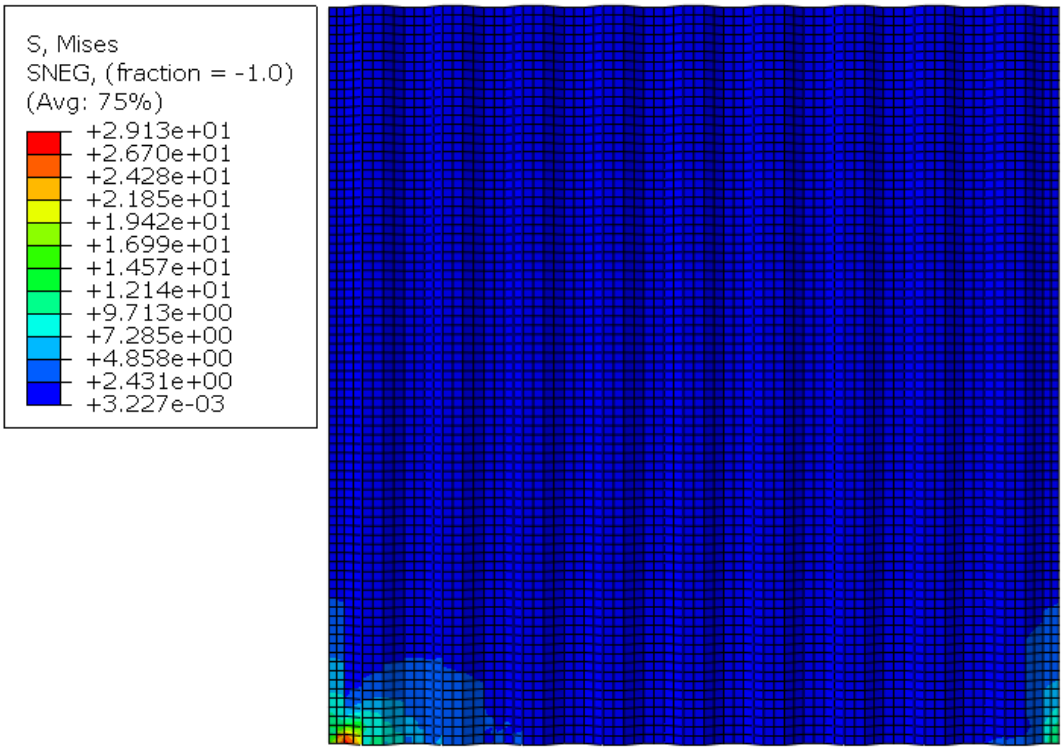

Appendix Figure 5 Stress Distribution of FEA Shell Model of End Wall Subject to Lateral Loading

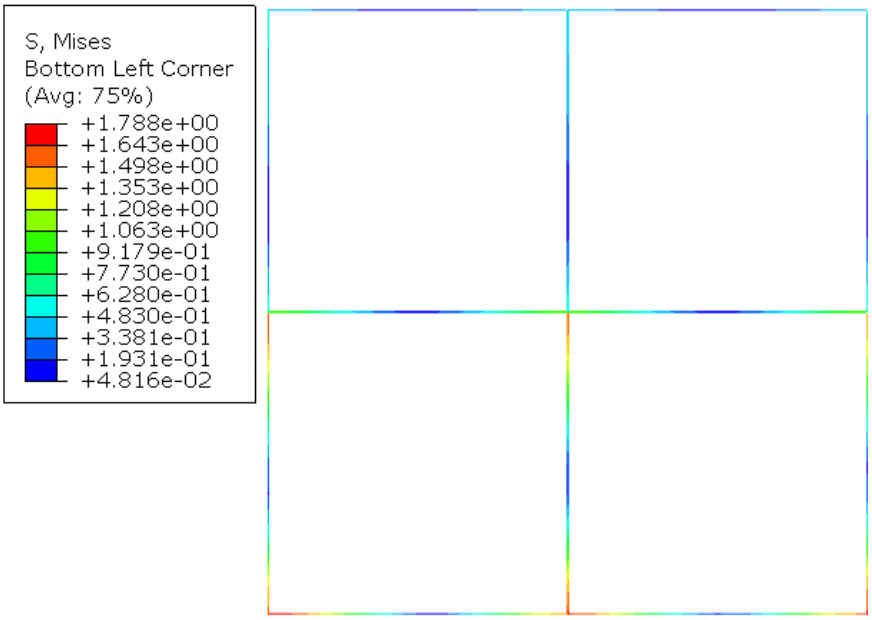

Appendix Figure 6 Stress Distribution of MBFM of End Wall Subject to Lateral Loading

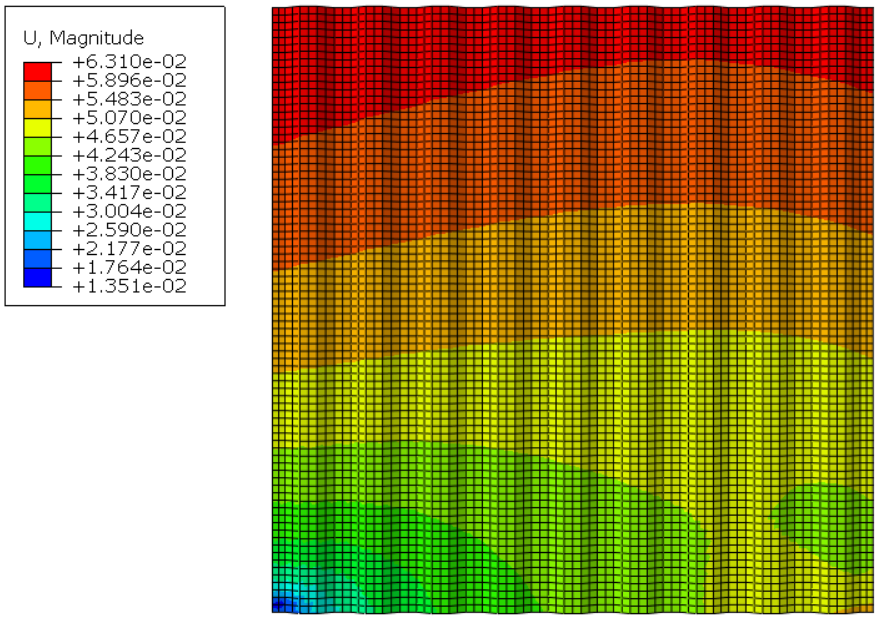

Appendix Figure 7 Displacement of FEA Shell Model of End Wall Subject to Lateral Loading

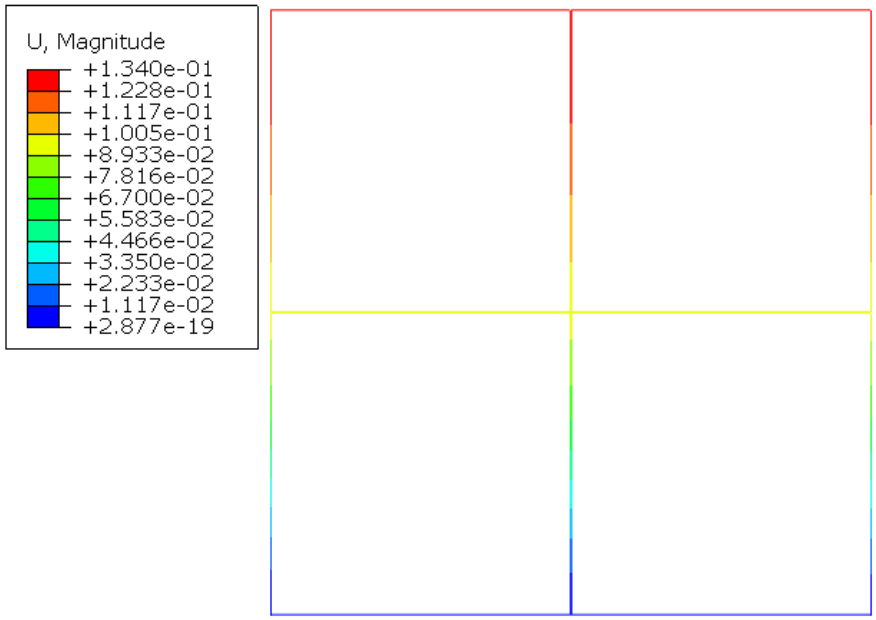

Appendix Figure 8 Displacement of MBFM of End Wall Subject to Lateral Loading

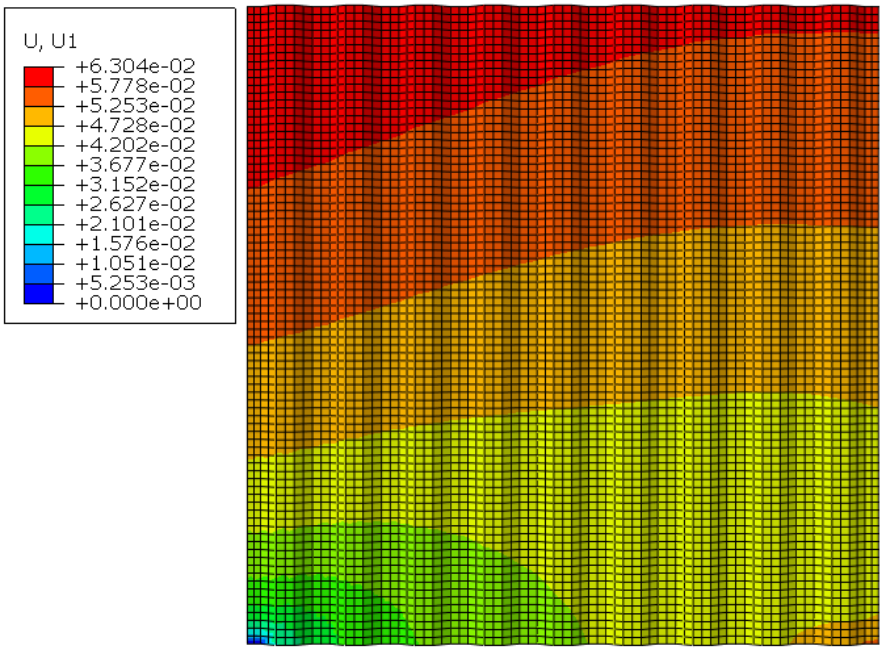

Appendix Figure 9 X-Axis Displacement of FEA Shell Model of End Wall Subject to Lateral Loading

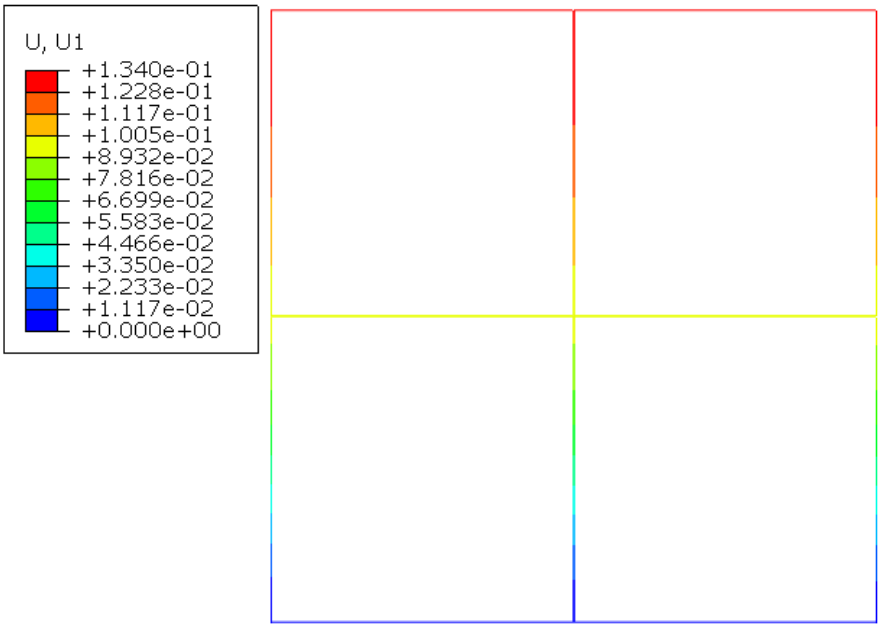

Appendix Figure 10 X-Axis Displacement of MBFM of End Wall Subject to Lateral Loading

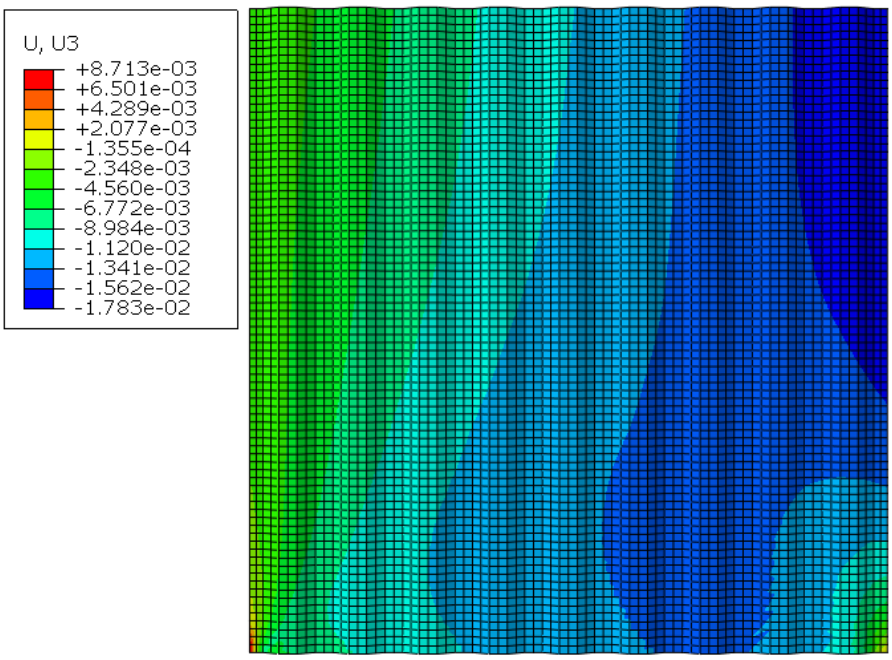

Appendix Figure 11 Displacement in Direction of Loading of FEA Shell Model of End Wall Subject to Lateral Loading

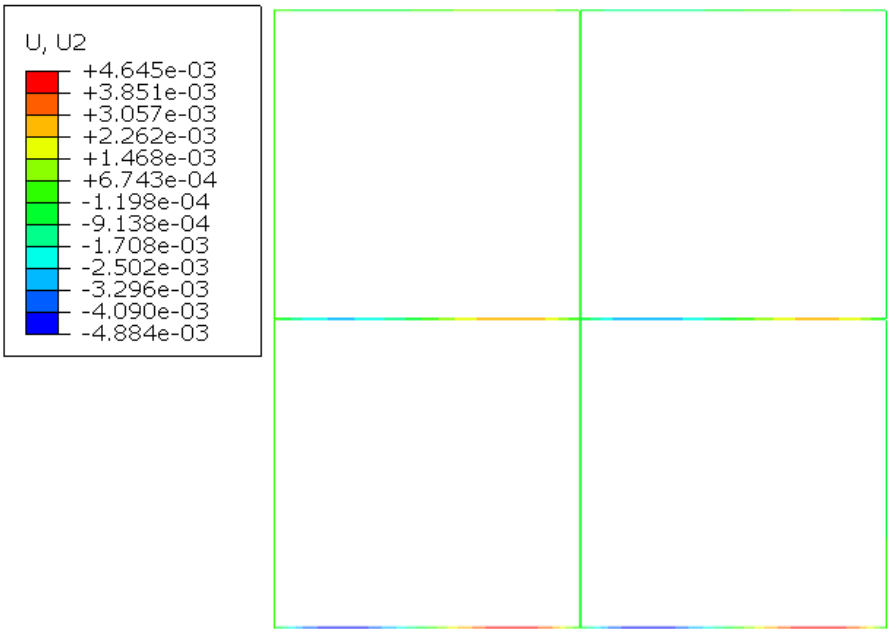

Appendix Figure 12 Displacement in Direction of Loading of MBFM of End Wall Subject to Lateral Loading

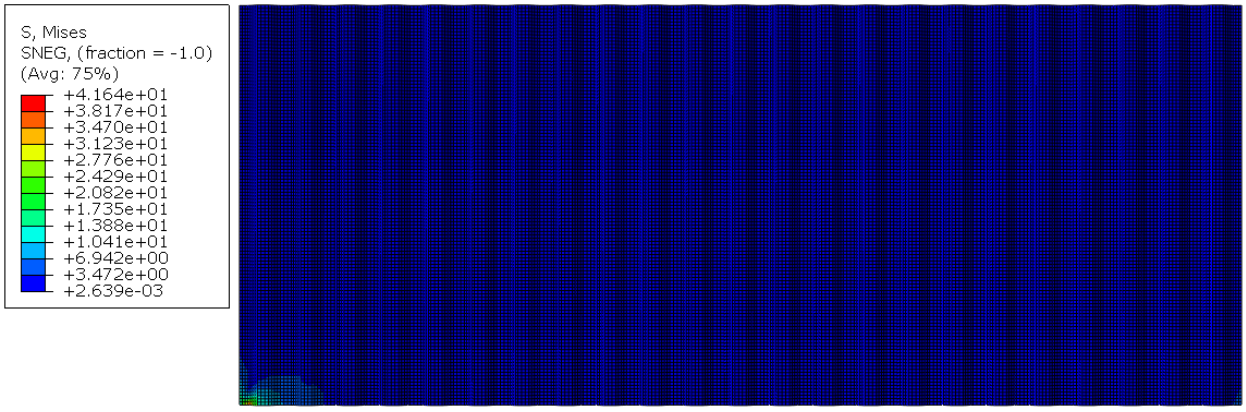

Appendix Figure 13 Stress Distribution of FEA Shell Model of Side Wall Subject to Lateral Loading

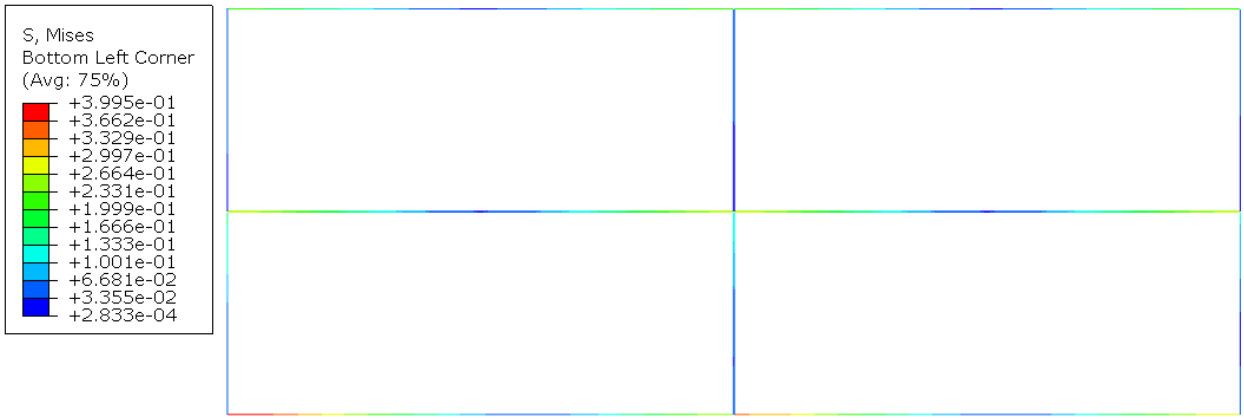

Appendix Figure 14 Stress Distribution of MBFM of Side Wall Subject to Lateral Loading

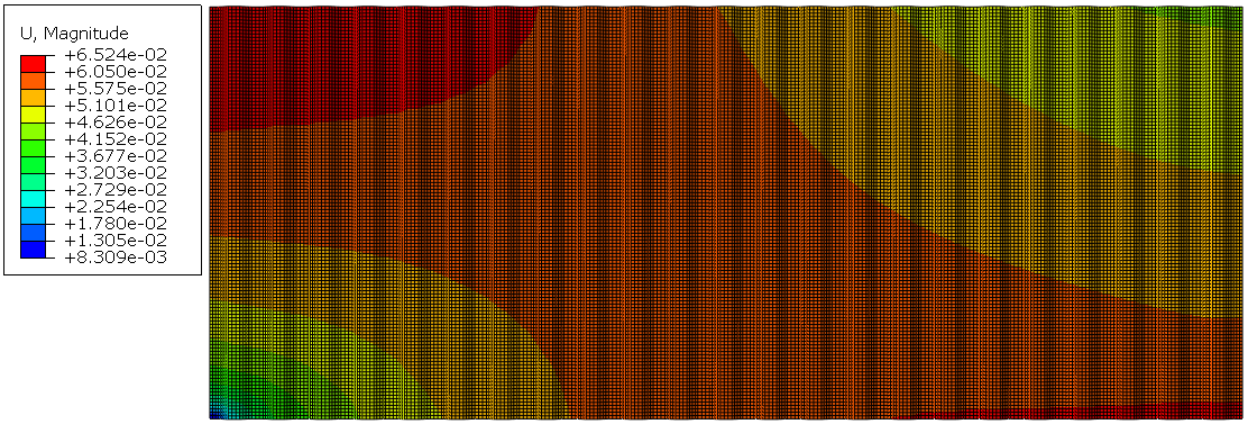

Appendix Figure 15 Displacement of FEA Shell Model of Side Wall Subject to Lateral Loading

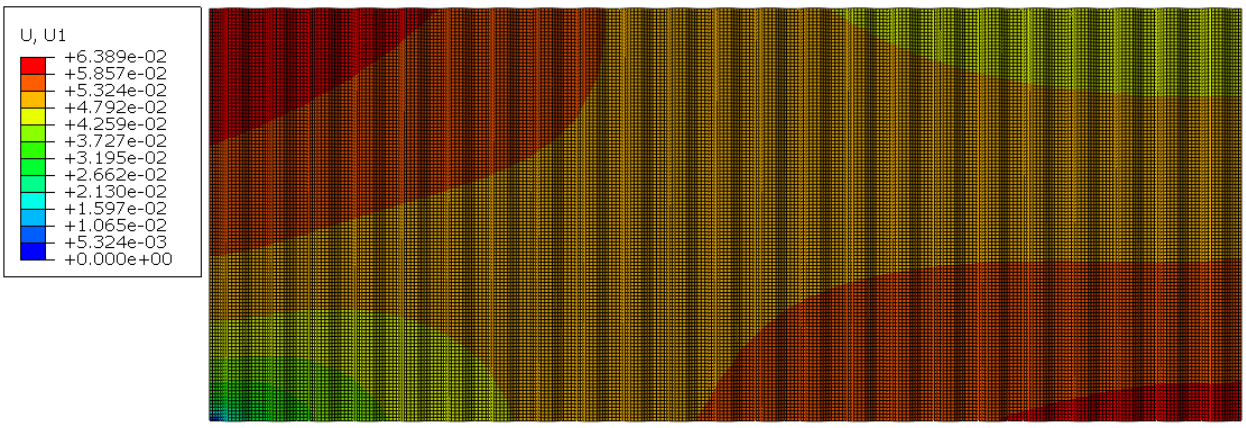

Appendix Figure 16 Displacement of FEA Shell Model of Side Wall Subject to Lateral Loading

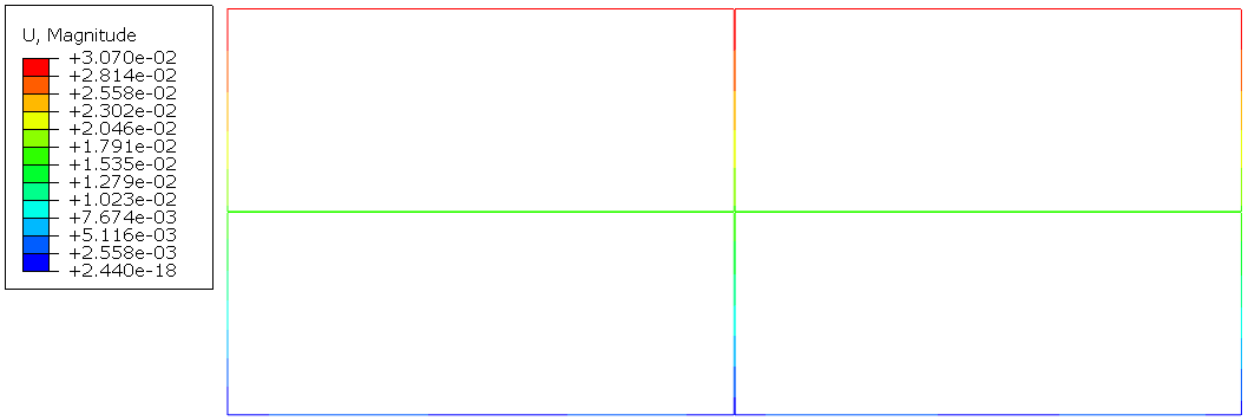

Appendix Figure 17 Displacement of MBFM of Side Wall Subject to Lateral Loading

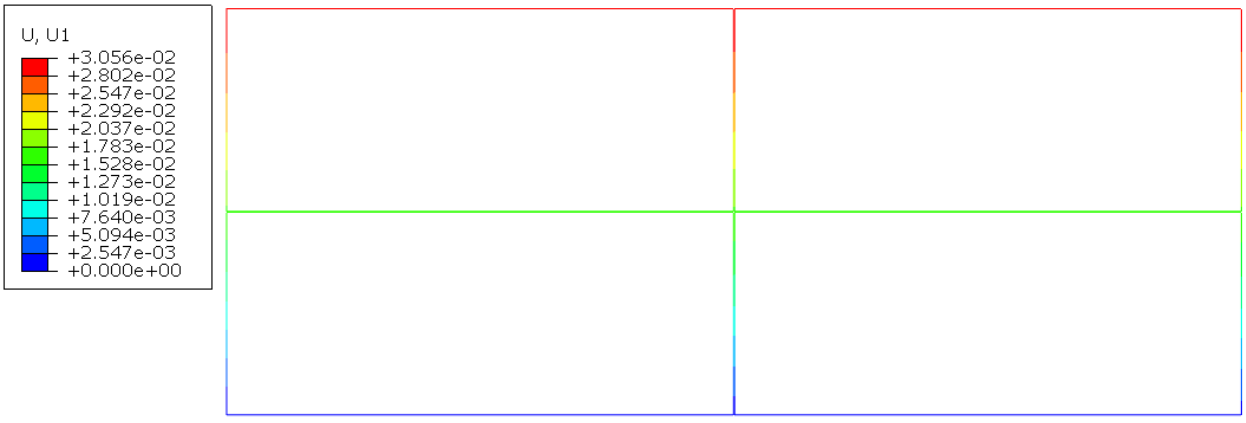

Appendix Figure 18 X-Axis Displacement of MBFM of Side Wall Subject to Lateral Loading

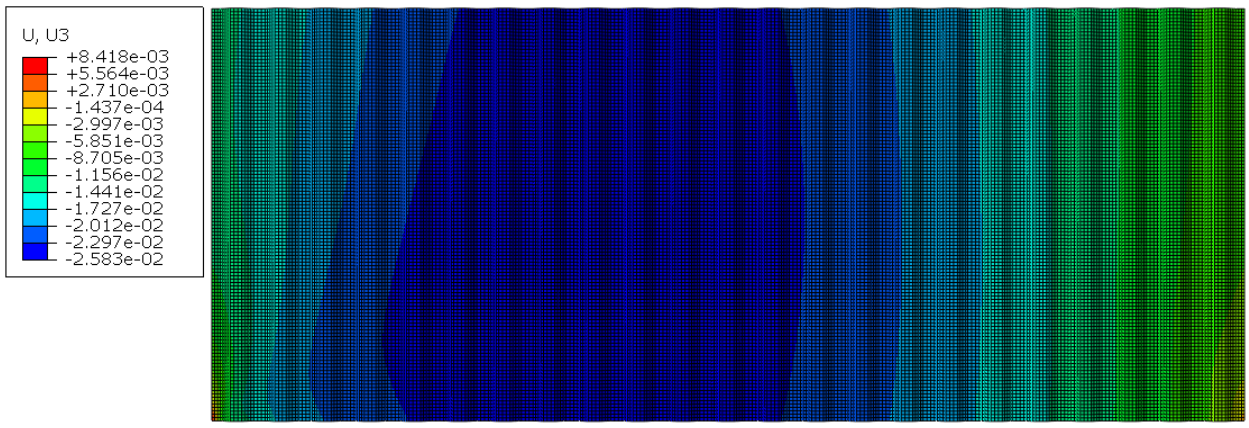

Appendix Figure 19 Displacement in Direction of Loading of FEA Shell Model of Side Wall Subject to Lateral Loading

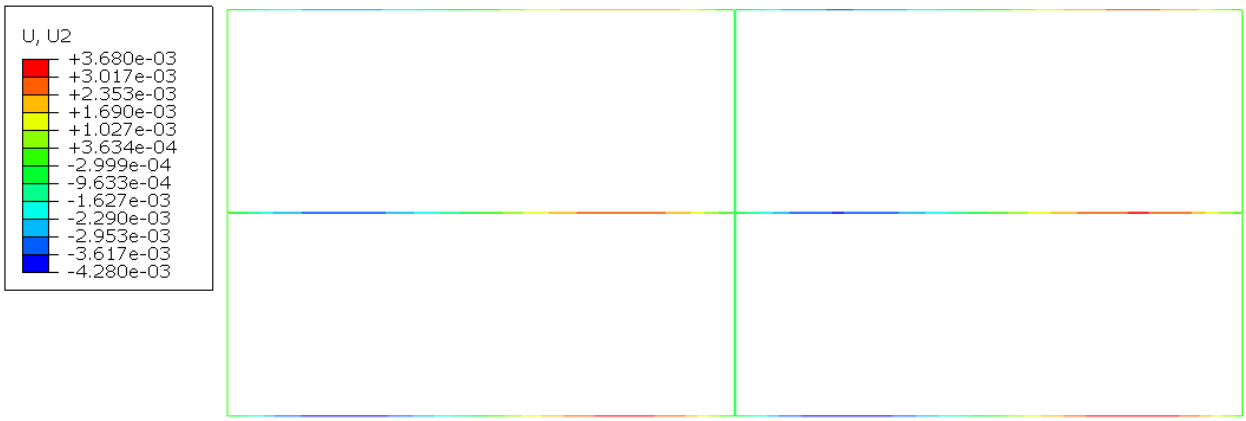

Appendix Figure 20 Displacement in Direction of Loading of MBFM of Side Wall Subject to Lateral Loading

Volume opening

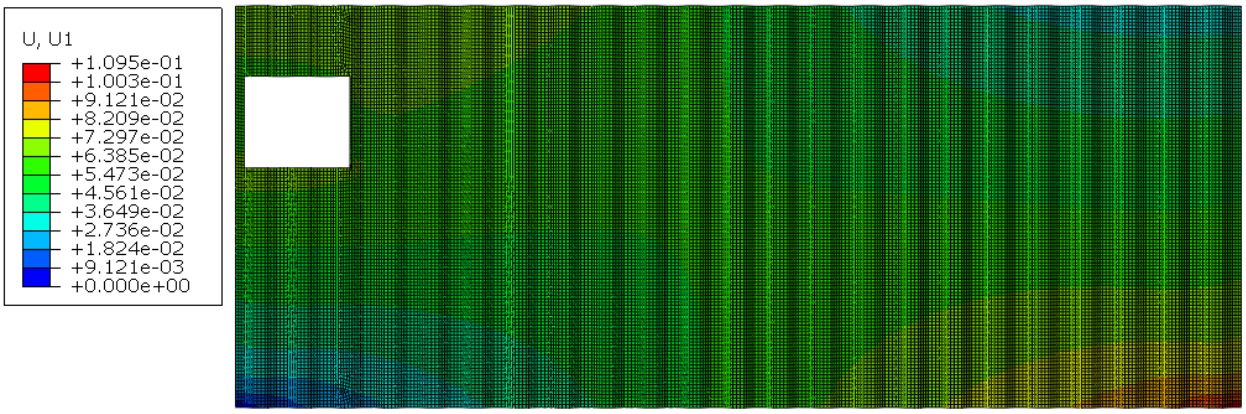

Appendix Figure 21 Displacement Distribution of FEA Shell Side Wall With Volume Opening

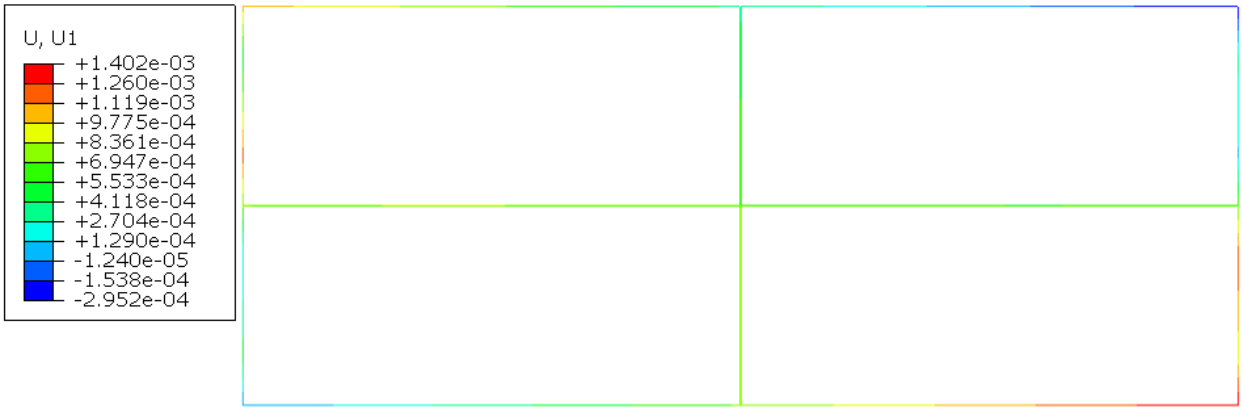

Appendix Figure 22 Displacement Distribution of MBFM Side Wall With Volume Opening

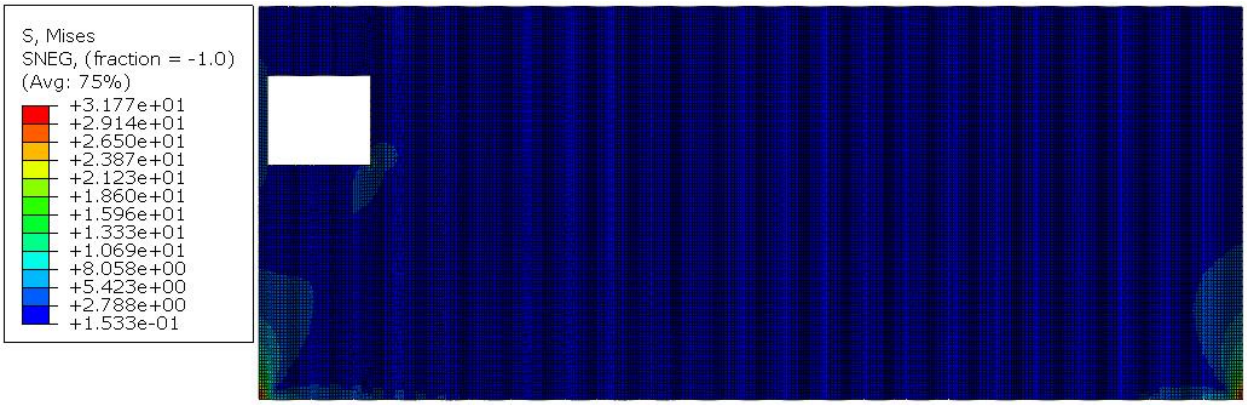

Appendix Figure 23 Stress Distribution of FEA Shell Side Wall With Volume Opening

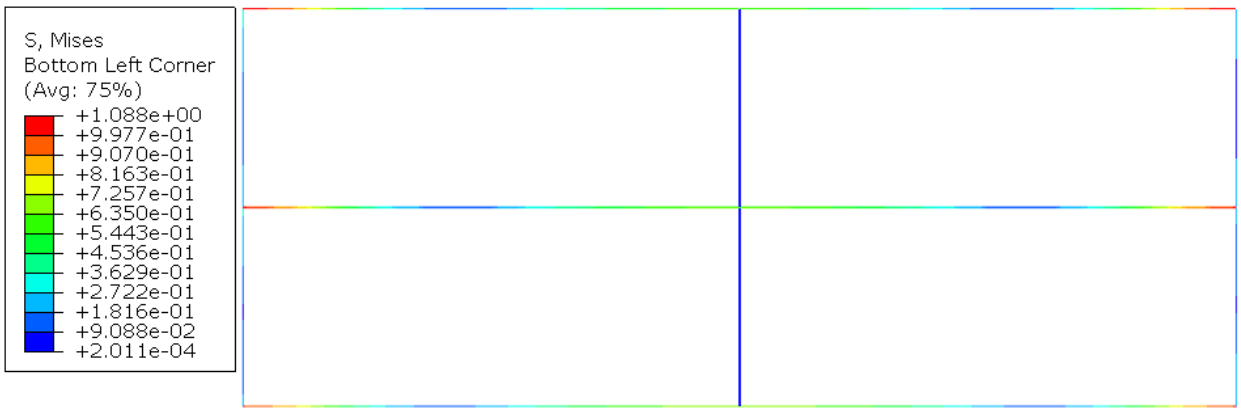

Appendix Figure 24 Stress Distribution of MBFM Side Wall With Volume Opening

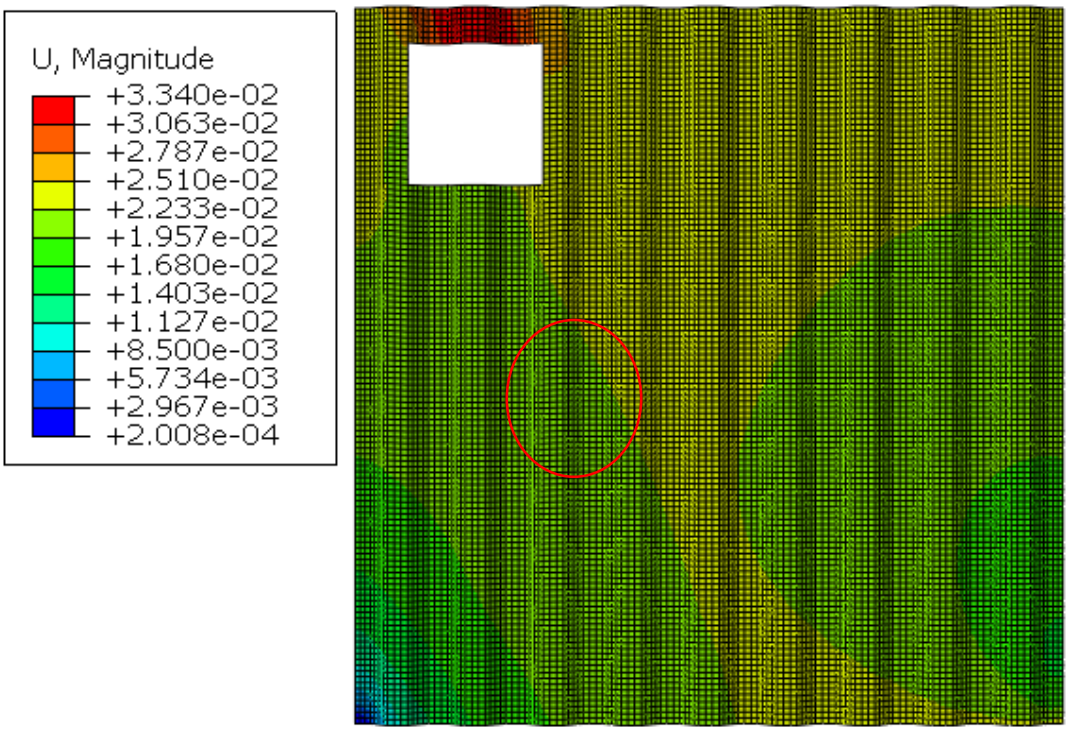

Appendix Figure 25 Displacement Distribution of MBFM End Wall With Volume Opening

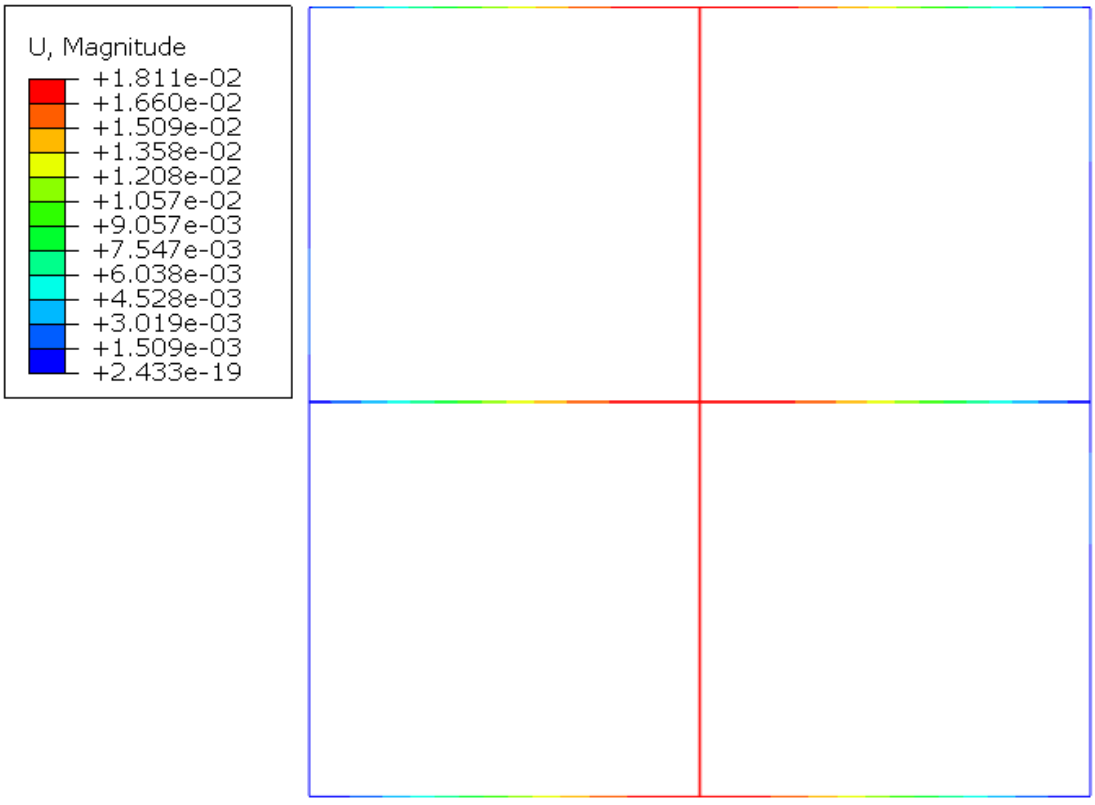

Appendix Figure 26 Displacement Distribution of MBFM End Wall With Volume Opening

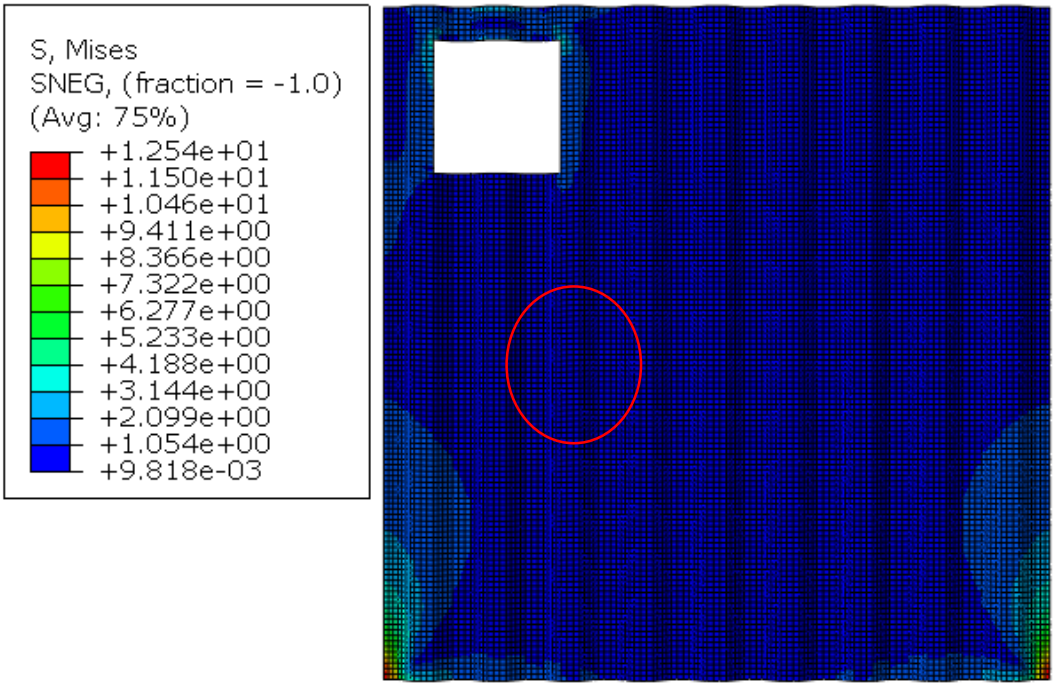

Appendix Figure 27 Stress Distribution of FEA Shell End Wall With Volume Opening

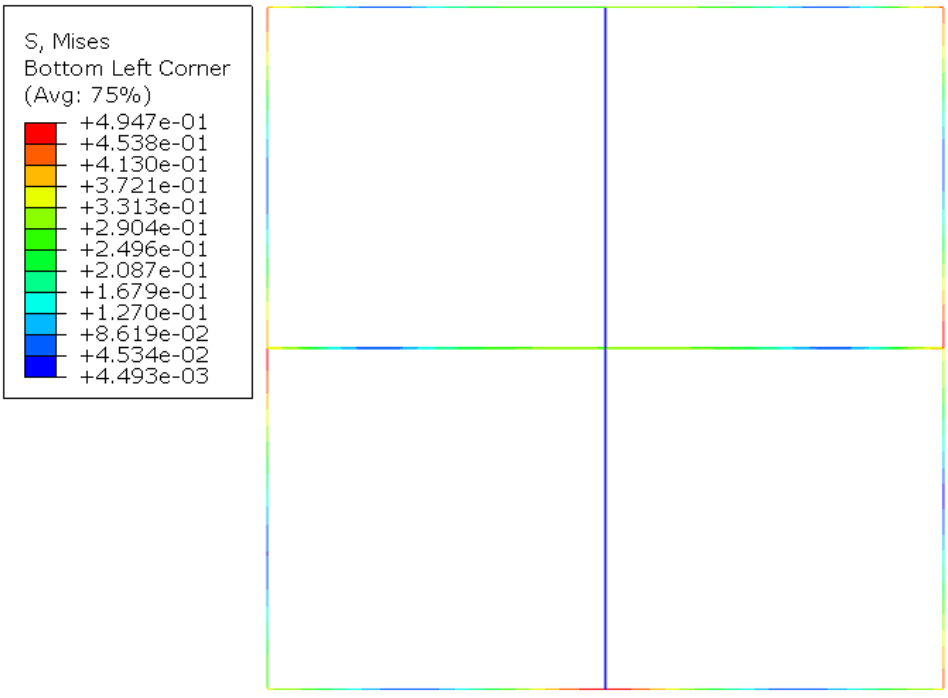

Appendix Figure 28 Stress Distribution of MBFM of End Wall With Volume Opening

Assembly

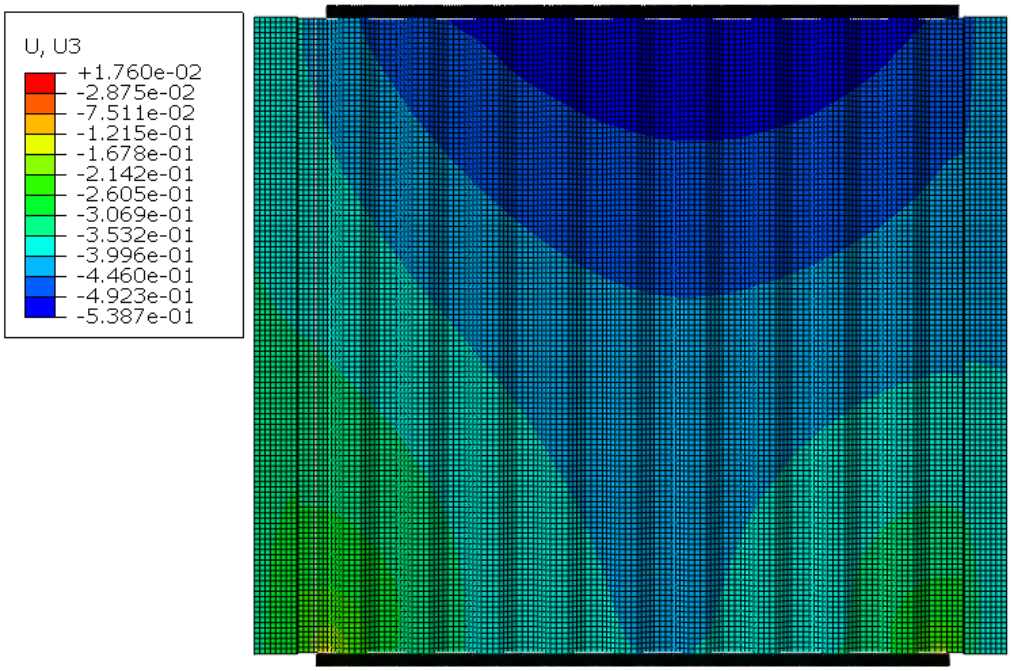

Appendix Figure 29 Displacement in Direction of Loading for FEA Shell End Wall Assembly

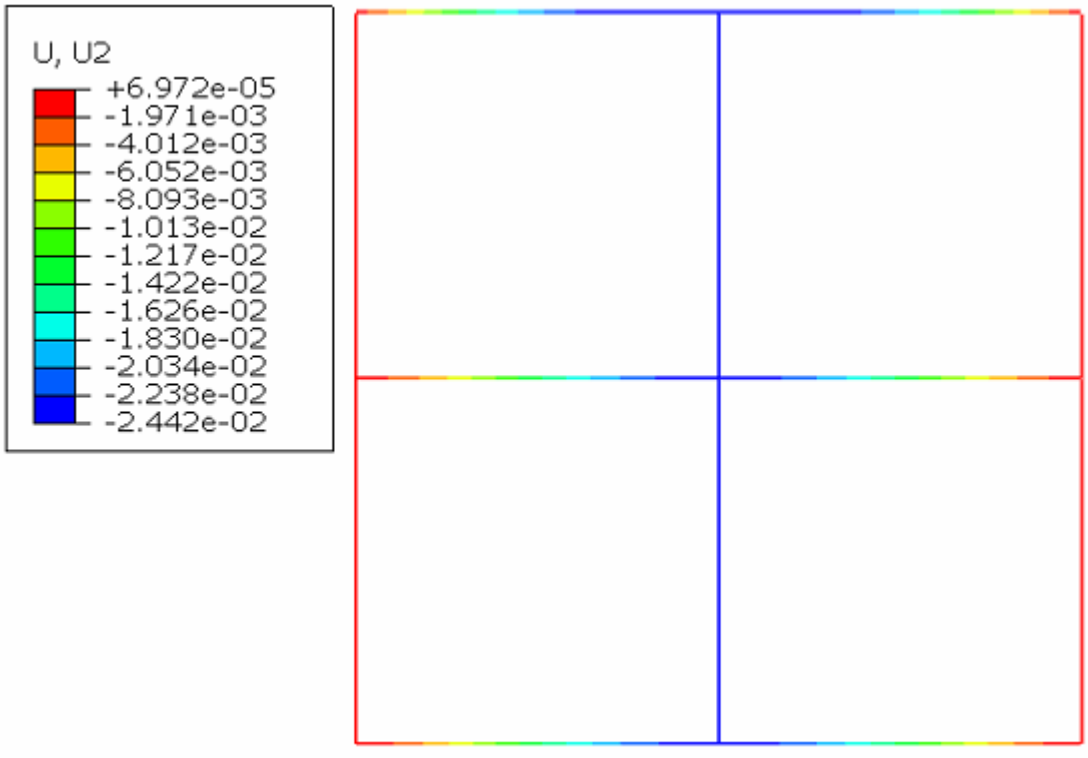

Appendix Figure 30 Displacement in Direction of Loading for MBFM End Wall Assmebly

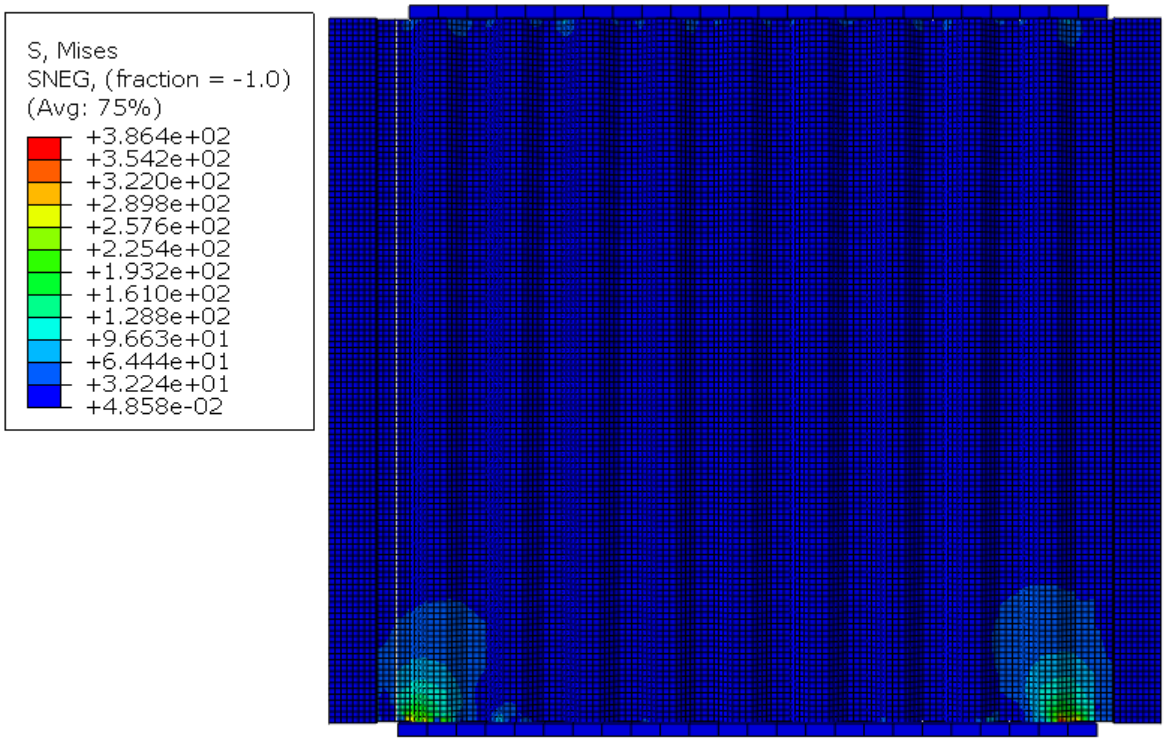

Appendix Figure 31 Stress Distribution for FEA End Wall Assembly

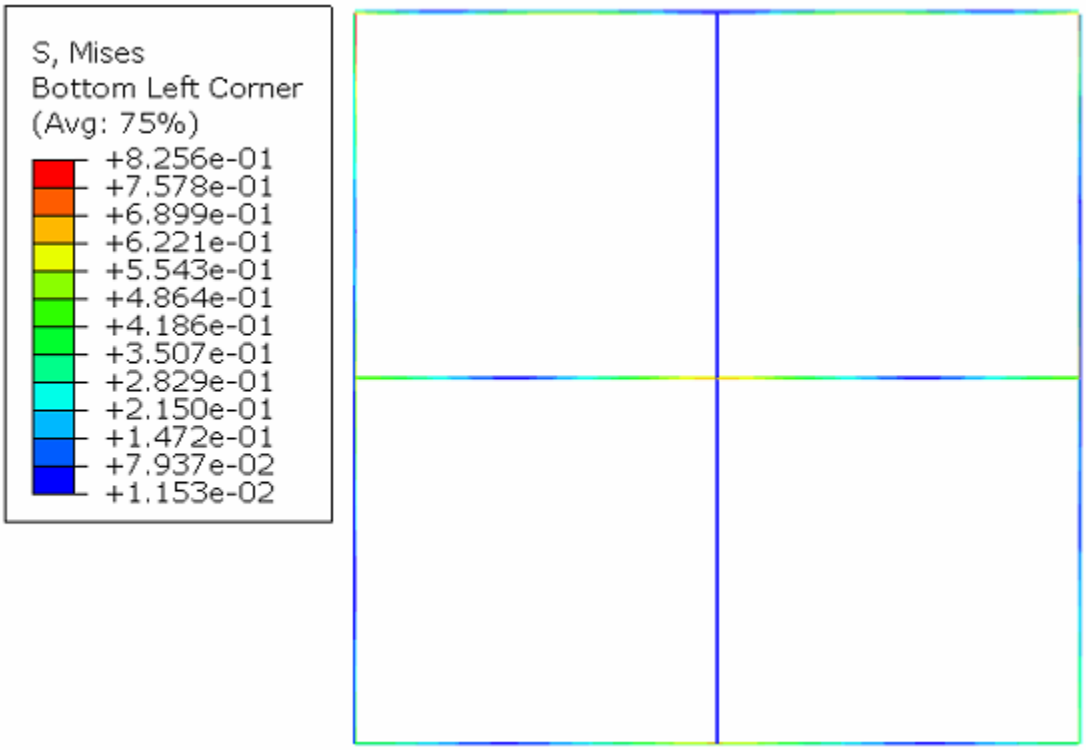

Appendix Figure 32 Stress Distribution for MBFM End Wall Assembly

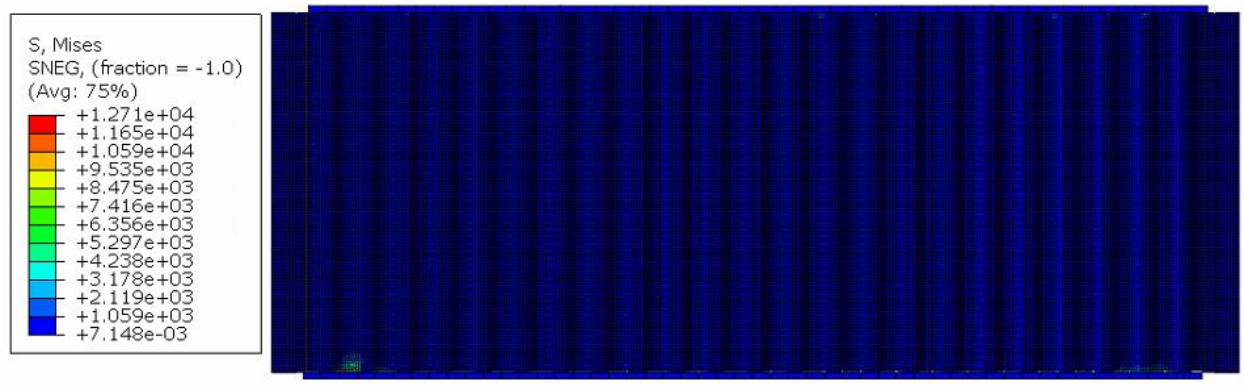

Appendix Figure 33 Stress Distribution for FEA Side Wall Assembly

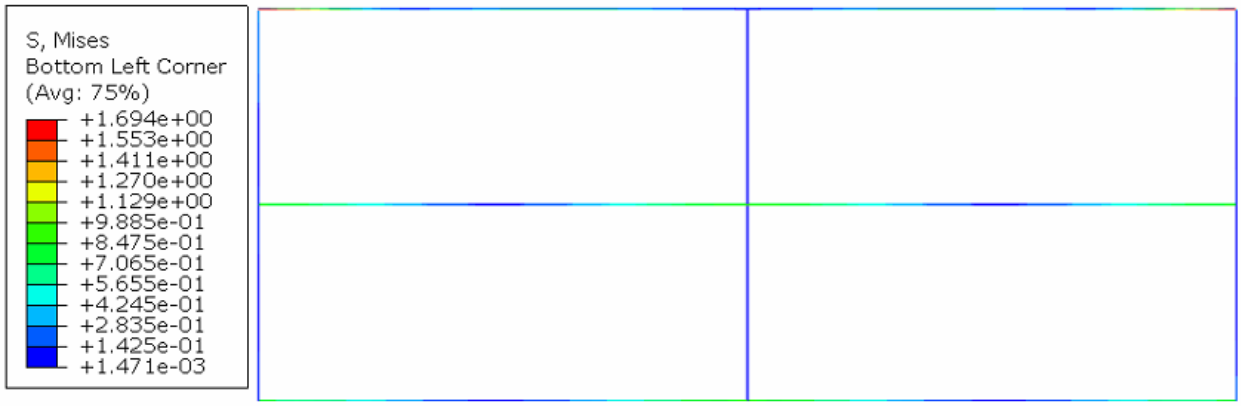

Appendix Figure 34 Stress Distribution for MBFM Side Wall Assembly

Appendix B

Hand Calculations

This Page Is Intentionally Left Blank

Department of Civil and Environmental Engineering
The University of New Hampshire
Kingsbury Hall
33 Academic Way
Durham, New Hampshire 03824

Project/Problem Set: Coupon Testing
Detail/Problem: Sample Calculations
Class: Thesis Prof: Dr. Henri

Sheet: 1 of 2
Calc. by: Dzieme Ntumi
Date: 8/28/18
Chck. by:
Date:

Specimen 6-2

data:

Width: $w = 0.499$ in
Thickness: $t = 0.0585$ in

Area $= 0.029092 in^2 = 18.7688 mm^2 = 1.88 * 10^{-5} m^2$

Time Sec	Position (X) mm	100kN (P) kN	8mm Ext (X') mm
0	-29.331	0.0675	-0.023215
0.1	-29.33	0.0864	-0.023129
0.2	-29.322	0.0988	-0.023147

$$\text{Nominal Strain} = \frac{X_n - X_o}{50}$$ where 50 is the gauge length of specimen

$\therefore$ $-29.331 - -29.331 = 0$ mm/mm

$-29.33 - -29.331 = 2 * 10^{-5}$ mm/mm

$-29.322 - -29.331 = 2 * 10^{-4}$ mm/mm

$$\text{Strain} = \frac{X'_n - X'_o}{25.4}$$ where 25.4 is the gauge length of the extensometer

$\therefore$ $-0.023215 - -0.023215 = 0$ mm/mm

$-0.023129 - -0.023215 = 3 * 10^{-6}$ mm/mm

$-0.023147 - -0.023215 = 3 * 10^{-6}$ mm/mm

$$\text{Stress} = \left(\frac{P}{A}\right) = \frac{0.0675}{1.88 * 10^{-5} * 10^6} = 0.003598 \text{ GPa} = \text{Offset Stress}$$

$$\frac{0.0864}{1.88 * 10^{-5} * 10^6} = 0.004601 \text{ GPa} = \text{Offset Stress}$$

$$\frac{0.0988}{1.88 * 10^{-5} * 10^6} = 0.005261 \text{ GPa} = \text{Offset Stress}$$

Offset Strain = Strain + 0.002

$\therefore$ $0 + 0.002 = 0.002$ mm/mm $\quad 2 * 10^{-4} + 0.002 = 0.002$ mm/mm

$2 * 10^{-5} + 0.002 = 0.002$ mm/mm

Department of Civil and
Environmental Engineering
The University of New Hampshire
Kingsbury Hall
33 Academic Way
Durham, New Hampshire 03824

Project/Problem Set: Coupon Testing
Detail/Problem: Sample Calculations
Class: Thesis Prof: Dr. Henry

Sheet: 2 of 2
Calc. by: Gillespie Nhum
Date: 3/30/18
Chck. by:
Date:

Ultimate yield Strength = maximum stress in data set

Yield Stress: Point at which 0.2% offset line crosses original data. (must graph data)

Elongation: Maximum elongation collected from extensometer

% Elongation: $\left(\frac{\text{Elongation}}{25.4}\right) * 100 = 2.19\%$ where 25.4 is the gauge length of the extencometer

Department of Civil and Environmental Engineering
The University of New Hampshire
Kingsbury Hall
33 Academic Way
Durham, New Hampshire 03824

Project/Problem Set: Chapter 6
Detail/Problem: Compressive Strength Calculation
Class: Thesis Prof: Dr. Henry

Sheet: 1 of 2
Calc. by: Desireme Ntumi
Date: 11/13/18
Chck. by:
Date:

AISC 14th Edition Chapter E Section 3

$1 in = 25.4 mm$

$50.3 mm * \frac{1 in}{25.4 mm} = 1.98 in$

$32.5 mm * \frac{1 in}{25.4 mm} = 1.28 in$

Eqs: $P_n = F_{cr} A_g$ (E3-1)

when $\frac{KL}{r} \leq 4.71\sqrt{\frac{E}{F_y}}$ or $\frac{F_y}{F_e} \leq 2.25$

$$F_{cr} = \left[0.658^{(F_y/F_e)}\right] F_y \quad (E3-2)$$

When $\frac{KL}{r} > 4.71\sqrt{\frac{E}{F_y}}$ or $\frac{F_y}{F_e} > 2.25$

$$F_{cr} = 0.877 F_e \quad (E3-3)$$

where: $F_e = \frac{\pi^2 E}{\left(\frac{KL}{r}\right)^2}$ (E3-4)

Solution

$A_g = 1.98 in * 1.28 in = 2.534 in^2$

$r_x = \sqrt{I_x/A_g}$ $r_y = \sqrt{I_y/A_g}$

AISC 1035 carbon steel $\rho = 0.284 lb/in^3$

Corner post is 8ft long = 96in

$V = 2.534 in^2 * 96 in = 243.3 in^3$

Mass = $V\rho = 243.3 in^3 * 0.284 lb/in^3 = 69.1 lbs$

$I_x = 1/12 bh^3 = 1/12 (1.28 in)(1.98 in)^3 = 0.828 in^4$

$I_y = 1/12 hb^3 = 1/12 (1.98 in)(1.28 in)^3 = 0.346 in^4$

Department of Civil and Environmental Engineering
The University of New Hampshire
Kingsbury Hall
33 Academic Way
Durham, New Hampshire 03824

Project/Problem Set: Chapter 6
Detail/Problem: Compressive Strength Calculation
Class: Thesis Prof: Dr. Henru

Sheet: 2 of 2
Calc. by: Dzifemi Nkansi
Date: 11/13/18
Chck. by:
Date:

$r_x = \sqrt{\frac{0.828 in^4}{2.534 in^2}} = 0.572 in$ $\quad r_y = \sqrt{\frac{0.346 in^4}{2.534 in^2}} = 0.370 in$

$F_y = 67 ksi$; $F_u = 80 ksi$; assume $K = 1.0$; $L = 32 in$, braced

$\frac{KL}{r_x} = \frac{1.0(32 in)}{0.572 in} = 55.9 \cong 56$ governs

$\frac{KL}{r_y} = \frac{1.0(32 in)}{0.370 in} = 86.5 \cong 87$

$4.71\sqrt{\frac{E}{F_y}} = 4.71\sqrt{\frac{29,000 ksi}{67 ksi}} = 97.99 \cong 98$

$\frac{KL}{r_y} < 4.71\sqrt{\frac{E}{F_y}}$ ∴ use equation (E3-3)

$F_e = \frac{\pi^2 E}{\left(\frac{KL}{r_x}\right)^2} = \frac{\pi^2 (29,000 ksi)}{56^2} = 94.6 ksi$

$F_{cr} = \left(0.658^{\left[F_y/F_e\right]}\right) * F_y$

$= \left(0.658^{(67/94.6)}\right) * 67 ksi$

$= 49.8 ksi$

$P_n = F_{cr} A_g = 49.8 ksi * 2.534 in^2 = 126.2 kips$

Department of Civil and Environmental Engineering
The University of New Hampshire
Kingsbury Hall
33 Academic Way
Durham, New Hampshire 03824

Project/Problem Set: Chapter 5
Detail/Problem: MBFM for Sidewall
Class: Thesis Prof: Dr. Henry

Sheet: 1 of 1
Calc. by: Dzijemo Nthemi
Date: 11/29/18
Chck. by:
Date:

Modified box frame Method for sidewall

Volume of siding = 23,143,156 mm^3 = V_s

$\frac{1}{4} V_s = \frac{23,143,156\ mm^3}{4} = 5,785,789\ mm^3$

$V_s = V_i$ ∴ $n = 3.1$ Eq 23 [6.2.2-4]

Horizontal Member

$L_{member} = \frac{1}{2}$ (Length of siding) = ½(6048 mm) = 3024 mm

Eq 20 [5 2.2-1]

$$b = \sqrt{\frac{0.25 V_s}{L_{member}}} * n$$

$$= \sqrt{\frac{5,785,789\ mm^3}{3024\ m}} * 3.1$$

$$= 135.598\ mm \cong 135.6\ mm$$

Vertical Member

L_{member} = ½ (height of siding) = ½(2440 mm) = 1220mm

$$b = \sqrt{\frac{5,785,789\ mm^3}{1220}} * 3.1$$

$$= 213.48\ mm \cong 213.5mm$$

Cross Section of horizontal member → 135.6 mm x 135.6mm

Cross Section of Vertical member → 213.5mm x 213.5 mm

Department of Civil and Environmental Engineering
The University of New Hampshire
Kingsbury Hall
33 Academic Way
Durham, New Hampshire 03824

Project/Problem Set: Chapter 5
Detail/Problem: MBFM for Endwall
Class: Thesis Prof: R. Henry

Sheet: 1 of 1
Calc. by: Dzivema Dlamini
Date: 11/29/2018
Chck. by:
Date:

Modified Box Frame Method for Endwall

Volume of Siding (V_s) = 9,132,870 mm^3

$\frac{1}{4} V_s = \frac{9,132,870 mm^3}{4} = 2,283,217.5 mm^3$

$V_s \neq V_i$

Eq 22 [5.2.2-3]

$V_f = \frac{V_i}{V_s} = \frac{23,143,156 mm^3}{9,132,870 mm^3} = 2.53 \cong 2.5$

Eq 21 [5.2.2-2]

$n = \frac{V_f^2}{S_i} = \frac{2.53^2}{3.1} = 2.07 \cong 2.10$

Horizontal Member

L_{member} = 1/2 (Length of Siding) = 1/2 (2394 mm) = 1197mm

Eq 20 [5.2.2-1]

$b = \sqrt{\frac{2,283,217.5 mm^3}{1197 mm}} * 2.10 = 78.89 m$

$b \cong 78.9 mm$

Vertical Member

L_{member} = (1/2)(height) = 1/2 (2440mm) = 1220 mm

$b = \sqrt{\frac{2,283,217.5 mm^3}{1220 mm}} * 2.10 = 78.15 mm$

$b \cong 78.2$

Cross Section of horizontal Member → 78.9mm x 78.9mm

Cross Section of Vertical Member → 78.2mm x 78.2mm